Exploring Novel Electrochemical Methods for Nitrate and Glucose Sensing

Damala, Polyxeni

UNIVERSITÉ DE GENÈVE
FACULTÉ DES SCIENCES
Section de chimie et biochimie
Département de chimie minérale et analytique
Professeur Eric Bakker

Exploring Novel Electrochemical Methods for Nitrate and Glucose Sensing

THÈSE

présentée à la Faculté des sciences de l'Université de Genève
pour obtenir le grade de Docteure ès sciences, mention chimie

par
Polyxeni DAMALA

de
Athènes (Grèce)

Thèse N° 5783

GENÈVE
Repromail
2023

UNIVERSITÉ DE GENÈVE

FACULTÉ DES SCIENCES

DOCTORAT ÈS SCIENCES, MENTION CHIMIE

Thèse de Madame Polyxeni DAMALA

intitulée :

«Exploring Novel Electrochemical Methods for Nitrate and Glucose Sensing»

La Faculté des sciences, sur le préavis de Monsieur E. BAKKER, professeur ordinaire et directeur de thèse (Département de chimie minérale et analytique), Monsieur R. MILTON, professeur assistant (Département de chimie minérale et analytique) et Monsieur A. RADU, professeur (School of chemistry, Universiy of Lincoln, Lincoln, United Kingdom), autorise l'impression de la présente thèse, sans exprimer d'opinion sur les propositions qui y sont énoncées.

Genève, le 4 décembre 2023

Thèse - 5783 -

Le Décanat

N.B. - La thèse doit porter la déclaration précédente et remplir les conditions énumérées dans les "Informations relatives aux thèses de doctorat à l'Université de Genève".

Abstract

Accurate monitoring, whether it be in environmental, clinical, or other context, is a prerequisite for maintaining and enhancing the common wellness and functionality of our society. Successful monitoring is grounded in the use of reliable sensors which ensure that real-time data reflect -as much as possible- the actual conditions. Numerous aspects influence the performance of sensors, including -but not limited to- environmental conditions, engineering features, maintenance needs and more, often making the task of ensuring accurate sensing quite challenging. The goal of this thesis is to explore some of these issues and provide alternative methods that can serve as a foundation for developing better performing sensors, with a special focus on the environmental and clinical field.

Nitrate constitutes a major analyte in the environmental context mainly due to its increased presence in the water bodies following the misuse of fertilizers and inadequate management of water resources. Potentiometry offers a simple and easy way to monitor nitrate levels using nitrate selective electrodes that typically rely their function on ion-exchangers. Despite their widespread use, these sensors often lack the desired selectivity and present interfering issues due to the presence of other components found in water, such as chloride. To overcome this challenge, nitrate ionophores have been developed and commercialized, with the hope of providing the required selective characteristics. Even though several studies have dedicated their resources on these compounds, nitrate still remains one of the analytes lacking a selective ionophore that can outperform the existing ion-exchangers, as we demonstrate by testing two commercially available nitrate ionophores. Apart from the prerequisite of selectivity, a well performing ion-selective electrode (ISE) requires a conditioning step prior to its use. This is typically a time-consuming procedure and several strategies have been suggested for decreasing the required time of conditioning. In this work we propose a method for completely avoiding the need for conditioning while maintaining stable potentiometric readings using solid-contact ISEs.

Transitioning from the environmental to the clinical setting, glucose emerges as another key analyte that continues to attract considerable attention. Today, the goal is to measure glucose in-situ with minimally invasive sensors that are reliable and affordable, and in view of this trend, the research field has experienced a surge of newly developed sensors. The downside of this development is that often there is a tendency to prioritize the engineering facets, neglecting the understanding of the fundamental working principles behind glucose sensing. As we demonstrate here, these core issues need to be carefully examined and addressed to enable the implementation of continuously operating biosensors. The majority of glucose sensors currently work in amperometric mode. Despite their popularity, owing to their ease of use, amperometric sensors suffer from undesired high charging currents and ohmic contributions. To circumvent these limitations, in the last part of this work we present a time-dependent potentiometric glucose biosensor with a readout similar to that of chronopotentiometry. The thesis is divided into five chapters:

Chapter 1: Introduction introduces critical aspects of nitrate and glucose sensing, including an overview of the challenges faced by nitrate sensors today and the evolution of glucose sensors over the decades. The reader is then navigated to the theory behind membrane electrodes to understand the principles of potentiometric response, the essential components of ISEs and other parameters affecting their performance. Next, an analysis of the basic concepts behind the operation of bioelectrochemical sensors follows, including discussions on the enzymes and mediators employed, the immobilization techniques put in place, the enzyme kinetics involved, and the electrochemical methods adopted in this work.

Chapter 2. Commercially Available Nitrate Ionophores in Potentiometric Sensors Are Not Superior to Common Ion-Exchangers examines the commercially available nitrate ionophores V and VI comparing their performance with the currently used ion-exchangers using conventional liquid-based ISEs. Selectivity coefficients and complex formation constants are calculated with the modified separate solution and sandwich membrane methods respectively, followed by few recommendations for improving the reporting of similar data in the literature.

Chapter 3: Unconditioned Symmetric Solid-Contact Electrodes for Potentiometric Sensing presents a symmetric setup with identical indicator and reference electrodes measured against each other, achieving potentiometric measurements using sold-contact ISEs “out-of-the-box”. The differential measurements cancel out all the potential drifts unrelated to the analyte activity giving stable potential readings from the first minutes. The symmetric system is then tested with freshwater samples affirming that nitrate concentration in river water can be measured using unconditioned ISEs.

Chapter 4. Avoiding Potential Pitfalls in Designing Wired Glucose Biosensors shifts the discussion on the challenges linked to the design of wired glucose biosensors. The case of a biosensor with diffusion limited response is used as an example to showcase the delicate relationship between the various forms of enzyme “wiring” and the time-dependent amperometric signal produced. In view of the pitfalls presented, suggestions for improving glucose biosensor design are provided at the end of the discussion.

Chapter 5. A novel time-dependent potentiometric glucose biosensor reports on a time-dependent potentiometric glucose biosensor based on a two-step procedure, including the oxidation of a redox mediator followed by the monitoring of open circuit potential. The transition time reflecting the jump of potential due to the changing redox state of mediator is used as the readout and correlated with the glucose concentration, yielding a linear relationship. The suggested method presents the advantages of rapid response and enhanced reproducibility when compared to the classic amperometry.

Resumé

Un suivi précis, que ce soit dans un contexte environnemental, clinique ou autre, est une condition préalable pour maintenir et améliorer le bien-être de notre société. Un suivi réussi repose sur l'utilisation de capteurs fiables qui garantissent que les données en temps réel reflètent, dans la mesure du possible, les conditions réelles. De nombreux aspects influencent la performance des capteurs, y compris, mais sans s'y limiter, les conditions environnementales, les caractéristiques techniques, les besoins de maintenance et autres, rendant souvent la tâche d'assurer une détection précise assez difficile. L'objectif de cette thèse est d'explorer certaines de ces questions et de fournir des méthodes alternatives qui peuvent servir de base pour développer des capteurs plus performants, avec une attention particulière sur le domaine environnemental et clinique.

Les nitrates constituent un analyte majeur dans le contexte environnemental, principalement en raison de leur présence accrue dans les masses d'eau à la suite d'une mauvaise utilisation des engrais et d'une gestion inadéquate des ressources en eau. La potentiométrie offre un moyen simple et facile pour surveiller les niveaux de nitrate en utilisant des électrodes sélectives au nitrate qui reposent généralement leur fonction sur des échangeurs d'ions. Malgré leur utilisation répandue, ces capteurs n'ont souvent pas la sélectivité souhaitée et présentent des problèmes d'interférences en raison de la présence d'autres composants présents dans l'eau, tels que le chlorure. Pour surmonter ce défi, des ionophores de nitrate ont été développés et commercialisés, dans l'espoir de fournir les caractéristiques sélectives requises. Bien que plusieurs études aient consacré leurs ressources à ces composés, les nitrates restent l'un des analytes pour lesquels il n'existe pas d'ionophore sélectif capable de surpasser la performance des échangeurs d'ions existants, comme nous le démontrons en testant deux ionophores de nitrate disponibles commercialement. Outre la condition préalable de sélectivité, une électrode ionosélective (EIS) performante nécessite une étape de conditionnement avant son utilisation. Cette procédure prend généralement beaucoup de temps et plusieurs stratégies ont été proposées pour réduire le temps de conditionnement nécessaire. Dans ce travail, nous proposons une méthode pour éviter complètement le besoin de conditionnement tout en maintenant des mesures potentiométriques stables en utilisant des EIS à contact solide.

Passant du contexte environnemental au contexte clinique, le glucose apparaît comme un autre analyte clé qui continue d'attirer une attention considérable. Aujourd'hui, l'objectif est de mesurer le glucose in situ à l'aide de capteurs peu invasifs, fiables et abordables, et compte tenu de cette tendance, ce domaine de recherche a connu une augmentation du nombre de nouveaux capteurs développés. L'inconvénient de ce développement est qu'il y a souvent une tendance à prioriser les facettes d'ingénierie, négligeant la compréhension des principes de fonctionnement fondamentaux derrière la détection du glucose. Comme nous le démontrons ici, ces questions fondamentales doivent être soigneusement examinées et traitées pour permettre la mise en œuvre de biocapteurs fonctionnant en continu. La majorité des

capteurs de glucose fonctionnent actuellement en mode ampérométrique. Malgré leur popularité, due à leur facilité d'utilisation, les capteurs ampérométriques souffrent de courants de charge élevés et de contributions ohmiques indésirables. Pour contourner ces limitations, nous présentons dans la dernière partie de ce travail un biocapteur de glucose potentiométrique à dépendance temporelle avec une réponse similaire à celle obtenue avec la chronopotentiométrie. Cette thèse est divisée en cinq chapitres:

Le **chapitre 1** présente les aspects essentiels de la détection du nitrate et du glucose, y compris une vue d'ensemble des défis auxquels sont confrontés les capteurs de nitrate aujourd'hui et l'évolution des capteurs de glucose au cours du temps. Le lecteur est ensuite guidé vers la théorie des électrodes à membrane pour comprendre les principes de réponse potentiométrique, les composants essentiels des EIS et d'autres paramètres affectant leur performance. Par la suite, une analyse des concepts de base derrière le fonctionnement des capteurs bioélectrochimiques est proposée, y compris des discussions sur les enzymes et les médiateurs employés, les techniques d'immobilisation mises en place, la cinétique enzymatique impliquée, et les méthodes électrochimiques adoptées dans ce travail.

Le **chapitre 2** examine les ionophores de nitrate V et VI disponibles commercialement en comparant leurs performances avec les échangeurs d'ions en utilisant des EIS conventionnelles à contact liquide. Les coefficients de sélectivité et les constantes de formation de complexe sont calculés avec la méthode modifiée de la solution séparée et la méthode de la membrane sandwich respectivement, suivis de quelques recommandations pour améliorer la présentation de données similaires dans la littérature.

Le **chapitre 3** présente une configuration symétrique avec des électrodes indicatrices et de référence identiques mesurées l'une par rapport à l'autre, réalisant des mesures potentiométriques en utilisant des EIS à contact solide "prêtes à l'emploi". Les mesures différentielles annulent toutes les dérives de potentiel non liées à l'activité de l'analyte, ce qui permet d'obtenir des lectures de potentiel stables dès les premières minutes. Le système symétrique est ensuite testé avec des échantillons d'eau douce, démontrant que la concentration de nitrate dans l'eau de rivière peut être mesurée en utilisant des EIS non conditionnées.

Le **chapitre 4** aborde les défis liés à la conception de biocapteurs de glucose de type "wired". Le cas d'un biocapteur dont la réponse est limitée par la diffusion est utilisé comme exemple pour mettre en évidence la relation délicate entre les différentes formes de "wiring" enzymatique et le signal ampérométrique généré. Compte tenu des pièges présentés, des suggestions visant à améliorer la conception des biocapteurs de glucose sont fournies à la fin de la discussion.

Le **chapitre 5** présente un biocapteur de glucose potentiométrique à dépendance temporelle, basé sur une procédure en deux étapes, comprenant l'oxydation d'un médiateur redox suivie du contrôle du potentiel en circuit ouvert. Le temps de transition reflétant le saut de potentiel dû au changement d'état redox du médiateur est utilisé comme réponse et corrélé à la concentration de glucose, ce qui donne une

relation linéaire. La méthode proposée présente les avantages d'une réponse rapide et d'une reproductibilité améliorée par rapport à l'ampérométrie classique.

List of Publications

1. Damala, P.; Zdrachek, E.; Bakker, E. Commercially Available Nitrate Ionophores in Potentiometric Sensors Are Not Superior to Common Ion-Exchangers. *Electroanalysis* **2023**, *35* (2), e202200247. https://doi.org/10.1002/elan.202200247

2. Damala, P.; Zdrachek, E.; Forrest, T.; Bakker, E. Unconditioned Symmetric Solid-Contact Electrodes for Potentiometric Sensing. *Anal. Chem.* **2022**, *94* (33), 11549–11556. https://doi.org/10.1021/acs.analchem.2c01728

3. Damala, P.; Tiuftiakov, Yu. N.; Bakker, E. Avoiding Potential Pitfalls in Designing Wired Glucose Biosensors, *ACS Sens.* **2024**, *9* (1), 2–8. https://doi.org/10.1021/acssensors.3c01960

4. Damala, P.; Bakker, E. A Novel Time-Dependent Potentiometric Glucose Biosensor, manuscript in preparation.

Table of Contents

Chapter 1: Introduction

The goal of this chapter is to lay out the scientific concepts discussed in the following chapters. This work focuses on two distinct analytes that have drawn significant attention in their respective fields: *nitrate* in the environmental context and *glucose* in the clinical context. To this end, several aspects related to the monitoring of these two analytes are presented, combined with a discussion on the electrochemical principles examined during the studies undertaken for this thesis.

1.1 Nitrate sensing: Challenges of transitioning from the lab to the market

The accurate monitoring of environmental compounds is crucial for maintaining and enhancing quality of life by identifying and addressing potentially harmful chemicals and pollutants. Nitrate is an essential ion for supporting life in aquatic systems and a fundamental nutrient to agriculture. The excessive use of fertilizers and the overall poor management of our water resources often lead to increased levels of nutrients in the water bodies that can cause excessive growth of phytoplankton, eutrophication, elevated water turbidity and other concerns, eventually leading to the malfunctioning of aquatic life and surrounding ecosystem. In view of these issues, during the last decades there has been a growing interest in developing robust analytical devices for nitrate monitoring that are reliable, have a long lifetime and require minimal maintenance. [1]

Meeting these criteria altogether has been a challenging task and today commercially available systems are still limited in terms of the detection methods employed, with the UV spectrophotometric devices still being the preferred choice for nitrate sensing. From this perspective, the goal of this Section is to briefly discuss on few aspects of the potentiometric nitrate sensors that limit their applicability and more widespread use, which may partly explain why they rarely find their way to commercialization.

The selectivity aspect remains one of the main concerns, especially with respect to chloride that is omnipresent in the aquatic systems. The detection of nitrate with potentiometric sensors relies mainly on the use of ion-exchangers that lack the desired selectivity offered (for other ions) by their counterparts, ionophores. Today there are no commercially available nitrate ionophores that perform better than the existing ion-exchangers, as discussed in *Chapter 2. Commercially Available Nitrate Ionophores in Potentiometric Sensors Are Not Superior to Common Ion-Exchangers.* However, there are a few studies that have reported increased selectivity against chloride, performing better than the available ion-exchangers. Ardakani et al. used a vanadyl-based compound as nitrate ionophore in a mixture of PVC, plasticizer, and a cation exchanger. Using conventional liquid-based ion-selective electrodes, they reported a logarithmic selectivity coefficient of -3.6 against chloride (approximately one order of magnitude lower compared to ion-exchangers) attributing the better selectivity to the possible interaction of anions with vanadyl (IV). [2] In a more recent study, Hassan et al. used solid-contact nitrate ISEs based on carbon nanotubes, and Nitron (1,4-diphenyl-endoanilino-dihydrotriazole) as the main sensing element incorporated in a plasticized PVC-based membrane mixture, reporting a

very good selectivity of nitrate over chloride with a logarithmic selectivity coefficient equal to -5.1. [3] Apart from these limited examples, occasionally one can find in the literature some newly developed ionophores that report an enhanced selectivity over nitrate tested with NMR or calorimetry titration studies in organic solvents. [4] Unfortunately, the information reported in this context is of limited use since the studies performed in the field of analytical chemistry for the determination of selectivity coefficients or binding constants are fundamentally different. Another option for circumventing the interference from chloride is to use an inline desalination unit coupled to the sensing flow cell. This approach has been successfully implemented for the nitrate measurement in seawater exhibiting fast response times and good reproducibility, with the additional possibility to use the desalination cell as a chloride sensor and salinity detector. [5] Another concern limiting the applicability of ISEs is the leaching of membrane components that drastically decreases their lifetime and overall performance. A strategy to overcome this is to covalently attach some or all the membrane components to the polymeric matrix. Le Goff et al. covalently attached betaine salts to cross-linked polystyrene-based polymers and used them as nitrate sensors for the measurement of moorland streams and natural waters with an extended lifetime of four months and with a selectivity over chloride similar to the one of ion-exchangers (logK= -2.47). [6]

In view of these issues, researchers have explored different electrochemical detection methods including amperometry, [7] chronocoulometry, [8] and other voltammetric techniques, [9–11] however, many of the developed sensors are still lacking field studies which are indispensable before becoming commercially available.

1.2 Evolution of glucose sensing

Glucose belongs to those analytes that have been studied, and continue to be studied, with an unwavering interest for almost two centuries now. If we attempt to track back the beginnings of the glucose story, we find ourselves in 1849, the year when Claude Bernard first demonstrated the presence of sugar in blood. [12] For the next half-century or so, different methods for the determination of sugar levels were proposed, most of which were either colorimetric or titrimetric, keeping as the main goal and requirement to use the smallest possible amounts of blood. [13] To mention a few of the landmark works, in 1915, Lewis and Benedict suggested the use of picric acid and sodium carbonate which, in presence of glucose and upon heating, gave a characteristic red color. [13] Four years later, Folin and Wu suggested the replacement of picric acid by the addition of a phenol reagent to a copper solution that reportedly gave a more intense and stable color. [14] Then, in 1923 Hagedorn and Jensen suggested the use of potassium ferricyanide which is reduced to ferrocyanide upon heating in alkaline solutions with specific reducing substances. [15] As reported by Hanes C.S. the advantage of replacing copper by ferricyanide was the elimination of the influence of oxygen on the reduction reaction in the latter case. [16]

The shift from the use of reducing agents to the use of enzymes takes place in the next two decades. Glucose oxidase (GOx), initially described and named as notatin, is one of the main protagonists in the field. It was discovered by Muller in 1928, who demonstrated that the enzyme catalyzes the oxidation of glucose to gluconic acid by molecular oxygen. [17] A decade later, Franke et al. using a more purified product showed that hydrogen peroxide was formed in the process from the reduction of oxygen. [18,19] In 1948, Keilin & Hartree estimated the glucose levels in blood plasma and studied the kinetics of glucose oxidase using a manometric method [20] and shortly after, Bentley & Neuberger reported another detailed study on the mechanism of its action. [21] Moving a decade forward, the next advancement in the field came from the introduction of continuous flow and automated procedures leading to repetitive analyses and more sensitive measurements. Malmstadt and Hicks, [22] and later, Blaedel and Hicks [23] developed automatic systems based on the classic colorimetric approach where glucose was oxidized by glucose oxidase forming hydrogen peroxide which then reacted with peroxidase and a dye to form a colored product. The latter study made it possible to analyse 15 samples per hour with a response time of less than 3 minutes. At the same time, different spectrophotometric and fluorometric methods based on the enzyme glucose dehydrogenase were promoted as an alternative that could offer less susceptibility to interferences. [24–27] Despite their widespread use, the systems based on colorimetric procedures suffered from fluctuations of calibration curves from day to day, unstable colored products and interferences by other redox processes originating from the used dyes. [28]

Electrochemistry on the frontline

In the meantime, the study of enzymatic methods that were not based on spectrophotometry was already underway. This progress was promoted partly by the recent advances in the continuous measurement of oxygen and carbon dioxide pressure and pH in the blood. [29–31] Therefore, many of the subsequent published works were based on the monitoring of the pH changes or the consumed oxygen originating from the enzymatic action. In 1962, Clark and Lyons reported an enzyme electrode system with glucose oxidase entrapped between two membranes and a pH electrode that could successfully correlate the pH drop observed from the oxidation of glucose to its concentration. The most known application of this system which led the way for the development of the first glucose biosensors used a pO_2 electrode (widely known as Clark oxygen electrode) and an oxygen permeable membrane incorporating glucose oxidase that allowed the measurement of glucose levels based on the oxygen consumed during the enzyme-catalysed oxidation of glucose. [31,32] In 1967, Updike & Hicks reported the first electrode with immobilized glucose oxidase in acrylamide gel, polymerized over an oxygen electrode. [33] Up until the 1970s, using amperometry to measure the concentration changes in pH, oxygen, hydrogen peroxide or products of the latter (e.g. ferrocyanide oxidized by the generated hydrogen peroxide) and relate those changes to glucose was the focus of most of the studies published. [28,34–39] Meanwhile, potentiometry also found some applications in the field, which were inspired by the introduction of precision null-point potentiometry in the late 50s. [40,41]

From the first to the second generation of glucose biosensors

When glucose oxidase is the principal enzyme used, oxygen plays the vital role of electron acceptor in the enzymatic reaction and hydrogen peroxide is the main product. The sensors relying on this principle belong to the first-generation glucose biosensors. The dependence on oxygen can become problematic when fluctuations in oxygen tension or stoichiometric limitations arise, which lead to alterations in the sensor response and the detection limit. One way to address this is to use mass transport limiting membranes that can adjust the flux of oxygen and glucose. The use of enzymes that do not require oxygen as the electron acceptor (e.g. glucose dehydrogenase) offers another possibility for oxygen independence. Another way is to use alternative compounds that can act as electron acceptors. [42] The study of such compounds for the enzymatic glucose oxidation started about 50 years ago. In 1970, Williams et al. reported an electrode system replacing oxygen by benzoquinone, which enabled the glucose measurements by monitoring the electro-oxidation of hydroquinone. [39] Few years later, Schlapfer et al. examined ten additional electron acceptors, including 2,6-dichlorophenolindophenol, pyocyanine, methylene blue and hexacyanoferrate(III). As with the study of Williams et al., these compounds were not bound or entrapped on the electrode, but added in the sample solution so they could diffuse through the semipermeable membrane that separated the enzyme from the bulk solution. Among the examined electron acceptors, hexacyanoferrate(III) showed the most satisfactory accuracy for the measurement of blood glucose in the clinical and research context. [43] These early investigations built the basis and led to the emergence of the so-called second-generation glucose biosensors, which rely on either immobilized or freely diffusing electron mediators able to reduce/oxidize the active redox center of the enzyme and shuttle the electrons to the electrode's surface and back. During this process, the mediator is cycled between its oxidized and reduced form while competing with the other available substrates (such as oxygen). In 1984, Cass et al. published a study on a second-generation glucose electrode based on ferrocene deposited on a graphite electrode with immobilized glucose oxidase covalently bound on top. [44] In 1987, this study brought to the market the first mediated amperometric glucose biosensor for use at home by a start-up company with facilities in the USA and the UK. The start-up was initially called Genetics International, later MediSense, before it was eventually bought by Abbott Laboratories in 1996. [45] From this time onwards, glucose biosensors incorporating electron mediators capture the research and market scene.

The wired enzyme

The study of electron transfer between enzymes and electrodes was well underway already from the 1980s, leading to more in-depth investigations on the electronic coupling between the active sites of the redox enzymes and the electrode surface. In most cases, the enzymes cannot exchange electrons with the electrode on which they are adsorbed because their active sites are located far from the electrode surface, making them electrically inaccessible. These sites are surrounded by the enzyme's glycosylation shell, which protects against the random electron exchanges that may happen and stabilizes the enzyme's

structure. For the enzymatic catalysis to take place, part of this protective casing needs to be either exposed or modified with other redox compounds that will act as "electron relays" between the enzyme and electrode. [46] The concept of modifying the electron mediator to covalently attach it on the enzyme gained particular attention during this decade and was marked by the important work of Heller et al. and other researchers working on various ferrocene derivatives. More specifically, in 1984, Hill et al. reported the attachment of ferrocene monocarboxylic acid to lysine residues of glucose oxidase. [47] Later on, Deganni and Heller extended the work to incorporate other enzyme residues and ferrocene derivatives, further demonstrating the idea that attaching electron relays to the enzymes is a successful way of establishing a direct electrical communication between the latter and the electrode. [48,49] These were the first attempts of "wiring the enzyme", as was later described by Heller in 1990. [46] Further studies on the stability, kinetics and enzyme activity of the modified glucose oxidase with ferrocene followed [50–52] while other compounds that could act as redox mediators were also under examination. [53,54] In the meantime, concerns on the long-term stability of similar sensors [55] urged the field to search for more efficient ways to maintain the sensing components in place and minimize leaching from the sensing layer.

In the ideal case, the enzyme and mediator should remain immobilized in a matrix that can also function as an electron-conducting relay. One solution came by the introduction of redox polymers that can meet both requirements. Redox polymers, i.e. polymers containing groups that can be reversibly reduced or oxidized, had already attracted attention from the late 70s for various applications, [56–59] but their coupling with enzymes, which marked the field of bioelectrochemistry and the development of biosensors, came somewhat later. In 1989, Heller et al. reported a covalently bound glucose oxidase on a polycationic redox polymer that could maintain fast electron transfer rates using osmium containing poly(vinylpyridine) (PVP) polymer enzyme complexes for the electrical contact between electrode and enzyme. [60] Shortly after, they published an optimized method with cross-linked PVP films that contained the covalently bound enzyme, offering a faster and simpler immobilization method that could be applied in a number of enzyme applications. [61] Additional studies with different redox polymers (e.g. siloxane, polypyrrole) were also reported soon after. [62–67] Today, several redox polymers have been studied (e.g. methacrylates, acrylamides, linear or branched poly(ethylenimines) and poly(vinylalcohols)) in a wide range of applications covering the fields of bioelectrocatalysis, biofuel cells, biosupercapacitors, biophotoelectrochemistry and biosensors. [68]

Amperometric glucose biosensors

The most significant application of the redox polymers is in amperometric biosensors that monitor the levels of various analytes in the human body. [69] Glucose biosensors particularly have seen a significant growth after the introduction of enzyme-wiring electron-conducting materials, with many commercialized products exhibiting enhanced sensitivity and low detection limits, as in the case of the Accu-Chek test strips by Roche. [70] Today, the goal is to perform glucose detection online, in situ,

continuously, at low cost, with high sensitivity and reliability. For this end, along with the traditional blood-based biosensors, many studies on non-invasive systems that target alternative biofluids, such as tears, saliva, sweat and urine have been developed where the glucose levels can be correlated to those in blood. [71,72]

1.3 Membrane electrodes

1.3.1 Origin of the potentiometric response

Membrane electrodes, which form the basis of this thesis, belong to the more general class of electrodes known as Ion-Selective Electrodes, abbreviated as ISEs. The origin of ISEs can be traced back to 1906 with the development of the pH-sensitive glass electrode by Max Cremer, which led to the first commercial pH glass electrode about two decades later. [73,74] Today, we can categorize ISEs into three groups depending on the material used: (i) glass electrodes, which were the earliest type of ISEs developed, (ii) solid-state ISEs, made of soluble salts of the ion under examination, and (iii) polymer membrane ISEs, which rely on the use of ionophores and/or ion-exchangers and can be further categorized in liquid- and solid-contact electrodes. [75]

In its simplest form, a membrane electrode is used to determine the activity of a specific ion of interest in the presence of other ions found in the same aqueous solution. Such an electrode, also known as indicator electrode, functions as a galvanic half-cell comprised of an ion-selective membrane, an inner solution (in liquid-contact ISEs) or a solid-contact material (in solid-contact ISEs) and an internal reference electrode, all of which are enclosed within a single casing. The second half-cell that completes the electrochemical system is an external reference electrode immersed in a reference electrolyte, while the connection between the two is established with a salt bridge that is typically found in the reference electrode. [76]

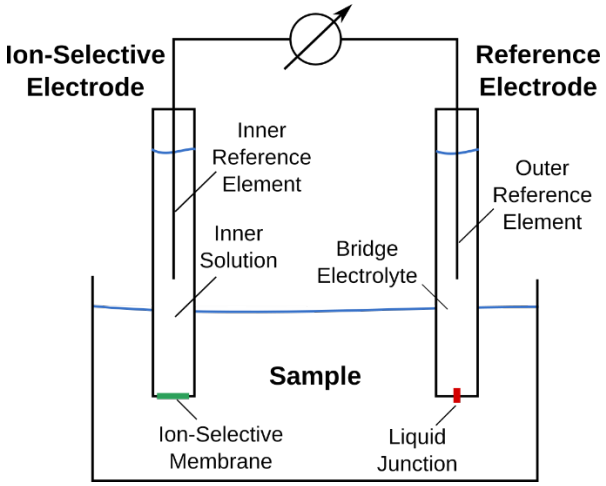

Figure 1.1: Two-electrode electrochemical cell with conventional liquid-contact ion-selective electrode

The potential difference across the cell is measured according to the potentiometric principle which requires the measuring current to be as low as possible. This is accomplished using a voltmeter that

works under high ohmic resistance. The measured electrical potential, commonly known as electromotive force (EMF), is the sum of all individual electrical potentials that arise between the solid-solid, solid-liquid and liquid-liquid interfaces in the cell, some of which being sample-dependent and others sample-independent.

Two key aspects for the development of successful ISEs are to ensure that (i) the activity of the target ion in the membrane phase is constant and independent of the sample composition, and (ii) all potential contributions to the measured EMF are also independent of the sample, except for the phase boundary potential developed at the interface of the sample and the ion-selective membrane. When these two conditions are met, the activity of the analyte ion in the membrane phase can be combined with the rest sample-independent potential contributions into a single term (E^0) and the potential of the ISE (E_M) against the reference electrode can be described by the Nernst equation [77]:

$$E_M = E^0 + \frac{RT}{z_I F} \ln a_I(aq) \tag{1.1}$$

where a_I and z_I the activity and charge of the analyte ion, F the Faraday constant, R the gas constant and T the absolute temperature.

The Nernst equation predicts that a ten-fold increase in the activity of ion I will result in a 59.2 mV/z_I increase in the EMF (25 ºC). In the case of interfering ions arising from the presence of different electrolytes in the sample, the potential of the cell can be approximated by the Nicolskii-Eisenman equation [76]:

$$E = E_I^0 + \frac{RT}{z_I F} \ln(a_I + \sum_J K_{IJ}^{pot} a_J^{z_I/z_J}) \tag{1.2}$$

where a_J the activity of the interfering ion in the solution and K_I^{pot} the selectivity coefficient (Nicolskii coefficient).

To determine the important components for the fabrication of an ISE membrane, we need first to understand the origin of the phase boundary potential developed at the interface of the membrane and the sample. Let's look at the case of a hydrophobic (water-immiscible) solution in contact with an aqueous phase. When the two solutions are brought in contact, the requirement for electroneutrality will impose a balance between the positive and negative charges in the bulk of the two phases. Meanwhile, the concentration of the same ion in the organic and aqueous phases will be different, depending on the energy of solvation of the ion for each phase. At the vicinity of the phase boundary between the two phases, the different nature of the positive and negative ions will manifest themselves resulting in an imbalance of the cationic and anionic charges at the interface. This local charge separation is the origin of the phase boundary potential that will manifest in a similar way in the case of a hydrophobic membrane when brought in contact with an aqueous sample solution. Since the response of an ISE

depends on ion movements that extend only at the nanoscale, they are characterized by fast response times. In addition, the fact that they are largely independent of ion fluxes and currents, gives them the additional advantage of being unaffected by components that may adsorb onto their surface and potentially deteriorate their response. [74]

1.3.2 Essential components of ion-selective membranes

As discussed above, the phase boundary potential developed at the interface between the sample and membrane depends heavily on ion-exchange processes between the two phases. To fulfil the condition of keeping constant the activity of the targeted ion in the membrane, which is a prerequisite for the establishment of a Nernstian response, ionic sites (also known as ion-exchangers) are added to the membrane. For an anion-selective membrane, a typical ion-exchanger will be a bulky lipophilic cation accompanied by a hydrophilic anion. Thanks to its lipophilic nature, the former will be retained in the membrane and will determine the activity of the primary anion in that phase, while preventing the transfer of counter ions to the membrane phase via the Donnan exclusion effect. Typical examples of anion- and cation- exchangers are shown in **Figure 1.2**.

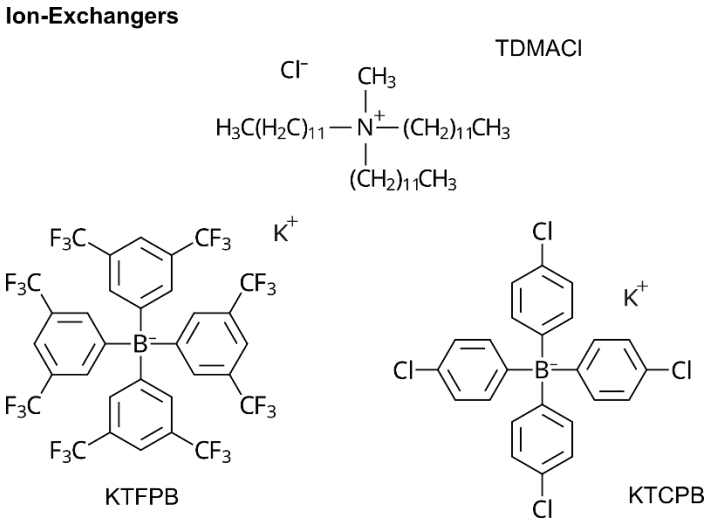

Figure 1.2: Examples of ion-exchangers: potassium tetrakis[3,5-bis(trifluoromethyl)phenyl]borate (KTFPB), tridodecylmethylammonium chloride (TDMACl) and potassium tetrakis(4-chlorophenyl)borate ion-exchanger (KTCPB)

ISEs relying solely on ion-exchangers are not highly selective since the transfer of the targeted ion to the membrane will essentially depend on its free energy of hydration based on the Hofmeister series. [78] For this reason, whenever available, ionophores, compounds capable of selectively complexing with the targeted ion, are added. A great number of cation-selective ionophores selective was already available by the end of 90s, but the development of new compounds has seen a drastic decrease during the last decades. The trend is even more prominent in the case of anion-selective compounds, which have traditionally been harder to synthesize partly because of the low affinity of hydrophilic anions to the non-polar membrane phase. [79] The synthetic pathways employed for the development of cation-and

anion-selective ionophores differ from each other. In the former case, the cation-dipole interactions are favored, while in the latter other interactions between the anion-ionophore are preferred, including hydrogen bonding, metal coordination and covalent bonding. Strategies for tailoring the interactions between anions and hosts for the development of anion-selective ionophores are discussed in *Chapter 2. Commercially Available Nitrate Ionophores in Potentiometric Sensors Are Not Superior to Common Ion-Exchangers*. **Figure 1.3** presents a few examples of anion- and cation- selective ionophores used today.

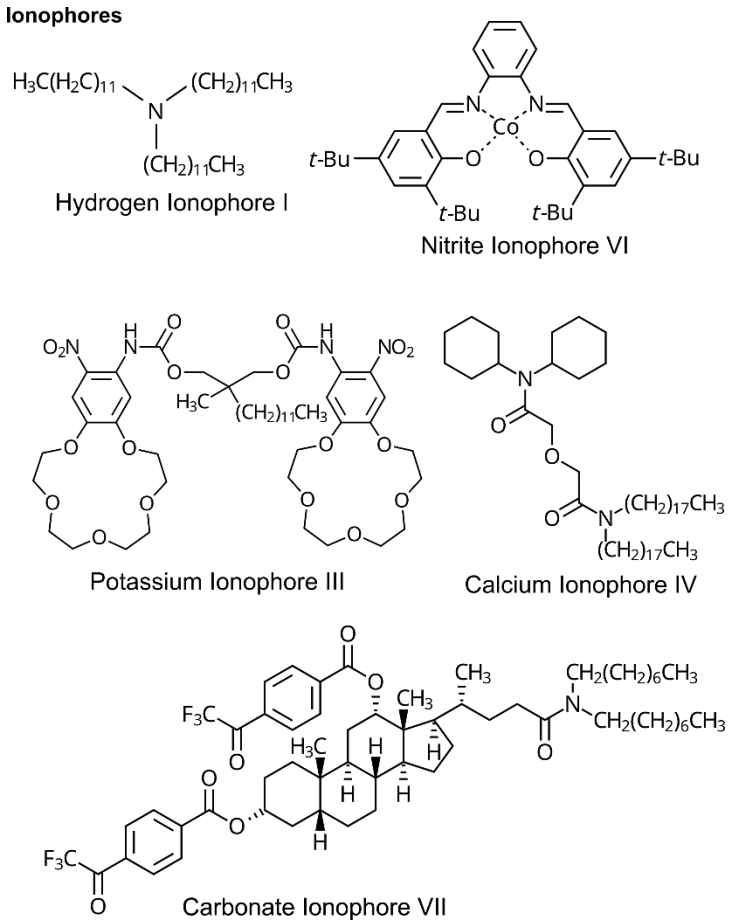

Figure 1.3: Examples of ionophores: hydrogen ionophore I, nitrite ionophore VI, potassium ionophore III, calcium ionophore IV, carbonate ionophore VII.

The selectivity attributed to the presence of ion-exchangers or ionophores is described by the selectivity coefficient (K_{I}^{pot}).

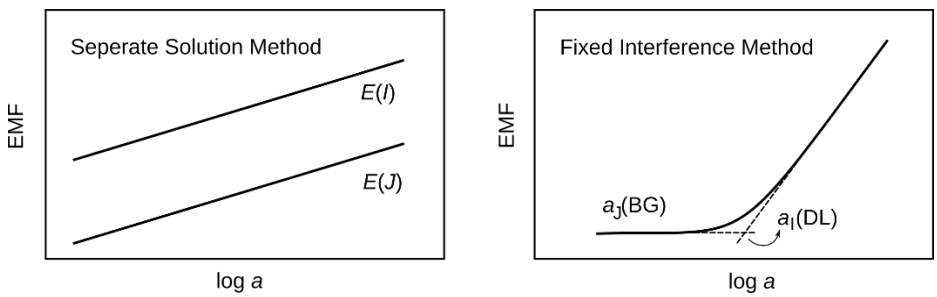

Figure 1.4: Separate solution method (SSM) and fixed interference method (FIM) for the calculation of selectivity coefficient

There are two principal methods for its calculation, the separate solution method (SSM) and fixed interference method (FIM) that both require that the measured ions exhibit Nernstian slopes (**Figure 1.4**). In SSM, the examined ions are measured in two separate solutions and the coefficients are calculated from the observed EMF value of each solution using eq. 1.3.

$$\log K_{IJ}^{pot} = \frac{(E_J - E_I)z_I F}{2.303RT} + \log(\frac{a_I}{a_J^{z_I/z_J}}) \quad (1.3)$$

In FIM, a single solution is used containing a fixed concentration of the interfering ion. The whole calibration curve is measured for the primary ion and the linear segment of the curve is extrapolated until it intersects with the potential of the interfering ion. The selectivity coefficient is then calculated with eq. 1.4.

$$\log K_{IJ}^{pot} = \log(\frac{a_I(DL)}{a_J(BG)^{z_I/z_J}}) \quad (1.4)$$

Both ionophores and ion-exchangers are incorporated within polymeric inert matrices, which were introduced in the membrane making process already from the 1970s. Among them, poly (vinyl chloride) (PVC) is still one of the principal polymeric matrices used. The main motivation for replacing the porous supports infused with ionophore solutions that were initially used, was the increased mechanical stability and resistance to pressure offered by these newly introduced polymeric materials. [74] Other important parameters are the immiscibility with water, minimal swelling, sufficient solubility of the membrane components as well as the possession of an amorphous structure and a glass transition temperature sufficiently low that will enable the free movement of ions in the membrane. [80] The accomplishment of the above requirements is often achieved with the addition of plasticizers, examples of which are shown in **Figure 1.5** together with the typical polymeric matrices employed today.

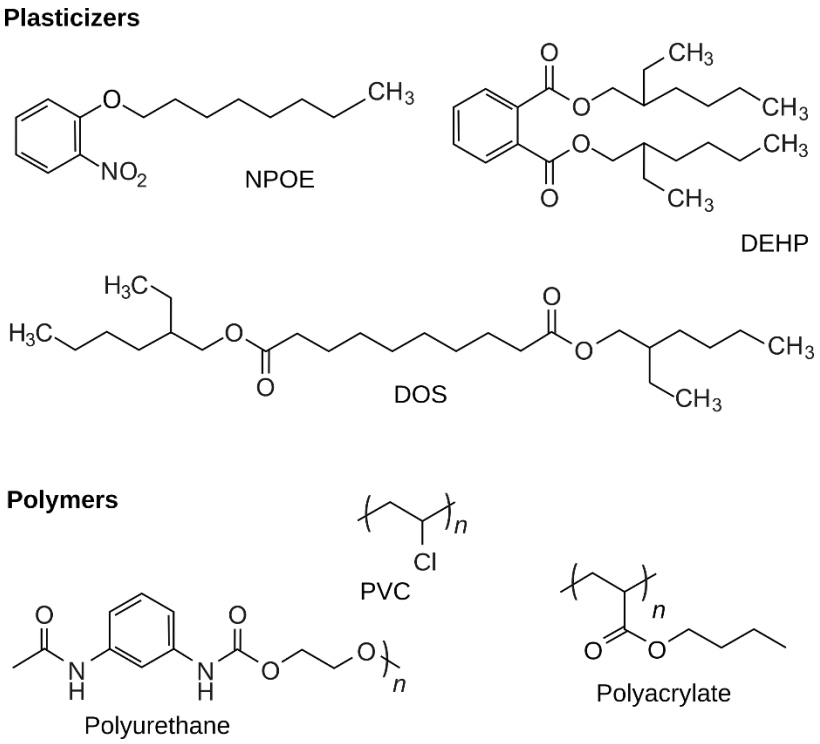

Figure 1.5: Examples of plasticizers, 2-Nitrophenyl octyl ether (NPOE), bis(2-ethylhexyl) sebacate (DOS) and bis(2-Ethylhexyl)Phthalate (DEHP), and of polymeric membrane materials.

1.3.3 Ion-to-electron transduction via solid-contact materials

In solid-contact ISEs (sc-ISEs), the inner solution and reference element are replaced by a solid ion-to-electron transducer and an electrically conducting material (**Figure 1.6**). The motivation for switching to solid-contact materials comes down to the inherent problems linked to the inner filling solution of the conventional ISEs. These include the constant need for maintenance to avoid the drying of solution, the careful orientation of the electrode, the insufficient resistance to pressure and the effect of temperature, to name a few. In addition, many agree that the biggest quality of sc-ISEs is found in their ability to be part of microfabrication technologies, which can lead to cost-effective mass production. [81]

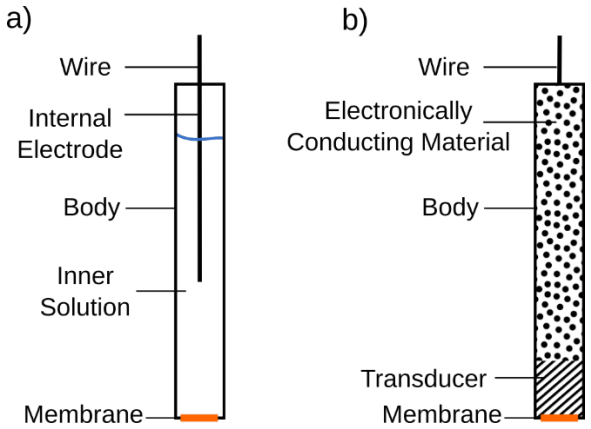

Figure 1.6: Conventional liquid-contact ISE (a) and solid-contact ISE (b) (adapted from [79])

The very first attempts to develop such electrodes date back in the early 1920s, with the development of the first glass electrode with solid internal contact made from an alkali metal. [82] Despite successfully achieving the transition between the electronic and ionic conductivity, the electrode did not find wider use due to safety concerns linked to the explosive nature of the materials used. In the following decades, several other solid-based systems were developed, including electrodes with solid crystal membranes and PVC-based ones, among which, the "coated-wire electrodes" (CWE) found extensive use. In CWEs the polymeric ion-selective membrane is directly applied on a metal wire. One of the first attempts to eliminate the internal solution applying this approach came by Freiser and Cattrall, who coated a platinum wire with a PVC membrane cocktail containing calcium didecylphosphate in dioctylphthalate to develop a calcium-responsive electrode. [83] Although the potential stability was not great, with the instabilities attributed to the interface between wire and membrane, these and similar findings from earlier studies [84,85] stimulated the research and development for more efficient solid-contacts.

Today, a wide range of materials has been tested in terms of their ability to act as ion-to-electron transducers, including several conducting polymers (e.g. poly(3-octylthiophene), poly(3,4-ethylenedioxythiophene), polyaniline, polypyrrole), carbon-based nanomaterials (e.g. carbon nanotubes, graphene, fullerene) and more. [86] Solid-contact transducers should possess both redox and ion-exchange properties to successfully establish the electrical connection between the electron-conducting solid support and a liquid-based ion selective membrane. This is a challenging task and many reported sensors suffer from potential drifts and poor reproducibility. One of the problems often encountered is the transport of small interfering molecules across the membrane (e.g. H_2O, CO_2, O_2). For example, the introduction of a water layer between the membrane and the solid-contact has been well documented and constitutes one of the main factors contributing to potential drifts. Another issue is that many of the developed materials are sensitive to either temperature, light or oxygen, often leading to electrode malfunctions and important discrepancies between the reported E^0 values. Lindner & Gyurcsányi describe in detail these issues in their thorough review on the quality standards and testing protocols for evaluating the performance of sc-ISEs, which also includes the discussion of common misconceptions and opposing viewpoints when reporting on the performance of sc-ISEs. [81]

Several aspects should be taken into consideration for the rational design of sc-ISEs. [87] Obtaining a reproducible E^0 value and stable EMF response remain the two major goals. Among the strategies tested for achieving E^0 reproducibility is the application of a potential or current and the short-circuiting of ISEs, [88,89] the use of well-defined redox buffers either alone or in combination with e.g. carbon-based materials, [90,91] and the careful selection of the electron-conducting substrate. [92] The stability of EMF response can be improved by preventing the uptake of water within the membrane choosing polymeric matrices that absorb only small amounts of water and solid-contact materials that are hydrophobic. This is particularly important for conducting polymers which often incorporate an excess of salt from the doping process that contributes to the formation of water layer. Conversely, carbon-based materials are

less affected by water uptake thanks to the hydrophobic nature of carbon. The choice of solid contacts with increased redox or double layer capacitance offering a large interfacial surface between the membrane and solid-contact is also crucial since materials with low redox capacity will be rapidly depleted even by the presence of very low measurement currents, resulting in undesired potential drifts. [80,87] In addition, efforts to minimize the leaching and decomposition of membrane components have been realized through the covalent bonding of plasticizers to the PVC polymeric matrix offering a convenient solution to the problem of plasticizer migration. [93] Finally, mechanical failures stemming from the decreased size of sc-ISEs should not be overlooked. As the sensor decreases in size, the risk of delamination and the formation of pinholes across the thin sensing membrane increase, which can eventually lead to the complete breakdown of response. [81,94]

1.3.4 Other parameters affecting sc-ISEs performance

In the above section we discussed the importance of reproducible E^0 value and stable EMF response for the development of successful ISEs. Here we will extend the discussion to other important parameters affecting their performance and examine some strategies employed to improve the performance.

To ensure a stable signal, ISEs need to be conditioned for a sufficient amount of time in order to hydrate and saturate the sensing membrane with the analyte ions of interest. When immersed in the conditioning solution, the sensor manifests a potential drift which is mainly attributed to the ion-exchange processes taking place between the sample and membrane and the resulting water uptake within the membrane and transuding material. Longer conditioning times have shown to improve the detection limit of ISEs, [95] which is another important consideration that will be examined next. As expected, the time of conditioning will be also affected by the properties of the membrane, with thicker membranes needing more time than thinner ones. [96] As will be discussed in *Chapter 3: Unconditioned Symmetric Solid-Contact Electrodes for Potentiometric Sensing*, avoiding the time-consuming conditioning step while maintaining the desired potential stability is possible by using a symmetric setup with identical indicator and reference solid-contact ISEs measured against each other. [97] By reducing the time of conditioning or even avoiding it completely, the risk of water layer formation between the sample and transducer is also decreased and the potentiometric measurement can take place in a faster time frame.

The detection limit is another parameter determining the performance of ISEs. The lower and upper detection limits that characterize every ISE are found at those activity levels where the electrode loses sensitivity towards the primary ion and its response becomes non-Nernstian (**Figure 1.7**). Ideally, the low detection limit can be calculated from the selectivity coefficient as follows:

$$a_I(DL) = K_{IJ}^{pot} a_J^{z_I/z_J} \tag{1.5}$$

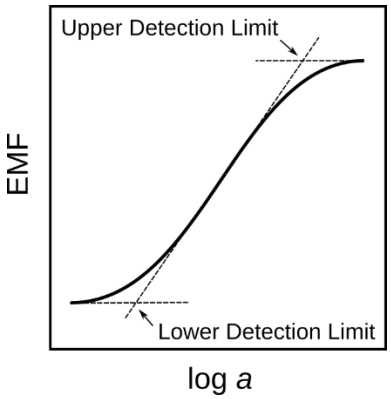

Figure 1.7: Definition of upper and lower detection limit

At low primary ion activity, the deviation from Nernstian response can be attributed either (i) to interfering ions present in the sample, or (ii) to the alteration of the interfacial sample activity by the continuous release of small amounts of primary ions from the membrane to the sample, rendering the electrode insensitive to changes of primary ion activity in the bulk of the sample. [77] In conventional ISEs, transmembrane ionic fluxes from the inner solution to the sample can dictate (by deteriorating) the lower detection limits. Once the research community came to this realization in the mid-90s, strategies targeting the minimization of such fluxes were put in place, achieving a significant decrease of the lower detection limits from the millimolar to the picomolar level. [98] One would imagine that since sc-ISEs lack the internal solution, their detection limits would be superior to the ones from conventional ISEs. However, both types of ISEs give similar detection limits, which has been attributed to contaminations arising from the membrane itself. [99]

Successful approaches that have been employed for lowering the detection limits of ISEs include the incorporation of primary ion-complexing agents within the solid-contact material to minimize the migration of primary ions from the membrane to the sample [100,101] and the use of highly lipophilic conducting polymers (poly(octylthiophene)) as ion-to-electron transducers combined with polymeric membranes (poly(methyl methacrylate)/poly(decylmethacrylate)) of low diffusivity. [102] In cases where the use of the conventional PVC polymer matrix is preferred, the increase of PVC in the cocktail membrane from 33 % (typical concentration used) to 40-50 wt% is suggested for significantly improving the detection limit while maintaining the desired mechanical properties. [103] Elaborate pretreatment protocols have also successfully resulted in the desired low detection limits. A long conditioning step in a significantly low concentration of the primary ion has worked remarkably well for a broad range of cations achieving detection limits at the nanomolar level. [104,105] Another approach which involves a drastically shorter pretreatment time is the conditioning of ISEs in a solution containing an excess of the ionophore. During the short conditioning step, the lipophilic ionophore complexes with the primary ions found at the sample-membrane interface and migrates into the membrane due to its lipophilic nature. This results in a decrease of primary ions in the sample and the minimization of the undesired ion fluxes.

This approach was tested with carbonate-selective electrodes in artificial seawater matrix achieving detection levels at the picomolar level. [106]

1.4 Bioelectrochemical sensors

The main function of a biosensor is to couple a biologically active compound to a transducer that can translate the physicochemical changes undergone at the compound to an output signal. Depending on the type of transducer used, biosensors are divided into optical, piezoelectric, calorimetric, and electrochemical ones. [107] In this work, we are examining the last category of biosensors which often constitute the most preferred choice for being fast, easy to manipulate and affordable. In addition, the discussion is limited to the use of enzymes acting as biologically active compounds, omitting references to bacteria or other redox-active proteins that do not have catalyzing properties. Finally, particular attention is given to the redox mediated systems, which have been introduced in Section **1.2** and employed in the studies presented in the following chapters.

1.4.1 Enzymes and redox mediators

Enzymes are nature's catalysts and facilitate a wide range of intricate reactions in living organisms through their unique catalytic properties. Among them, oxidoreductases are probably the most frequently used enzymes in electrochemistry thanks to their high selectivity for their substrate and their ability to retain their activity under ambient temperature and close to neutral pH. The main goal of enzymes coupled with electrodes is to enable the electron transfer from the surface of electrode to their redox-active site (and vice versa) establishing a link between the two, which is also known as "electrical wiring". [108] Redox enzymes typically used in biosensing applications consist of the apoenzyme, a proteinaceous component that is enzymatically inactive, and the cofactor, a small non-proteinaceous compound that is electroactive. The cofactor is responsible for establishing the electrical communication between the enzyme's active site and the electrode and can stay bound to the enzyme or be liberated during the enzymatic reaction. Examples of cofactors are flavin adenine dinucleotide (FAD), pyrroloquinoline quinone (PQQ) and nicotinamide adenine dinucleotide (NAD). [109] The latter, NAD+ (NAD in its oxidized form), which is found in certain reductases or dehydrogenases is an example of a cofactor that is loosely bound, or completely unbound from the enzyme backbone. The active sites of enzymes can be found buried within the enzyme's structure or at the edge of their scaffold. In the second case, a direct electron transfer (DET) between the enzyme and electrode can take place. As expected, the enzyme orientation is of crucial importance. Sensors based on enzymes that can perform DET belong to the third-generation biosensors. [110] The major downside of the convenient DET process is that few enzymes possess this ability and glucose oxidase, which is used in this work, is not one of them [111,112] even though this has been a subject for debate since a long time. The supporters of the idea that GOx can perform DET base their arguments on the presence of the reductive current typically found around the potential window of the FAD (cofactor of GOx) which transitions to the "less reductive" currents in

the presence of glucose, leading to increased current readings. However, it is increasingly accepted that the FAD redox response originates from its dissociation (from GOx) and adsorption on the electrode surface, while part of the active GOx remains attached to the electrode. In this case, the observed reductive current comes from the reduction of oxygen by the electrode, while upon addition of glucose in the system oxygen is consumed by the enzyme and thus, less it becomes reduced at the electrode. [113] Despite its inability to perform DET, glucose oxidase presents some advantages compared to its counterparts, namely a good thermostability, a low redox potential (-420 mV vs Ag/AgCl at pH 7.4) and a high specificity for glucose. On the downside, the production of hydrogen peroxide can be harmful for the enzyme, while the competition for electrons between oxygen and redox mediators and the placement of active redox centre in the enzyme that are far from the electrode surface can affect the electron transfer rates. [114]

When the enzyme's active site is not easily accessible for electron transfer, artificial electron transfer compounds, known as redox mediators, can be used as "electron relays" to electrically "wire" the enzyme and electrode surface. These are typically low molecular weight redox couples that are either immobilized or freely diffusing where the enzyme is located. Examples of such compounds include ferrocene, tetrathiafulvalene (TTF), conducting salts, quinones and the ferricyanide/ferrocyanide couple, among others. [107] As briefly discussed in Section **1.2**, these redox compounds perform the mediated electron transfer (MET) between the enzyme and electrode usually within a redox polymer that is housing all the essential components for the enzymatic catalysis, bringing in proximity the enzyme, redox couple, and electrode. This typically results in increased current densities that are crucial for the successful development of enzyme biosensors. Another advantage of using redox polymers is the possibility to act as a protecting environment for e.g. enzymes that are sensitive to oxygen, a feature which has significantly increased the popularity of these polymers for their use in new directions. [115]

Despite the plethora of available redox couples, the compounds intended to be used as mediators have certain prerequisites that are not always easy to fulfil. Ideally, they should interact rapidly with the enzyme to minimize competition from oxygen. They should have chemically stable reduced and oxidized forms, be insoluble in the aqueous phase to minimize leaching, have good electrochemical characteristics and reversible heterogeneous kinetics and be non-toxic. Possessing the above properties altogether is not common among the existing mediators while the omnipresent oxygen may also participate in the oxidation of the enzyme's sites despite the use of the mediator, thus reducing the accuracy of measurements. [42,107] Nevertheless, even if the perfect electron mediator were to be found, a successful electron transfer between enzyme and electrode is not always given. A key element in this regard is the positioning of the enzyme's active sites and the attachment of the mediators and enzymes on the electrode surface.

1.4.2 Immobilization techniques

For all practical purposes, the enzyme, as the main sensing component of the biosensor, should remain anchored at the proximity of the electrode surface. There are three main methods for enzyme immobilization: (i) adsorption, which relies heavily on the charge and polarity of the enzyme and typically results in a milder immobilization effect, (ii) cross-linking, which provides increased stability, but often to the detriment of decreased enzyme activity, and (iii) entrapment within a polymer, which is usually done by polymerizing the monomer or small polymer unit around the enzyme. Overall, before choosing the best immobilization strategy, factors that should be considered include the enzyme size, polarity and charge, the protein's surface groups, and the enzyme's ability to withstand the potentially harsh environment of immobilization that is particularly relevant in the case of cross-linking. [116,117]

1.4.3 Enzyme kinetics and key considerations

The activity and kinetics of enzymes catalysing redox reactions can be measured electrochemically and described mathematically by expressing the relationship between the rate of reaction and concentration of reactants. Through the mathematical description of reaction kinetics one can qualitatively understand how the examined system works and quantitatively determine its rate constants. The earliest attempts of studying enzyme kinetics came by Victor Henri in 1903 who first reported that enzyme reactions begin with a bond formation between the enzyme and its substrate. [118] Work towards this direction was followed by Michaelis and Menten who were studying enzymes catalysing the hydrolysis of saccharose. [119] These studies built the foundations of what we know today as the Michaelis-Menten equation:

$$v = \frac{v_{\max}[S]}{K_m + [S]} \tag{1.6}$$

where v the initial velocity of the enzyme reaction, *[S]* the substrate concentration, K_m the Michaelis constant (which is equal to the substrate concentration when the rate is half of the maximum velocity) and v_{max} the maximum velocity rate at saturating substrate concentration.

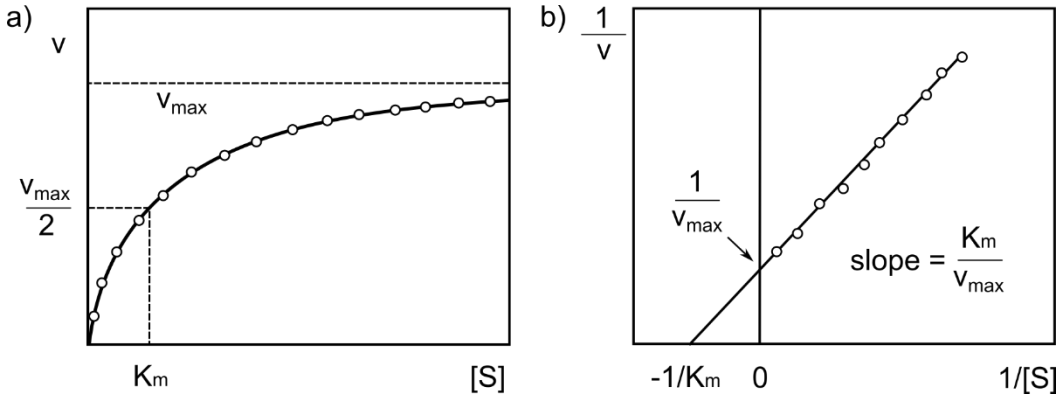

Figure 1.8: Michaelis-Menten (a) and Lineweaver-Bruk (b) plots

The Michaelis-Menten method is the best-known kinetic model to predict enzyme activity when simple and straightforward kinetics can be assumed. In **Figure 1.8**a, a typical Michaelis-Menten plot is shown where the measured reaction velocity *v* is plotted against substrate concentration *S*. The reaction velocities are calculated from separate experiments where the product formation rate over time is measured for different substrate concentrations. The resulting v-S plot can then be fitted to the Michaelis-Menten model for obtaining the desired kinetic information. For an easier interpretation of the results, the Lineweaver-Burk model is typically used to retrieve the v_{max} and K_m parameters from the following equation:

$$\frac{1}{v} = \frac{1}{v_{\max}} + \frac{K_m}{v_{\max}} \frac{1}{[S]} \tag{1.7}$$

For the electrochemist, a more practical description of the model can be given by plotting the peak current I_{max} measured at different substrate concentrations, instead of the velocity. This analogy is generally accepted given that a proportional number of electrons is released per substrate molecule during the enzymatic reaction. [120] Ideally, the equation can then take the form:

$$I = \frac{I_{\max}[S]}{K_m^{'} + [S]} \tag{1.8}$$

❖ *Key considerations before applying the Michaelis-Menten model.*

Undoubtedly, the Michaelis-Menten model holds a historical significance and continues to be a very useful tool in the study of enzyme kinetics. However, it is important to bear in mind that not all enzymes follow this kinetic model. First and foremost, the experimental data should guide our conclusions on whether the model can be applied, paying attention to discrepancies from theory which can be due to substrate inhibition, for example. As with all scientific models, the Michaelis-Menten equation stems from certain assumptions and conditions made during its formulation which should hold for any system examined. Two of these conditions are that the kinetic data used are derived from initial velocities, and the total enzyme concentration is very small compared to the total substrate concentration.

Another important consideration is the knowledge of the rate-limiting process controlling the response of the system. This is particularly relevant in the case of immobilized enzymes and other membrane components, which may introduce diffusion limits to the system and shift the electrochemistry from being enzyme-limited to diffusion-limited. A description of the rate-limiting steps controlling the conversion of substrate (glucose, in our case) is given in *Chapter 4. Avoiding Potential Pitfalls in Designing Wired Glucose Biosensors*. The use of diffusion limiting membranes is very common during the preparation of biosensors due to the advantages they offer, including increased stability of the membrane components, elimination of interferents, and more. In these electrodes, ideally the current is limited by the diffusion of substrate across the membrane. However, in special conditions, for example

when the enzyme is lost by denaturation, this condition may no longer hold and the enzyme kinetics may become the rate-limited step.

An interesting discussion initiated by Silverstein and Goodney [121] pointed out these and similar issues when reporting the performance of enzyme based biosensors, commenting on the fairly common misconception that biosensors relying on enzymes should forcedly obey the Michaelis-Menten kinetics. Using as an example a tyrosinase-based phenol biosensor which was previously published to be used in the laboratory context, [122] they underline the importance of evaluating the origin of saturated response observed at high substrate concentrations. Notably, when the saturation is non-hyperbolic, the Michaelis-Menten model is not applicable and the response cannot be attributed to enzyme kinetics. In their example, in the linear response region the current is diffusion limited, influenced only by the substrate concentration in the bulk of solution. In this regime, all of the substrate arriving at the electrode surface is catalytically converted to product. Above this point, the enzyme cannot convert all of the incoming substrate to product, and as the substrate concentration increases approaching the one of the bulk solution, the system starts to become truly limited by enzyme kinetics. In this sense, the response is not solely limited by enzyme kinetics within the whole range of examined concentrations. The discussion emphasizes another interesting point mentioned above. The application of scientific models often comes with various simplifications and assumptions. In the above example where the enzyme is immobilized, factors such as the local environment, adsorption phenomena, physicochemical changes of the protein, thickness layer and more, make it difficult to accurately define the origin of the response and assess whether it is solely diffusion or enzyme limited. In these cases, the application of kinetic models may serve better for the qualitative description of the examined systems.

1.4.4 Electrochemical methods for studying mediated biosensors

In the case of mediated enzymatic biosensors, extracting information solely about the enzyme using electrochemical methods is challenging because its electrochemical response is often convoluted with the response of the redox mediator. [108] However, electroanalytical techniques are powerful tools to examine reactions involving electron transfer and can provide us with important insights on the electrochemical properties of the examined redox polymers, the efficiency of the charge transfer, the application of the appropriate potential for efficient catalytic conversion with the minimal interference from the external environment, and more. For both cyclic voltammetry and amperometry/chronoamperometry techniques that are presented below, a three-electrode system is required, composed of the working (WE), reference (RE), and counter (CE) electrodes. The applied potential of the working electrode against the reference electrode is controlled by a potentiostat. The electrochemical event of interest is taking place at the working electrode which is modified accordingly (physically, chemically, or electrochemically) to house the sensing components under examination. The counter electrode is completing the electrical circuit by recording the resulting current flowing in the cell.

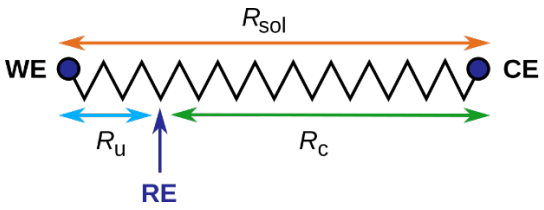

Figure 1.9: Resistances in a three-electrode electrochemical cell (WE: working electrode, CE: counter electrode, RE: reference electrode) (adapted from [123])

The electrochemical cell is characterized by an intrinsic resistance R_{sol} which is composed of the solution resistance R_c (typically compensated by the potentiostat) and a part of uncompensated resistance R_u between the working and reference electrodes (**Figure 1.9**). The latter term is linked to the appearance of the so-called ohmic drop that characterizes some systems where the potential recorded by the potentiostat differs from what the analyte experiences. By increasing the conductivity of the solution, we can decrease its resistance R_{sol}, and thereby decrease the uncompensated resistance R_u, which can also be decreased by decreasing the distance between the working and reference electrodes. [123]

Cyclic Voltammetry

Cyclic voltammetry (CV) is a versatile method that is easy to use and can convey important information on the examined system. In CV, the potential is swept linearly across the desired potential range and the resulting current is measured. The starting potential is typically found in a region where no electrochemical process is taking place. As it is swept towards the positive or negative direction, it crosses over the formal potential of the investigated species (e.g. redox mediator or enzyme) which undergoes oxidation or reduction, and then swept back to the opposite direction. When it reaches the starting potential, the cycle is completed, and a new scan can be initiated. The change of potential over time is defined by the chosen scan rate ($V\ s^{-1}$). An example of a typical voltammogram is given in **Figure 1.10**.

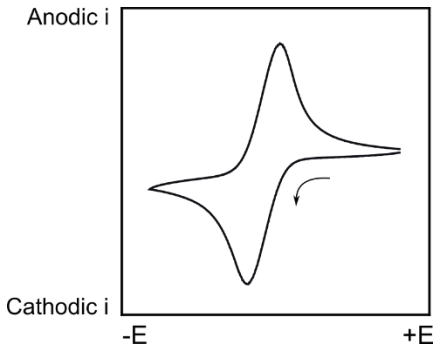

Figure 1.10: Example of a typical cyclic voltammogram

The oxidation/reduction process of the redox active species is manifested by the appearance of distinct peaks in the voltammogram. In mediated biosensors, the redox reaction can take place either with the redox mediator (e.g. the ferrocene/ferrocenium couple) or the redox active part of the enzyme (e.g. the FAD/$FADH_2$ cofactor). In this method the faradaic response will overlay an approximately constant

charging current, the magnitude of which is hard to estimate, making the measurement of peak currents relatively imprecise. Hence, CV is not an ideal technique for quantitatively assessing the system properties through the measurement of peak heights, e.g. for the concentration of the electroactive species, and should rather be used as a diagnostic tool by interpreting the qualitative or semi-quantitative information given by the positioning of the peaks, the shape of voltammogram, etc. [124]

A key information directly extracted by the cyclic voltammogram is the position of the oxidation and reduction peaks, which is used to define the redox potential of the examined redox polymer, the peak-to-peak separation and the electrochemical reversibility of the system. The redox potential is typically defined by the type of electron mediator attached to the redox polymer. In the case of amperometric biosensors, where the enzymatic catalysis and current measurement take place at a defined potential, it should be low enough to avoid co-oxidation of potential interfering compounds. At the same time, if oxygen is a concern, it should be fine-tuned to avoid oxygen reduction at the electrode or through the mediator, as has been the case with certain osmium complexes. The standard apparent reduction potential of the oxygen/hydrogen peroxide couple is +60 mV vs Ag/AgCl (at pH 7.2 and 37 ºC) so operating at a lower potential range is desired when the oxygen interference should be ruled out. [125,126]

Peak-to-peak separation is the difference between the anodic and cathodic current peak potential values. If a system is chemically and electrochemically reversible and the current is diffusion-limited, theory predicts a peak-to-peak separation of approximately 57 mV (at 25 ºC). A chemically reversible species will remain stable during the oxidation and subsequent reduction process. Similarly, in an electrochemically reversible system the electron transfer kinetics to and from the electrode will be fast and the Nernstian equilibrium will be rapidly established upon the changing applied potential. Conversely, in an electrochemically quasi-reversible or irreversible system the electron transfer kinetics will be slow and more positive or negative potential will be needed for the oxidation or reduction reactions, which will result in a larger peak-to-peak separation. [123] In addition, by performing cyclic voltammetry at different scan rates and comparing the resulting peak currents with the square root of the scan rate, one can obtain information on the type of electron transfer and evaluate whether it is diffusion controlled, in which case the data should agree with the Randles-Sevcik equation: [124]

$$i_p = (2.69 \cdot 10^5) n^{3/2} A D_e^{1/2} c_R v^{1/2} \quad (1.9)$$

where i_p the anodic or cathodic peak current (in A), n the electrons involved in the redox reaction, A the electrode surface area (in cm_2), D_e the apparent electron diffusion coefficient of the redox polymer (in $cm^2\ s^{-1}$), c_R the concentration of the electroactive species (in mol mL^{-1}) and v the scan rate (in V s^{-1}).

A linear dependence between i_p and $v^{1/2}$ is indicative of a diffusion-limited electron transfer process. The application of Randles-Sevcik equation is also useful for the calculation of the apparent electron diffusion coefficient when the concentration of electroactive species is known. Finally, the extent of the current decay at the extremes of the applied potential together with the peak positioning can provide

insights on whether the electroactive species are surface bound on the electrode or extending on a three-dimensional network within the redox polymer, which is often the case in the mediated biosensors with the enzyme and redox mediator immobilized within the polymeric network. A detailed discussion on these cases is found in *Chapter 4. Avoiding Potential Pitfalls in Designing Wired Glucose Biosensors*.

Amperometry/Chronoamperometry

Amperometry is one of the most frequently applied methods for assessing the performance of biosensors. It is not only widespread in glucose sensing (with the majority of commercially available glucose sensors being amperometric), but in environmental monitoring applications as well, targeting pesticides, peroxides, aromatic compounds and explosives, among others. [108] To perform amperometry, a potential is applied to the working electrode and the resulting current is recorded over the time. The choice of applied potential depends on the electrochemical properties of the system under examination, namely the redox potential of the polymer hosting the enzyme/redox mediator couple. As discussed above, the careful consideration of the applied potential is needed to ensure that the catalytic conversion of substrate by the enzyme will take place with minimal influence of interfering agents that may also be electroactive within the same potential window.

In chronoamperometry the potential can be applied at various steps, which are followed by the current measurement. While both are step techniques that apply potentials and measure currents, the following distinction can be made: typically, an amperometric experiment involves the application of a single potential over an extended period of time during which the substrate concentration may change and the resulting current is measured in response. During a chronoamperometric experiment the interest is more on the decay of the resulting current over time at a constant substrate concentration.

In the case of a planar electrode, the diffusion-controlled current $i_d(t)$ resulting from the application of a constant potential can be estimated by the Cottrell equation [124] (which may be adapted for the case of redox-active species confined in polymers):

$$i_d(t) = \frac{nFAD_e^{1/2}c_R}{\pi^{1/2}t^{1/2}} \tag{1.10}$$

As in the case of Randles-Sevcik equation, a Cottrell experiment can be used for the calculation of the apparent electron diffusion coefficient when the rest parameters (geometrical area, concentration of redox species) are known.

Chronopotentiometry

In chronopotentiometry, a constant current is applied between the working and counter electrode, and the potential of the former is monitored over time (against the reference electrode). In this controlled-current experiment a redox reaction must take place at the electrode surface to support the applied current. In the simplest terms, if we consider the most basic electron transfer reaction where an oxidized

species *O* is reduced at the electrode surface to species *R* upon application of a constant reducing current, the potential of the electrochemical cell will depend on the Nernst equation (simplified version for 25ºC):

$$E = E^{0'} + \frac{0.059}{z} \log \frac{c_O^S}{c_R^S} \tag{1.11}$$

where c_O^S and c_R^S the concentrations of oxidized and reduced species at the electrode surface, which will vary with time resulting in the observed potential variations. The time needed for the *O* species to become depleted at the electrode surface (because of their reduction to *R*) is characterized by the time τ, the magnitude of which will be defined by the applied current *i* and is described by the Sand equation:

$$i\tau^{1/2} = \frac{nFAD^{1/2}\pi^{1/2}c}{2} \tag{1.12}$$

where *c* the bulk concentration of the species and *D* its diffusion coefficient.

An advantage of constant current methods is that they are characterized by a constant ohmic drop that can be easily corrected by setting a potential offset, as opposed to the above examined potentiostatic techniques where the current varies with the potential, which also leads to variations of the ohmic drop making its correction more challenging. [127] In the context of this thesis, an equivalent technique to chronopotentiometry will be used, which is the measurement of open circuit potential (OCP) over time after the application of an oxidation step, as discussed in *Chapter 5. A novel time-dependent potentiometric glucose biosensor*.

1.5 References

(1) Mahmud, M. A. P.; Ejeian, F.; Azadi, S.; Myers, M.; Pejcic, B.; Abbassi, R.; Razmjou, A.; Asadnia, M. Recent Progress in Sensing Nitrate, Nitrite, Phosphate, and Ammonium in Aquatic Environment. *Chemosphere* **2020**, *259*, 127492. https://doi.org/10.1016/j.chemosphere.2020.127492.

(2) Mazloum Ardakani, M.; Salavati-Niasari, M.; Jamshidpoor, M. Selective Nitrate Poly(Vinylchloride) Membrane Electrode Based on Bis(2-Hydroxyacetophenone)Ethylenediimine Vanadyl (IV). *Sensors and Actuators B: Chemical* **2004**, *101* (3), 302–307. https://doi.org/10.1016/j.snb.2004.03.011.

(3) S. M. Hassan, S.; Galal Eldin, A.; E. Amr, A. E.-G.; A. Al-Omar, M.; H. Kamel, A.; Khalifa, N. M. Improved Solid-Contact Nitrate Ion Selective Electrodes Based on Multi-Walled Carbon Nanotubes (MWCNTs) as an Ion-to-Electron Transducer. *Sensors* **2019**, *19* (18), 3891. https://doi.org/10.3390/s19183891.

(4) Watt, M. M.; Zakharov, L. N.; Haley, M. M.; Johnson, D. W. Selective Nitrate Binding in Competitive Hydrogen Bonding Solvents: Do Anion–π Interactions Facilitate Nitrate Selectivity? *Angewandte Chemie International Edition* **2013**, *52* (39), 10275–10280. https://doi.org/10.1002/anie.201303881.

(5) Cuartero, M.; Crespo, G.; Cherubini, T.; Pankratova, N.; Confalonieri, F.; Massa, F.; Tercier-Waeber, M.-L.; Abdou, M.; Schäfer, J.; Bakker, E. In Situ Detection of Macronutrients and Chloride in Seawater by Submersible Electrochemical Sensors. *Anal. Chem.* **2018**, *90* (7), 4702–4710. https://doi.org/10.1021/acs.analchem.7b05299.

(6) Le Goff, T.; Braven, J.; Ebdon, L.; Scholefield, D. High-Performance Nitrate-Selective Electrodes Containing Immobilized Amino Acid Betaines as Sensors. *Anal. Chem.* **2002**, *74* (11), 2596–2602. https://doi.org/10.1021/ac010985i.
(7) Gokhale, A. A.; Lu, J.; Weerasiri, R. R.; Yu, J.; Lee, I. Amperometric Detection and Quantification of Nitrate Ions Using a Highly Sensitive Nanostructured Membrane Electrocodeposited Biosensor Array. *Electroanalysis* **2015**, *27* (5), 1127–1137. https://doi.org/10.1002/elan.201400547.
(8) Kim, D.; Goldberg, I. B.; Judy, J. W. Microfabricated Electrochemical Nitrate Sensor Using Double-Potential-Step Chronocoulometry. *Sensors and Actuators B: Chemical* **2009**, *135* (2), 618–624. https://doi.org/10.1016/j.snb.2008.09.022.
(9) Bagheri, H.; Hajian, A.; Rezaei, M.; Shirzadmehr, A. Composite of Cu Metal Nanoparticles-Multiwall Carbon Nanotubes-Reduced Graphene Oxide as a Novel and High Performance Platform of the Electrochemical Sensor for Simultaneous Determination of Nitrite and Nitrate. *Journal of Hazardous Materials* **2017**, *324*, 762–772. https://doi.org/10.1016/j.jhazmat.2016.11.055.
(10) Wang, J.; Diao, P. Simultaneous Detection of Ammonia and Nitrate Using a Modified Electrode with Two Regions. *Microchemical Journal* **2020**, *154*, 104649. https://doi.org/10.1016/j.microc.2020.104649.
(11) Liang, J.; Zheng, Y.; Liu, Z. Nanowire-Based Cu Electrode as Electrochemical Sensor for Detection of Nitrate in Water. *Sensors and Actuators B: Chemical* **2016**, *232*, 336–344. https://doi.org/10.1016/j.snb.2016.03.145.
(12) Bernard, C. De l'origine Du Sucre Dans l'économie Animale. *Mem. Soc. Biol.* **1849**, 121–133.
(13) Lewis, R. C.; Benedict, S. R. A METHOD FOR THE ESTIMATION OF SUGAR IN SMALL QUANTITIES OF BLOOD. *Journal of Biological Chemistry* **1915**, *20* (1), 61–72. https://doi.org/10.1016/S0021-9258(18)88273-4.
(14) Folin, O.; Wu, H. A SYSTEM OF BLOOD ANALYSIS. *Journal of Biological Chemistry* **1919**, *38* (1), 81–110. https://doi.org/10.1016/S0021-9258(18)87378-1.
(15) Hagedorn, H. C.; Jensen, B. N. The Microdetermination of Blood Sugar by Means of Ferricyanide. *Biochem. Z.* **1923**, *135* (43).
(16) Hanes, C. S. An Application of the Method of Hagedorn and Jensen to the Determination of Larger Quantities of Reducing Sugars. *Biochem J* **1929**, *23* (1), 99–106. https://doi.org/10.1042/bj0230099.
(17) Müller, D. Oxidation von Glukose Mit Extrakten Aus Aspegillus Niger. *Biochem. Z.* **1928**, *199*, 136–170.
(18) Franke, W.; Lorenz, F. *Liebigs Ann.* **1937**, *531*.
(19) Franke, W.; Deffner, M. Zur Kenntnis Der Sog. Glucose-Oxydase. II. *Justus Liebigs Annalen der Chemie* **1939**, *541* (1), 117–150. https://doi.org/10.1002/jlac.19395410107.
(20) Keilin, D.; Hartree, E. F. The Use of Glucose Oxidase (Notatin) for the Determination of Glucose in Biological Material and for the Study of Glucose-Producing Systems by Manometric Methods. *Biochemical Journal* **1948**, *42* (2), 230–238. https://doi.org/10.1042/bj0420230.
(21) Bentley, R.; Neuberger, A. The Mechanism of the Action of Notatin. *Biochemical Journal* **1949**, *45* (5), 584–590. https://doi.org/10.1042/bj0450584.
(22) Malmstadt, H. V.; Hicks, G. P. Determination of Glucose in Blood Serum by New Rapid and Specific Automatic System. *Anal. Chem.* **1960**, *32* (3), 394–398. https://doi.org/10.1021/ac60159a027.
(23) Blaedel, W. J.; Hicks, G. P. Continuous Analysis by Measurement of the Rate of Enzyme Catalyzed Reactions. Glucose Determination. *Anal. Chem.* **1962**, *34* (3), 388–394. https://doi.org/10.1021/ac60183a025.
(24) Schmidt, F. H. [Enzymatic determination of glucose and fructose simultaneously]. *Klin Wochenschr* **1961**, *39*, 1244–1247. https://doi.org/10.1007/BF01506150.
(25) Scherstén, B.; Tibbling, G. A Fluorometric Method for the Enzymatic Determination of Normal Concentrations of Urinary Glucose. *Clinica Chimica Acta* **1967**, *18* (3), 383–393. https://doi.org/10.1016/0009-8981(67)90035-6.
(26) Peterson, J. I.; Young, D. S. Evaluation of the Hexokinase-Glucose-6-Phosphate Dehydrogenase Method of Determination of Glucose in Urine. *Anal Biochem* **1968**, *23* (2), 301–316. https://doi.org/10.1016/0003-2697(68)90361-8.

(27) Guilbault, G. G. Use of Enzymes in and Kinetic Aspects of Analytical Chemistry. *Anal. Chem.* **1970**, *42* (5), 334–349. https://doi.org/10.1021/ac60287a031.
(28) Guilbault, G. G.; Tyson, B. C.; Kramer, D. N.; Cannon, P. L. Electrochemical Determination of Glucose Oxidase Using Diphenylamine Sulfonic Acid as a Potential Poiser. *Anal. Chem.* **1963**, *35* (4), 582–586. https://doi.org/10.1021/ac60197a014.
(29) Clark, L. C.; Kaplan, S.; Matthews, E. C.; Edwards, P. K.; Helmsworth, J. A. MONITOR AND CONTROL OF BLOOD OXYGEN TENSION AND PH DURING TOTAL BODY PERFUSION. *Journal of Thoracic Surgery* **1958**, *36* (4), 488–496. https://doi.org/10.1016/S0096-5588(20)30126-4.
(30) Severinghaus, J. W.; Bradley, A. F. Electrodes for Blood PO2 and PCO2 Determination. *J Appl Physiol* **1958**, *13* (3), 515–520. https://doi.org/10.1152/jappl.1958.13.3.515.
(31) Clark, L. C.; Wolf, R.; Granger, D.; Taylor, Z. *Continuous Recording of Blood Oxygen Tensions by Polarography*. *Journal of Applied Physiology* **1953**, *6* (3), 189–193. https://doi.org/10.1152/jappl.1953.6.3.189.
(32) Clark, L. C.; Lyons, C. Electrode Systems for Continuous Monitoring in Cardiovascular Surgery. *Ann N Y Acad Sci* **1962**, *102*, 29–45. https://doi.org/10.1111/j.1749-6632.1962.tb13623.x.
(33) Updike, S. J.; Hicks, G. P. The Enzyme Electrode. *Nature* **1967**, *214* (5092), 986–988. https://doi.org/10.1038/214986a0.
(34) Pardue, H. L.; Simon, R. K. Automatic Amperometric Assay of Glucose Oxidase. *Analytical Biochemistry* **1964**, *9* (2), 204–210. https://doi.org/10.1016/0003-2697(64)90104-6.
(35) Blaedel, W. J.; Olson, Carter. Continuous Analysis by the Amperometric Measurement of Reaction Rate. *Anal. Chem.* **1964**, *36* (2), 343–347. https://doi.org/10.1021/ac60208a031.
(36) Pardue, H. L. Automatic Amperometric Measurement of Reaction Rates. Enzymatic Determination of Glucose in Serum, Plasma, and Whole Blood. *Anal. Chem.* **1963**, *35* (9), 1240–1243. https://doi.org/10.1021/ac60202a008.
(37) Kadish, A. H.; Hall, D. A. A New Method for the Continuous Monitoring of Blood Glucose by Measurement of Dissolved Oxygen. *Clin Chem* **1965**, *11* (9), 869–875.
(38) Kadish, A. H.; Litle, R. L.; Sternberg, J. C. A New and Rapid Method for the Determination of Glucose by Measurement of Rate of Oxygen Consumption. *Clinical Chemistry* **1968**, *14* (2), 116–131. https://doi.org/10.1093/clinchem/14.2.116.
(39) Williams, D. Lloyd.; Doig, A. R.; Korosi, Alexander. Electrochemical-Enzymatic Analysis of Blood Glucose and Lactate. *Anal. Chem.* **1970**, *42* (1), 118–121. https://doi.org/10.1021/ac60283a032.
(40) Malmstadt, H. V.; Winefordner, J. D. Precision Null-Point Potentiometry: A Simple, Rapid and Accurate Method for Low Concentration Chloride Determinations. *Analytica Chimica Acta* **1959**, *20*, 283–291. https://doi.org/10.1016/0003-2670(59)80066-0.
(41) Malmstadt, H. V.; Pardue, H. L. Quantitative Analysis by an Automatic Potentiometric Reaction Rate Method. Specific Enzymatic Determination of Glucose. *Anal. Chem.* **1961**, *33* (8), 1040–1047. https://doi.org/10.1021/ac60176a054.
(42) Wang, J. Electrochemical Glucose Biosensors. *Chem. Rev.* **2008**, *108* (2), 814–825. https://doi.org/10.1021/cr068123a.
(43) Schläpfer, P.; Mindt, W.; Racine, P. H. Electrochemical Measurement of Glucose Using Various Electron Acceptors. *Clinica Chimica Acta* **1974**, *57* (3), 283–289. https://doi.org/10.1016/0009-8981(74)90408-2.
(44) Cass, A. E. G.; Davis, Graham.; Francis, G. D.; Hill, H. A. O.; Aston, W. J.; Higgins, I. John.; Plotkin, E. V.; Scott, L. D. L.; Turner, A. P. F. Ferrocene-Mediated Enzyme Electrode for Amperometric Determination of Glucose. *Anal. Chem.* **1984**, *56* (4), 667–671. https://doi.org/10.1021/ac00268a018.
(45) Turner, A. P. F. Biosensors: Sense and Sensibility. *Chem. Soc. Rev.* **2013**, *42* (8), 3184–3196. https://doi.org/10.1039/C3CS35528D.
(46) Heller, A. Electrical Wiring of Redox Enzymes. *Acc. Chem. Res.* **1990**, *23* (5), 128–134. https://doi.org/10.1021/ar00173a002.
(47) Hill, H. A. O. *Eur. Pat. Appl. EPO* **1984**, *125*, 45−46.
(48) Degani, Y.; Heller, Adam. Direct Electrical Communication between Chemically Modified Enzymes and Metal Electrodes. I. Electron Transfer from Glucose Oxidase to Metal Electrodes

via Electron Relays, Bound Covalently to the Enzyme. *J. Phys. Chem.* **1987**, *91* (6), 1285–1289. https://doi.org/10.1021/j100290a001.
(49) Degani, Yinon.; Heller, Adam. Direct Electrical Communication between Chemically Modified Enzymes and Metal Electrodes. 2. Methods for Bonding Electron-Transfer Relays to Glucose Oxidase and D-Amino-Acid Oxidase. *J. Am. Chem. Soc.* **1988**, *110* (8), 2615–2620. https://doi.org/10.1021/ja00216a040.
(50) N. Bartlett, P.; G. Whitaker, R.; J. Green, M.; Frew, J. Covalent Binding of Electron Relays to Glucose Oxidase. *Journal of the Chemical Society, Chemical Communications* **1987**, *0* (20), 1603–1604. https://doi.org/10.1039/C39870001603.
(51) Bartlett, P. N.; Bradford, V. Q.; Whitaker, R. G. Enzyme Electrode Studies of Glucose Oxidase Modified with a Redox Mediator. *Talanta* **1991**, *38* (1), 57–63. https://doi.org/10.1016/0039-9140(91)80009-O.
(52) Badia, A.; Carlini, R.; Fernandez, A.; Battaglini, F.; Mikkelsen, S. R.; English, A. M. Intramolecular Electron-Transfer Rates in Ferrocene-Derivatized Glucose Oxidase. *J. Am. Chem. Soc.* **1993**, *115* (16), 7053–7060. https://doi.org/10.1021/ja00069a001.
(53) Ikeda, T.; Katasho, I.; Kamei, M.; Senda, M. Electrocatalysis with a Glucose-Oxidase-Immobilized Graphite Electrode. *Agricultural and Biological Chemistry* **1984**, *48* (8), 1969–1976. https://doi.org/10.1080/00021369.1984.10866431.
(54) Albery, W. J.; Bartlett, P. N.; Craston, D. H. Amperometric Enzyme Electrodes: Part II. Conducting Salts as Electrode Materials for the Oxidation of Glucose Oxidase. *Journal of Electroanalytical Chemistry and Interfacial Electrochemistry* **1985**, *194* (2), 223–235. https://doi.org/10.1016/0022-0728(85)85006-3.
(55) Schuhmann, W.; Wohlschläger, H.; Lammert, R.; Schmidt, H.-L.; Löffler, U.; Wiemhöfer, H.-D.; Göpel, W. Leaching of Dimethylferrocene, a Redox Mediator in Amperometric Enzyme Electrodes. *Sensors and Actuators B: Chemical* **1990**, *1* (1), 571–575. https://doi.org/10.1016/0925-4005(90)80275-5.
(56) Kaufman, F. B.; Engler, E. M. Solid-State Spectroelectrochemistry of Crosslinked Donor Bound Polymer Films. *J. Am. Chem. Soc.* **1979**, *101* (3), 547–549. https://doi.org/10.1021/ja00497a009.
(57) Rubinstein, I.; Bard, A. J. Polymer Films on Electrodes. 4. Nafion-Coated Electrodes and Electrogenerated Chemiluminescence of Surface-Attached Tris(2,2'-Bipyridine)Ruthenium(2+). *J. Am. Chem. Soc.* **1980**, *102* (21), 6641–6642. https://doi.org/10.1021/ja00541a080.
(58) Buttry, D. A.; Anson, F. C. Electron Hopping vs. Molecular Diffusion as Charge Transfer Mechanisms in Redox Polymer Films. *Journal of Electroanalytical Chemistry and Interfacial Electrochemistry* **1981**, *130*, 333–338. https://doi.org/10.1016/S0022-0728(81)80402-0.
(59) Anson, F. C.; Saveant, J. M.; Shigehara, K. Self-Exchange Reactions at Redox Polymer Electrodes. A Kinetic Model and Theory for Stationary Voltammetric Techniques. *J. Phys. Chem.* **1983**, *87* (2), 214–219. https://doi.org/10.1021/j100225a008.
(60) Degani, Y.; Heller, A. Electrical Communication between Redox Centers of Glucose Oxidase and Electrodes via Electrostatically and Covalently Bound Redox Polymers. *J. Am. Chem. Soc.* **1989**, *111* (6), 2357–2358. https://doi.org/10.1021/ja00188a091.
(61) Gregg, B. A.; Heller, Adam. Cross-Linked Redox Gels Containing Glucose Oxidase for Amperometric Biosensor Applications. *Anal. Chem.* **1990**, *62* (3), 258–263. https://doi.org/10.1021/ac00202a007.
(62) Foulds, N. C.; Lowe, C. R. Immobilization of Glucose Oxidase in Ferrocene-Modified Pyrrole Polymers. *Anal. Chem.* **1988**, *60* (22), 2473–2478. https://doi.org/10.1021/ac00173a008.
(63) Schuhmann, W.; Lammert, R.; Uhe, B.; Schmidt, H.-L. Polypyrrole, a New Possibility for Covalent Binding of Oxidoreductases to Electrode Surfaces as a Base for Stable Biosensors. *Sensors and Actuators B: Chemical* **1990**, *1* (1), 537–541. https://doi.org/10.1016/0925-4005(90)80268-5.
(64) Gorton, L.; Karan, H. I.; Hale, P. D.; Inagaki, T.; Okamoto, Y.; Skotheim, T. A. A Glucose Electrode Based on Carbon Paste Chemically Modified with a Ferrocene-Containing Siloxane Polymer and Glucose Oxidase, Coated with a Poly(Ester-Sulfonic Acid) Cation-Exchanger. *Analytica Chimica Acta* **1990**, *228*, 23–30. https://doi.org/10.1016/S0003-2670(00)80474-2.
(65) De Taxis Du Poet, P.; Miyamoto, S.; Murakami, T.; Kimura, J.; Karube, I. Direct Electron Transfer with Glucose Oxidase Immobilized in an Electropolymerized Poly(N-Methylpyrrole) Film on a

Gold Microelectrode. *Analytica Chimica Acta* **1990**, *235*, 255–263. https://doi.org/10.1016/S0003-2670(00)82082-6.
(66) Lee, H. S.; Liu, L.-F.; Hale, P. D.; Okamoto, Y. Amperometric Enzyme-Modified Electrodes Based on Tetrathiafulvalene Derivatives for the Determination of Glucose. *Heteroatom Chemistry* **1992**, *3* (3), 303–310. https://doi.org/10.1002/hc.520030316.
(67) Contractor, A. Q.; Sureshkumar, T. N.; Narayanan, R.; Sukeerthi, S.; Lal, R.; Srinivasa, R. S. Conducting Polymer-Based Biosensors. *Electrochimica Acta* **1994**, *39* (8), 1321–1324. https://doi.org/10.1016/0013-4686(94)E0054-4.
(68) Ruff, A. Redox Polymers in Bioelectrochemistry: Common Playgrounds and Novel Concepts. *Current Opinion in Electrochemistry* **2017**, *5* (1), 66–73. https://doi.org/10.1016/j.coelec.2017.06.007.
(69) Heller, A. Electron-Conducting Redox Hydrogels: Design, Characteristics and Synthesis. *Current Opinion in Chemical Biology* **2006**, *10* (6), 664–672. https://doi.org/10.1016/j.cbpa.2006.09.018.
(70) Cha, K. H.; Qin, Y.; Meyerhoff, M. E. Origin of Low Detection Limit and High Selectivity of Roche Accu-Chek Test Strips That Enables Measurement of Tear Glucose Levels. *Electroanalysis* **2015**, *27* (3), 670–676. https://doi.org/10.1002/elan.201400576.
(71) Pullano, S. A.; Greco, M.; Bianco, M. G.; Foti, D.; Brunetti, A.; Fiorillo, A. S. Glucose Biosensors in Clinical Practice: Principles, Limits and Perspectives of Currently Used Devices. *Theranostics* **2022**, *12* (2), 493–511. https://doi.org/10.7150/thno.64035.
(72) Lee, H.; Hong, Y. J.; Baik, S.; Hyeon, T.; Kim, D.-H. Enzyme-Based Glucose Sensor: From Invasive to Wearable Device. *Adv Healthc Mater* **2018**, *7* (8), e1701150. https://doi.org/10.1002/adhm.201701150.
(73) Scholz, F. From the Leiden Jar to the Discovery of the Glass Electrode by Max Cremer. *J Solid State Electrochem* **2011**, *15* (1), 5–14. https://doi.org/10.1007/s10008-009-0962-7.
(74) Bühlmann, P.; Chen, L. D. Ion-Selective Electrodes With Ionophore-Doped Sensing Membranes. In *Supramolecular Chemistry*; John Wiley & Sons, Ltd, 2012. https://doi.org/10.1002/9780470661345.smc097.
(75) Radu, A.; Radu, T.; Mcgraw, C.; Dillingham, P.; Anastasova-Ivanova, S.; Diamond, D. Ion Selective Electrodes in Environmental Analysis. *Journal of the Serbian Chemical Society* **2013**, *78* (11), 1729–1761.
(76) Morf, W. E. *The Principles of Ion-Selective Electrodes and of Membrane Transport*; Studies in analytical chemistry; Akadémiai Kiadó Elsevier Scientific Pub. Co: Budapest Amsterdam, Netherlands, 1981.
(77) Bakker, E.; Bühlmann, P.; Pretsch, E. Carrier-Based Ion-Selective Electrodes and Bulk Optodes. 1. General Characteristics. *Chem. Rev.* **1997**, *97* (8), 3083–3132. https://doi.org/10.1021/cr940394a.
(78) Hofmeister, F. Zur Lehre von der Wirkung der Salze. *Archiv f. experiment. Pathol. u. Pharmakol* **1888**, *24* (4), 247–260. https://doi.org/10.1007/BF01918191.
(79) Mikhelson, K. N.; Peshkova, M. A. Advances and Trends in Ionophore-Based Chemical Sensors. *Russ. Chem. Rev.* **2015**, *84* (6), 555. https://doi.org/10.1070/RCR4506.
(80) Bieg, C.; Fuchsberger, K.; Stelzle, M. Introduction to Polymer-Based Solid-Contact Ion-Selective Electrodes—Basic Concepts, Practical Considerations, and Current Research Topics. *Anal Bioanal Chem* **2017**, *409* (1), 45–61. https://doi.org/10.1007/s00216-016-9945-6.
(81) Lindner, E.; Gyurcsányi, R. E. Quality Control Criteria for Solid-Contact, Solvent Polymeric Membrane Ion-Selective Electrodes. *J Solid State Electrochem* **2009**, *13* (1), 51–68. https://doi.org/10.1007/s10008-008-0608-1.
(82) Nikolskii, B. P.; Materova, E. A. Solid Contact in Membrane Ion-Selective Electrodes. In *Ion-Selective Electrode Reviews*; Thomas, J. D. R., Ed.; Ion-Selective Electrode Reviews; Elsevier, 1985; Vol. 7, pp 3–39. https://doi.org/10.1016/B978-0-08-034150-7.50005-X.
(83) Cattrall, R. W.; Freiser, Henry. Coated Wire Ion-Selective Electrodes. *Anal. Chem.* **1971**, *43* (13), 1905–1906. https://doi.org/10.1021/ac60307a032.
(84) E. Pungor. *Anal. Chem.* **1967**, *39* (13).
(85) Hirata, H.; Dato, K. Copper(I) Sulphide-Impregnated Silicone Rubber Membranes as Selective Electrodes for Copper(II) Ions. *Talanta* **1970**, *17* (9), 883–887. https://doi.org/10.1016/0039-9140(70)80185-0.

(86) Zdrachek, E.; Bakker, E. Potentiometric Sensing. *Anal. Chem.* **2021**, *93* (1), 72–102. https://doi.org/10.1021/acs.analchem.0c04249.
(87) Hu, J.; Stein, A.; Bühlmann, P. Rational Design of All-Solid-State Ion-Selective Electrodes and Reference Electrodes. *TrAC Trends in Analytical Chemistry* **2016**, *76*, 102–114. https://doi.org/10.1016/j.trac.2015.11.004.
(88) Vanamo, U.; Bobacka, J. Electrochemical Control of the Standard Potential of Solid-Contact Ion-Selective Electrodes Having a Conducting Polymer as Ion-to-Electron Transducer. *Electrochimica Acta* **2014**, *122*, 316–321. https://doi.org/10.1016/j.electacta.2013.10.134.
(89) Vanamo, U.; Bobacka, J. Instrument-Free Control of the Standard Potential of Potentiometric Solid-Contact Ion-Selective Electrodes by Short-Circuiting with a Conventional Reference Electrode. *Anal. Chem.* **2014**, *86* (21), 10540–10545. https://doi.org/10.1021/ac501464s.
(90) Zou, X. U.; Zhen, X. V.; Cheong, J. H.; Bühlmann, P. Calibration-Free Ionophore-Based Ion-Selective Electrodes With a Co(II)/Co(III) Redox Couple-Based Solid Contact. *Anal. Chem.* **2014**, *86* (17), 8687–8692. https://doi.org/10.1021/ac501625z.
(91) Hu, J.; Zou, X. U.; Stein, A.; Bühlmann, P. Ion-Selective Electrodes with Colloid-Imprinted Mesoporous Carbon as Solid Contact. *Anal. Chem.* **2014**, *86* (14), 7111–7118. https://doi.org/10.1021/ac501633r.
(92) Zou, X. U.; Cheong, J. H.; Taitt, B. J.; Bühlmann, P. Solid Contact Ion-Selective Electrodes with a Well-Controlled Co(II)/Co(III) Redox Buffer Layer. *Anal. Chem.* **2013**, *85* (19), 9350–9355. https://doi.org/10.1021/ac4022117.
(93) Skelly, P. W.; Li, L.; Braslau, R. Internal Plasticization of PVC. *Polymer Reviews* **2022**, *62* (3), 485–528. https://doi.org/10.1080/15583724.2021.1986066.
(94) Lindner, E.; Cosofret, V. V.; Ufer, S.; Buck, R. P.; Kusy, R. P.; Ash, R. B.; Nagle, H. T. Flexible (Kapton-Based) Microsensor Arrays of High Stability for Cardiovascular Applications. *J. Chem. Soc., Faraday Trans.* **1993**, *89* (2), 361–367. https://doi.org/10.1039/FT9938900361.
(95) Chumbimuni-Torres, K. Y.; Rubinova, N.; Radu, A.; Kubota, L. T.; Bakker, E. Solid Contact Potentiometric Sensors for Trace Level Measurements. *Anal. Chem.* **2006**, *78* (4), 1318–1322. https://doi.org/10.1021/ac050749y.
(96) Forrest, T.; Zdrachek, E.; Bakker, E. Thin Layer Membrane Systems as Rapid Development Tool for Potentiometric Solid Contact Ion-Selective Electrodes. *Electroanalysis* **2020**, *32* (4), 799–804. https://doi.org/10.1002/elan.201900674.
(97) Damala, P.; Zdrachek, E.; Forrest, T.; Bakker, E. Unconditioned Symmetric Solid-Contact Electrodes for Potentiometric Sensing. *Anal. Chem.* **2022**, *94* (33), 11549–11556. https://doi.org/10.1021/acs.analchem.2c01728.
(98) Sokalski, T.; Ceresa, A.; Zwickl, T.; Pretsch, E. Large Improvement of the Lower Detection Limit of Ion-Selective Polymer Membrane Electrodes. *J. Am. Chem. Soc.* **1997**, *119* (46), 11347–11348. https://doi.org/10.1021/ja972932h.
(99) Bühlmann, P.; Yajima, S.; Tohda, K.; Umezawa, K.; Nishizawa, S.; Umezawa, Y. Studies on the Phase Boundaries and the Significance of Ionic Sites of Liquid Membrane Ion-selective Electrodes. *Electroanalysis* **1995**, *7* (9), 811–816. https://doi.org/10.1002/elan.1140070905.
(100) Michalska, A.; Konopka, A.; Maj-Zurawska, M. All-Solid-State Calcium Solvent Polymeric Membrane Electrode for Low-Level Concentration Measurements. *Anal Chem* **2003**, *75* (1), 141–144. https://doi.org/10.1021/ac025916y.
(101) Konopka, A.; Sokalski, T.; Michalska, A.; Lewenstam, A.; Maj-Zurawska, M. Factors Affecting the Potentiometric Response of All-Solid-State Solvent Polymeric Membrane Calcium-Selective Electrode for Low-Level Measurements. *Anal. Chem.* **2004**, *76* (21), 6410–6418. https://doi.org/10.1021/ac0492158.
(102) Sutter, J.; Radu, A.; Peper, S.; Bakker, E.; Pretsch, E. Solid-Contact Polymeric Membrane Electrodes with Detection Limits in the Subnanomolar Range. *Analytica Chimica Acta* **2004**, *523* (1), 53–59. https://doi.org/10.1016/j.aca.2004.07.016.
(103) Radu, A.; Peper, S.; Bakker, E.; Diamond, D. Guidelines for Improving the Lower Detection Limit of Ion-Selective Electrodes: A Systematic Approach. *Electroanalysis* **2007**, *19* (2–3), 144–154. https://doi.org/10.1002/elan.200603741.

(104) Sutter, J.; Lindner, E.; Gyurcsányi, R. E.; Pretsch, E. A Polypyrrole-Based Solid-Contact Pb(2+)-Selective PVC-Membrane Electrode with a Nanomolar Detection Limit. *Anal Bioanal Chem* **2004**, *380* (1), 7–14. https://doi.org/10.1007/s00216-004-2737-4.
(105) Lai, C.-Z.; Joyer, M. M.; Fierke, M. A.; Petkovich, N. D.; Stein, A.; Bühlmann, P. Subnanomolar Detection Limit Application of Ion-Selective Electrodes with Three-Dimensionally Ordered Macroporous (3DOM) Carbon Solid Contacts. *J Solid State Electrochem* **2009**, *13* (1), 123–128. https://doi.org/10.1007/s10008-008-0579-2.
(106) Mendecki, L.; Fayose, T.; Stockmal, K. A.; Wei, J.; Granados-Focil, S.; McGraw, C. M.; Radu, A. Robust and Ultrasensitive Polymer Membrane-Based Carbonate-Selective Electrodes. *Anal. Chem.* **2015**, *87* (15), 7515–7518. https://doi.org/10.1021/acs.analchem.5b01756.
(107) Chaubey, A.; Malhotra, B. D. Mediated Biosensors. *Biosensors and Bioelectronics* **2002**, *17* (6), 441–456. https://doi.org/10.1016/S0956-5663(01)00313-X.
(108) Bedendi, G.; De Moura Torquato, L. D.; Webb, S.; Cadoux, C.; Kulkarni, A.; Sahin, S.; Maroni, P.; Milton, R. D.; Grattieri, M. Enzymatic and Microbial Electrochemistry: Approaches and Methods. *ACS Meas. Au* **2022**, acsmeasuresciau.2c00042. https://doi.org/10.1021/acsmeasuresciau.2c00042.
(109) Leech, D.; Kavanagh, P.; Schuhmann, W. Enzymatic Fuel Cells: Recent Progress. *Electrochimica Acta* **2012**, *84*, 223–234. https://doi.org/10.1016/j.electacta.2012.02.087.
(110) Bollella, P.; Katz, E. Enzyme-Based Biosensors: Tackling Electron Transfer Issues. *Sensors* **2020**, *20* (12), 3517. https://doi.org/10.3390/s20123517.
(111) Wilson, G. S. Native Glucose Oxidase Does Not Undergo Direct Electron Transfer. *Biosensors and Bioelectronics* **2016**, *82*, vii–viii. https://doi.org/10.1016/j.bios.2016.04.083.
(112) Bartlett, P. N.; Al-Lolage, F. A. There Is No Evidence to Support Literature Claims of Direct Electron Transfer (DET) for Native Glucose Oxidase (GOx) at Carbon Nanotubes or Graphene. *Journal of Electroanalytical Chemistry* **2018**, *819*, 26–37. https://doi.org/10.1016/j.jelechem.2017.06.021.
(113) Milton, R. D.; Minteer, S. D. Direct Enzymatic Bioelectrocatalysis: Differentiating between Myth and Reality. *Journal of The Royal Society Interface* **2017**, *14* (131), 20170253. https://doi.org/10.1098/rsif.2017.0253.
(114) Mano, N. Engineering Glucose Oxidase for Bioelectrochemical Applications. *Bioelectrochemistry* **2019**, *128*, 218–240. https://doi.org/10.1016/j.bioelechem.2019.04.015.
(115) Cadoux, C.; Milton, R. D. Recent Enzymatic Electrochemistry for Reductive Reactions. *ChemElectroChem* **2020**, *7* (9), 1974–1986. https://doi.org/10.1002/celc.202000282.
(116) Hanefeld, U.; Gardossi, L.; Magner, E. Understanding Enzyme Immobilisation. *Chem. Soc. Rev.* **2009**, *38* (2), 453–468. https://doi.org/10.1039/B711564B.
(117) Moehlenbrock, M. J.; Minteer, S. D. Introduction to the Field of Enzyme Immobilization and Stabilization. In *Enzyme Stabilization and Immobilization: Methods and Protocols*; Minteer, S. D., Ed.; Methods in Molecular Biology; Humana Press: Totowa, NJ, 2011; pp 1–7. https://doi.org/10.1007/978-1-60761-895-9_1.
(118) Henri, Victor. *Lois Générales de l'action Des Diastases*; Librairie Scientifique A. Hermann, 1903.
(119) Michaelis, L. Die Kinetik Der Invertinwirkung. *Biochem.* **1913**, *49* (352), 333–369.
(120) Cooney, M. J. Kinetic Measurements for Enzyme Immobilization. *Methods Mol Biol* **2017**, *1504*, 215–232. https://doi.org/10.1007/978-1-4939-6499-4_17.
(121) Silverstein, T. P.; Goodney, D. E. Enzyme-Linked Biosensors: Michaelis−Menten Kinetics Need Not Apply. *J. Chem. Educ.* **2010**, *87* (9), 905–907. https://doi.org/10.1021/ed100381r.
(122) Njagi, J.; Warner, J.; Andreescu, S. A Bioanalytical Chemistry Experiment for Undergraduate Students: Biosensors Based on Metal Nanoparticles. *J. Chem. Educ.* **2007**, *84* (7), 1180. https://doi.org/10.1021/ed084p1180.
(123) Elgrishi, N.; Rountree, K. J.; McCarthy, B. D.; Rountree, E. S.; Eisenhart, T. T.; Dempsey, J. L. A Practical Beginner's Guide to Cyclic Voltammetry. *J. Chem. Educ.* **2018**, *95* (2), 197–206. https://doi.org/10.1021/acs.jchemed.7b00361.
(124) Allen J. Bard; Larry R. Faulkner. *Electrochemical Methods: Fundamentals and Applications*, 2nd ed.; 2000.

(125) Prévoteau, A.; Mano, N. Oxygen Reduction on Redox Mediators May Affect Glucose Biosensors Based on "Wired" Enzymes. *Electrochimica Acta* **2012**, *68*, 128–133. https://doi.org/10.1016/j.electacta.2012.02.053.
(126) Prévoteau, A.; Mano, N. How the Reduction of O2 on Enzymes and/or Redox Mediators Affects the Calibration Curve of "Wired" Glucose Oxidase and Glucose Dehydrogenase Biosensors. *Electrochimica Acta* **2013**, *112*, 318–326. https://doi.org/10.1016/j.electacta.2013.08.173.
(127) Bott, A. W.; Avenue, K. Controlled Current Techniques. *Current Separations* **2000**, 3.

Chapter 2. Commercially Available Nitrate Ionophores in Potentiometric Sensors Are Not Superior to Common Ion-Exchangers

(This chapter is based on the following paper: Damala, P.; Zdrachek, E.; Bakker, E. Commercially Available Nitrate Ionophores in Potentiometric Sensors Are Not Superior to Common Ion-Exchangers. *Electroanalysis* 2023, *35* (2), e202200247. https://doi.org/10.1002/elan.202200247)

2.1 Introduction

Anion recognition chemistry dates to the late 1960s but it was only after two decades that a considerable interest in the complex anion-binding phenomena started to develop. The selective detection of anions through the design of suitable receptors is more challenging compared to that of cations. Several reasons lie behind this inconvenient aspect. The larger size of anionic species gives them a smaller charge-to-radius ratio which does not favor strong electrostatic interactions. Many anions are greatly influenced by pH perturbations as they become protonated at low pH to lose their negative charge. In addition, their geometry varies widely, including spherical, linear, trigonal planar and tetrahedral, making the design of receptors with sizes complementary to the anions a complex procedure. Solvation effects may also influence the anion-receptor interactions. As an example, anions may form strong hydrogen bonds with protic solvents with which the receptors have to compete for complexation. The choice of solvent in this case becomes particularly important. Hydrogen bonding is one type of noncovalent interaction between anions and receptors. Others include electrostatic interactions and coordination to metal ions, as well as combinations between them. Additional critical factors for the selectivity are the hydrophobicity of the anion, the receptor's binding sites and the environment where complexation occurs.[1]

Several strategies and recommendations are nowadays available for tailoring the anion-host interactions while designing new receptors. A general approach for designing molecules to coordinate with anions is favoring the hydrogen bonding by adding hydrogen bond donor groups to the backbone of the molecule. Interestingly, electrostatic potential surface studies have shown that nitrate possesses six positions for placing positive charges around the anion. Hence, the ideal nitrate host would provide six sites for hydrogen bonding. However, in practice only half of the sites are usually occupied, likely due to steric crowding. [2] In this context matching the size and shape of the guest ion is an important consideration. In the case of (thio)urea-based receptors (one of the simplest and most widely used neutral receptors for anions) this can be achieved by finding a suitable linker that can organize the urea units in the form of a cavity whose size and shape is complementary to the targeted anion. [3] (Thio)ureas have been suggested as suitable candidates for nitrate recognition, however, the association constant reported for nitrate was relatively small (K_{11} = 17.1 ± 0.4 M^{-1}) and overall the lowest among acetate, cyanide, bromide and hydrogensulfate. [4] Also, the authors stated that small structural variations of the ionophore

can result in complete loss of binding affinity with nitrate. Indeed, an earlier study showed that bis-thioureas selectively bind dihydrogenphosphate over acetate, chloride, sulfate and nitrate. [5] The enhanced selectivity was attributed to the complex geometry and basicity of the guest anions. Interestingly, the association constant for nitrate was remarkably smaller ($K_{11} < 1\ M^{-1}$) than the one reported in the previous work while in both studies the binding was examined by NMR titration. The fact that the binding affinity of an ion-receptor complex can be completely lost even by minor structural changes underlines how delicate the design process is. [3,4] Another strategy for enhancing complexation is to use the metal-ligand coordination chemistry for initiating conformational changes in the ligand so that its hydrogen-bond donor sites favor the anion binding. Alternatively, metal ions can be used to coordinate ligands and bring together their functional groups that can form hydrogen bonds with the target anion.[6]

The majority of the studies reporting on binding affinities of different synthetic receptors for nitrate originate in the field of supramolecular chemistry. In those studies the complexation between the in-house synthetized receptors and nitrate is usually examined in organic solvents such as dimethyl sulfoxide, dichloromethane, acetonitrile and chloroform. The choice of solvent is crucial and can significantly influence the binding interactions. As an example, in the case of a metal-based anion receptor changing the polarity of the solvent led to a shift in the orientation of its –CH and –NH groups and to a subsequent competition between the solvent and anion binding. [6] Receptors examined for nitrate recognition include tripodal thiophene- and urea-based structures, guanidinium- and acyclic amide-based receptors, as well as bicyclic cyclophanes. [7–11] The investigated receptors typically contain a variety of hydrogen bond donor groups. The advantage of hydrogen bonds is that they are directional which, in principle, enables the design of structures including cavities that are complementary to the size and shape of the target ion. [2] The most common techniques for quantifying their binding interactions and stoichiometry of the complexes include ^{1}H NMR titration, isothermal titration calorimetry and X-Ray analysis.

In this study we aim to assess the selectivity and complexation of nitrate ionophores and ion-exchangers in potentiometric ion-selective electrodes (ISEs). Such ISEs typically use a plasticized polymeric (typically PVC-based) membrane to encapsulate the ionophore or ion-exchanger that is responsible for the selective binding with nitrate. Hence, despite the abundance of studies reporting quantitative data on binding affinities and stoichiometries of several synthetized receptors with nitrate, the practical use of these data is often limited given the different nature of solvents used during the complexation studies. Indeed, complexation studies in solvents of high polarity (methanol, ethanol) have reported lower complex formation constants than those obtained in a typical membrane composition and the differences are attributed to the weak solvation properties of the typically apolar membranes of ISEs. [12] Besides, the methods to examine the complexation and selectivity of ionophores in the fields of organic and analytical chemistry are inherently different. In potentiometry, the selectivity of ISEs was initially described by

the Nicolsky equation. [13] Later on, this equation was proved inadequate for ions of different charges and subsequently a new formalism was described for the electrode response in the presence of analytes and interfering ions with different charges. [14] The selectivity coefficients are valid only if Nernstian slopes are observed for both primary and interfering ions. This prerequisite was not always met and efforts to eliminate the factors resulting in the non-Nernstian behavior were made. A procedure was then suggested by conditioning the membrane to the most discriminated ion before any contact with the preferred ion. [15] This adapted protocol allowed the determination of improved and unbiased selectivity coefficients.

Most of the studies on potentiometric nitrate selective electrodes examined in this paper use either the separate solution method (SSM) or the fixed interference method (FIM) for the determination of selectivity coefficients. In the first case, the potential of the ISE is recorded in separate solutions for each of the ions tested while in the second case, one solution contains both the primary and interfering ion and the selectivity coefficient is obtained by using separate sections of the calibration curve. [16] In the present study we used the modified separate solution method (mSSM), an extension of the classic SSM where entire calibration curves need to be recorded for each ion tested and use the potentials that fall in the Nernstian section of the curves. In order to avoid frequent biases made with this method, we applied the recommendations provided in the literature [17] and thus calculated the selectivity coefficients by using the highest concentration of interfering ions and avoiding the contact of membranes with the primary ion before measuring all the interfering ions.

For the determination of the complex formation constant, a potentiometric technique referred as the segmented sandwich membrane method is typically employed. The method, originally proposed by Russian researchers, [18,19] requires the use of a two-layer membrane from which only one contains the ionophore. By recording the initial membrane potential of this sandwich membrane one may obtain information on the ion activity ratio in both aqueous-membrane phases and calculate the resulting complex formation constant. [20] Many studies using the sandwich method are available in the literature examining both cation- [21–26] and anion-selective [27–31] ionophores. Nevertheless, none of them addresses nitrate-selective receptors. With the classic segmented sandwich membrane method, two distinct cases are examined: one that considers strong ion-pairing in the membrane and one that neglects it. Experiments with plasticized PVC membranes have shown that ions are completely associated in the membrane. However, the ion-pairs formed are rather non-specific and their effect on the ion-extraction equilibria can be neglected considering that the respective ion-pair formation constants will have similar values. [20] In that case, the complex formation constants calculated are expected to be close to the true values. This assumption was made in many of the above mentioned studies where ion-pairing is neglected. [21,24,25,27,28,31] The sandwich method distinguishes the cases where ion-pairing is strong or weak but it does not allow for the estimation of ion-pair formation constants. Modified versions of the method were consequently suggested to address this issue enabling the successful quantification of ion-pairing formation constants in membranes of variant compositions. [32,33]

Despite the considerable importance of nitrate measurements, especially in the environmental context, the existing research on nitrate ionophores (which has been ongoing since the 90s) has not found a wider application. Up until the end of the 1990s, the field of potentiometric nitrate sensing was dominated by the use of ion-exchangers, mainly nickel(II)-based ones. [34] This trend has not changed much until today with the main difference being the use of different ion-exchangers which are usually tetralkylammonium-based salts. [35,36] Ion-exchangers are used as the main components for ion-recognition when selective ionophores are lacking. The resulting selectivity order is named the Hofmeister sequence based on the studies of Franz Hofmeister who originally studied the effect of salts on the coagulation of proteins. [37] Despite the plethora of studies examining nitrate-selective electrodes using tetralkylammonium-based ion-exchangers [38–46], there are a few exceptions. These include studies using ionophores that have been identified as nitrate-selective and are commercially available (**Figure 2.1**) [47–50] as well as a few others that have been synthesized in-house [51–53] and whose selectivity has been examined with the same methods used in this study.

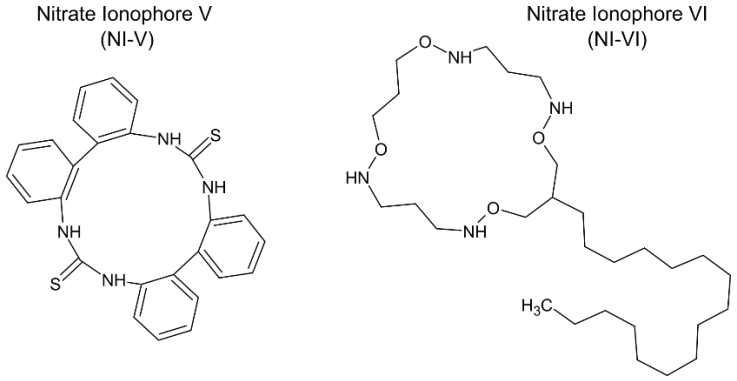

Figure 2.1: Commercially available nitrate ionophores V and VI

Here we aim to compare the performance of those nitrate ionophores and ion-exchangers in terms of their selectivity and complexation to nitrate. The interest for realizing this study was initially triggered by the roughly tenfold price difference between the commercially available nitrate ionophores (namely nitrate ionophores V and VI) and the commonly used ion-exchangers, and our desire to prioritize responsible spending of available resources. In addition, we aim to provide an overview of the potentiometric nitrate sensors developed during the last two decades focusing on the available selectivity and complexation data and highlight the improvements that can be made when reporting such information.

2.2 Experimental

2.2.1 Reagents

Tridodecymethylammonium chloride (TDMAC) ≥ 97.0% was purchased from Fluka, 9,11,20,22-tetrahydrotetrabenzo[1,3,8,10]tetraazacyclotetradecine-10,21-dithione (Nitrate Ionophore V, or else NI-V) ≥ 98.0% was purchased from Santa Cruz Biotechnology Inc., 9-hexadecyl-1,7,11,17-tetraoxa-

2,6,12,16-tetraazacycloeicosane (Nitrate Ionophore VI, or else NI-VI), tridodecymethylammonium nitrate (TDMAN) ≥ 99.0%, tetradodecylammonium tetrakis(4-chlorophenyl)borate (ETH500), 2-nitrophenyl octyl ether ≥ 99.0% (NPOE), bis(2-ethylhexyl)phthalate (DEHP), dibutyl phthalate (DBP), high molecular weight poly(vinyl chloride) (PVC) and tetrahydrofuran ≥ 99.5% (THF) were of Selectophore grade and purchased from Sigma Aldrich, tetradodecylammonium chloride (TDDAC) ≥ 97.0%, sodium nitrate (≥99 %), sodium chloride (≥ 99.5%), sodium nitrite (≥97 %), sodium bromide (≥99 %), sodium iodide (≥99 %), sodium thiocyanate (≥98 %), and sodium perchlorate (≥98 %) were purchased from Sigma Aldrich. Aqueous solutions were prepared by dissolving the respective salts in Milli-Q water (18.2 MΩ cm).

2.2.2 Preparation of Ion-Selective Electrodes

For the selectivity study, six different nitrate-selective membranes were tested which are referred with the numerals (I) to (IV) and have the following compositions: (I) 4.1 mmol·kg^{-1} TDDAC, PVC:DBP (1:1), (II) 100.6 mmol·kg^{-1} NI-VI, 4.1 mmol·kg^{-1} (4.1 % mol) TDDAC, PVC:DBP (1:1) (composition similar to manufacturer's recommendation), (III) 22 mmol·kg^{-1} NI-VI, 11 mmol·kg^{-1} (50 % mol) TDMAC, PVC:DEHP (1:2), (IV) 11 mmol·kg^{-1} TDMAC, PVC:NPOE (1:2), (V) 22 mmol·kg^{-1} NI-V, 11 mmol·kg^{-1} (50 % mol) TDMAC, PVC:NPOE (1:2) (composition used in [50]) and (VI) 11 mmol·kg^{-1} TDMAC, 15 mmol·kg^{-1} ETH500, PVC:DEHP (1:2). The PVC:plasticizer ratios refer to membrane masses. For each composition 200 mg membrane solution was prepared and dissolved in 2 mL THF. The membrane solution was poured to a 22 mm glass ring attached on a glass plate and left to dry overnight in ambient air. Then, three circular pieces of 8 mm were cut from the dried membrane and mounted in three OSTEC electrode bodies manually. The same procedure was followed for all membrane compositions and the resulting electrodes were filled with their respective inner filling solutions and conditioned before use. For the complexation study, four of the above mentioned membranes were prepared afresh, namely membranes (I) and (II) (without and with nitrate ionophore VI), and membranes (IV) and (V) (without and with nitrate ionophore V). In addition, two new membrane compositions were prepared to determine whether the ion-exchangers TDMAC and TDDAC can be used interchangeably in the ion-selective membrane solutions. These had the following compositions: 10 mmol·kg^{-1} TDDAC, PVC:DEHP (1:2) and 10 mmol·kg^{-1} TDMAC, PVC:DEHP (1:2). More details on the concentrations of the solutions used for the selectivity and complexation studies are given in the respective sections below.

2.2.3 Electrochemical equipment and corrections in potential

A high impedance input 16-channel EMF monitor (Lawson Laboratories, Malvern, PA) was used for the potentiometric measurements. The potential values were corrected for the liquid junction potentials arising from the double junction reference electrode (Ag/AgCl/ 3 M KCl/1 M LiOAc, Metrohm,

Switzerland) used in the selectivity study based on the Henderson equation (detailed numbers provided in the Supporting Information).

2.2.4 Selectivity coefficients and data processing

The selectivity study was performed with the modified separate solution method (mSSM) as follows: a 1 mM NaCl solution was used both as the inner filling and conditioning solution of the electrodes which were conditioned for 4 h prior to the study. Then, the electrodes were immersed sequentially in separate solutions of nitrate and interfering anions with the order of the Hofmeister series and their potentials were recorded for the concentrations tested (starting from 10^{-4} M up to 10^{-1} M). The selectivity coefficients were calculated using the following general equation adapted for nitrate:

$$\log K^{pot}_{NO_3^-,j} = \frac{\left(E_{NO_3^-} - E_j\right)}{s} + \log \frac{a_{NO_3^-}}{a_j}$$

where $E_{NO_3^-}$ and E_j are the corrected potential values corresponding to 0.1 M solution of nitrate or interfering anion respectively, $a_{NO_3^-}$ and a_j are the activities of nitrate and interfering anions respectively corresponding to 0.1 M ion solutions (detailed numbers provided in the Supporting Information), and s is the average slope calculated for each membrane composition from the individual Nernstian slopes of the tested ions using the two highest activities tested (logα equal to -1.4 and -1.1.). The ions with slopes that were far from Nernstian even at these high activities (having values above -55 mV/dec or below -64 mV/dec) were excluded from the averaging process and a relevant mention is made in the respective tables below. As a result, the values of the average slopes corresponding to the membranes (I) – (VI) were ranging between 56 mV·kg^{-1} and 60 mV·dec^{-1} (see **Table 2.1** & **Table 2.2**). For each membrane composition the average slope was subsequently used to perform a linear fit of the experimental data (after being corrected for the junction potentials) which resulted in a new set of fitted equations, all having the same slope (see red lines in **Figure 2.3** and **Figure 2.5**).

2.2.5 Complex formation constants

The complex formation constants of the commercially available nitrate ionophores V and VI were examined using the segmented sandwich membrane method. [20] In the case of nitrate ionophore V, the freshly prepared membranes (IV) and (V) were conditioned overnight in a solution of 10 mM $NaNO_3$ and 0.1 mM NaCl. The same composition was used for the inner filling solution and measuring solution. The membranes were firstly conditioned overnight. After conditioning, they were mounted in OSTEC bodies and immersed in the measuring solution to record the potentials corresponding to the single membranes under unstirred conditions. Subsequently, the electrodes were taken out of solution and were disassembled to re-obtain the single membranes which were gently dried and swiftly pressed together to obtain a fused two-layer membrane (one layer with the examined ionophore and one without). The

two-layer membrane, or else sandwich membrane, was then mounted back to the electrode making sure that the layer containing the ionophore was the one to face the measuring solution and not the inner filling solution. The re-assembled electrodes were again immersed in the measuring solution and potentials were recorded for approximately 2 h. The same procedure was followed for nitrate ionophore VI with the membranes (I) and (II). A similar experiment was performed with membranes containing the TDDAC and TDMAC ion-exchangers (see section with preparation of ISEs for their detailed composition) to examine the potential differences observed in the single and sandwich membranes and to determine whether they can be used interchangeably. The complex formation constant β_{IL} was calculated combining the membrane potential that corresponds to the two-layer membrane and the charge balances at the individual segments. Detailed calculations are provided in the Supporting Information.

2.3 Results and discussion

The selectivity of nitrate ionophore VI (NI-VI) was evaluated based on the membrane composition recommended by the manufacturer [54] which in this study is denoted as membrane (II). This composition has an uncommonly low proportion of ion-exchanger with respect to the ionophore which is typically maintained at a molar percentage around 50 % as opposed to the 4 % recommended. For comparison purposes, a membrane with the same composition but without ionophore (denoted as membrane (I)) and one with the same ionophore in different concentration and with different plasticizer (denoted as membrane (III)) were also prepared and tested. As shown in **Figure 2.*2*** and **Table 2.1** the selectivity coefficients among the three membrane compositions do not show significant differences. More importantly, the composition which lacks the ionophore presents the best results in terms of selectivity towards chloride which is the most common interfering ion in most applications.

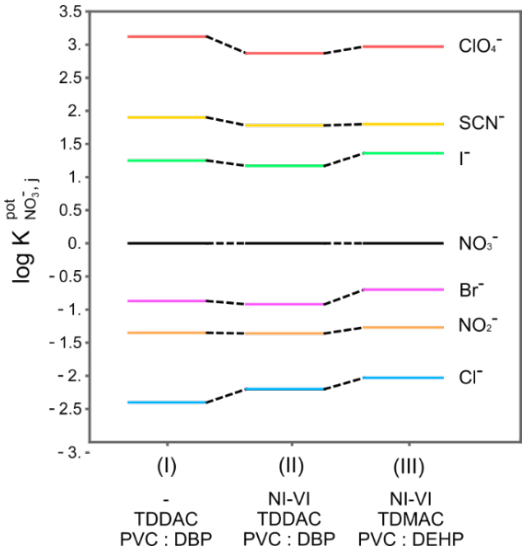

Figure 2.2: Selectivity coefficients ($\log K^{pot}_{NO_3^-,j}$) for plasticized PVC membranes with compositions (I) 4.1 mmol·kg^{-1} TDDAC, PVC:DBP (1:1), (II) 100.6 mmol·kg^{-1} NI-VI, 4.1 mmol·kg^{-1} (4.1 % mol)

TDDAC, PVC:DBP (1:1) (same to manufacturer's recommendation) and (III) 22 mmol·kg^{-1} NI-VI, 11 mmol·kg^{-1} (50 % mol) TDMAC, PVC:DEHP (1:2).

Table 2.1: Selectivity coefficients for nitrate-selective membranes with and without NI-VI.

	$\log K_{NO_3^-,j}^{pot}$ [a]		
Ion j	(I) (slope -57.8 ± 1.6 mV·dec^{-1}) [b]	(II) (slope = -56.2 ± 0.7 mV·dec^{-1}) [b]	(III) (slope = -60.7 ± 1.2 mV·dec^{-1}) [b]
Cl^-	-2.40 ± 0.10	-2.20 ± 0.15 [c]	-2.03 ± 0.00
NO_2^-	-1.35 ± 0.04	-1.36 ± 0.10	-1.27 ± 0.01
Br^-	-0.87 ± 0.04	-0.92 ± 0.09	-0.70 ± 0.00
NO_3^-	0.00	0.00 [c]	0.00
I^-	1.25 ± 0.05	1.17 ± 0.01	1.36 ± 0.01 [c]
SCN^-	1.90 ± 0.03	1.78 ± 0.02	1.80 ± 0.01
ClO_4^-	3.12 ± 0.03	2.87 ± 0.02 [c]	2.97 ± 0.01

[a] Average and standard deviations from three electrodes, [b] Slope: average value of the individual Nernstian slopes of the examined ions between logα -1.4 and -1, [c] The slopes for these ions were far from Nernstian and thus excluded from the calculation of the average slope (see section of "Selectivity coefficients and data processing" for more information)

For membrane (II), chloride did not show a Nernstian behavior even at high concentrations (s = -42.4 mV·dec^{-1}) hence the reported selectivity coefficient should be regarded as an approximation of the actual value. With the exception of three other similar cases (**Figure 2.3**) all ions showed a potentiometric response that correlated well with the calculated average slope of each composition, as shown from their individual curves in **Figure 2.3**. Moreover, the calculated selectivity coefficients are close to the reported values provided by the manufacturer (logarithmic selectivity coefficients equal to -2.5, -1.2 and -1.1 for chloride, nitrite and bromide respectively) confirming the validity of the reported data [54] for which no reference is available.

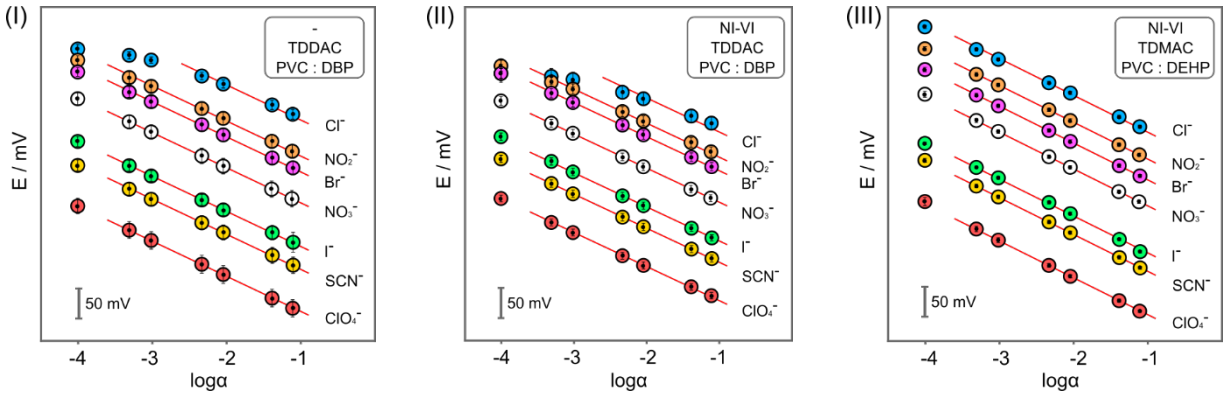

Figure 2.3: EMF responses of plasticized PVC membranes with compositions (I), (II) and (III) with the modified separate solutions method.

Only one study was found in the literature reporting on NI-VI. [47] The separate solutions method was used for the calculation of selectivity coefficients which were shown significantly improved compared to the ones obtained here. More specifically, the logarithmic selectivity coefficients for chloride, nitrite, bromide and perchlorate were calculated as -3.6, -1.9, -2.9 and 2.8. The membrane composition used was 39 mmol·kg^{-1} NI-VI, 50 % mol TDMAC and PCV:NPOE at a ratio 1:2, which is similar to the composition of membrane (III) examined here with the exception of the plasticizer used. The goal of that study was to examine the performance of solid-contact electrodes using thiol-functionalized reduced graphene oxide as transducer but it is unclear whether these electrodes or the traditional liquid-based electrodes were used for the selectivity study. Nevertheless, even in the first case, the use of a solid-contact electrode for the selectivity study should not significantly influence the results. This was demonstrated in two separate studies [43,45] where selectivity results based on solid-contact electrodes were compared with the ones from liquid-based electrodes confirming the absence of influence of the transducer on selectivity. Hence, the differences in selectivity are expected to be based on the membrane composition rather than the transducer.

To further investigate the binding properties of NI-VI, the sandwich membrane method was employed for the determination of its complex formation constant. This is a potentiometric method used to examine the complexation of ionophores in solvent polymeric membranes [20] the details of which are presented in the Experimental section. Unfortunately, the results obtained did not allow for the calculation of the constant due to the increased potential observed after immersing the sandwich membrane in the measuring solution (**Figure 2.6**, curve (i)). In general, when the sandwich membrane is immersed in the solution of the measuring ion i, the activity of i at the membrane-sample interface is expected to be lower than the one at the membrane-inner solution due to the ion-ionophore complexation. Based on the well-known membrane potential, in the case of anions this should result in a measured sandwich membrane potential lower than the measured potential of the single membrane segments. For nitrate ionophore VI the sandwich membrane potential was somewhat higher than the potentials of the individual segments which made the calculation of the complex formation constant meaningless.

The selectivity of nitrate ionophore V (NI-V) was evaluated based on a membrane composition found in the literature showing significant selectivity over chloride ($\log K^{pot}_{NO_3^-,Cl^-} = -3.5$) reported in a study which is used here as a reference. [50] This composition is represented by membrane (V). Similarly, two other compositions were tested for comparison purposes, one with the same composition but without ionophore (denoted as membrane (IV)) and one with the composition we typically use in our group for nitrate sensing [55–58] (denoted as membrane (VI)) with the exception that TDMAC was used instead of TDMAN to avoid the presence of nitrate in the membrane. As shown in **Table 2.2** the selectivity coefficient obtained here ($\log K^{pot}_{NO_3^-,Cl^-} = -2.4$) is worse than the one reported in the abovementioned reference study. In our case the slope for chloride response was equal to -53.0 mV·dec^{-1}, which is close to Nernstian. In contrast, the slope for chloride presented in [50] was -47.8 mV·dec^{-1} which, despite the uncertainty on whether this slope was used for the calculation selectivity coefficient, raises concerns on the validity of the reported values. Also, the authors reported data for a membrane composition without ionophore which are close to our reported values (membrane (IV) in **Table 2.2**). One aspect that should be taken into consideration and could explain the observed differences is that the nitrate ionophore in the above study was synthetized in-house in contrast to our case where the ionophore was purchased by a manufacturer.

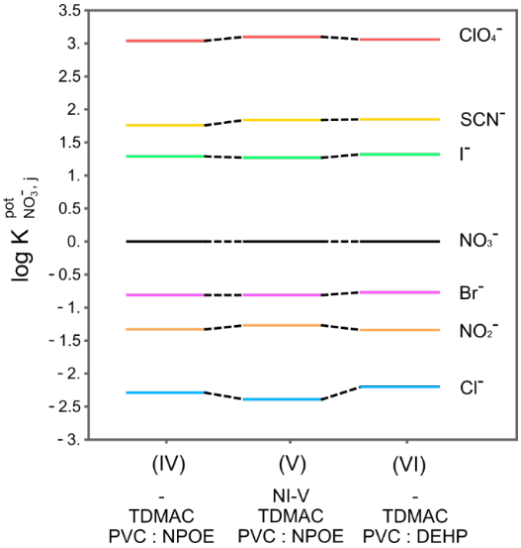

Figure 2.4: Selectivity coefficients ($\log K^{pot}_{NO_3^-,j}$) for plasticized PVC membranes with compositions (IV) 11 mmol·kg^{-1} TDMAC, PVC:NPOE (1:2), (V) 22 mmol·kg^{-1} NI-V, 11 mmol·kg^{-1} (50 % mol) TDMAC, PVC:NPOE (1:2) (same to reference [50]) and (VI) 11 mmol·kg^{-1} TDMAC, 15 mmol·kg^{-1} ETH500, PVC:DEHP (1:2).

Table 2.2: Selectivity coefficients for nitrate-selective membranes with and without NI-V.

	$\log K^{pot}_{NO_3^-,j}$ [(a)]		
Ion j	(IV) (slope = -59.2 ± 1.0 mV·dec^{-1}) [(b)]	(V) (slope = -58.2 ± 1.6 mV·dec^{-1}) [(b)]	(VI) (slope = -59.9 ± 0.7 mV·dec^{-1}) [(b)]
Cl^-	-2.29 ± 0.02	-2.39 ± 0.01 [(c)]	-2.20 ± 0.01
NO_2^-	-1.33 ± 0.03	-1.27 ± 0.00 [(c)]	-1.34 ± 0.01
Br^-	-0.81 ± 0.01	-0.81 ± 0.00	-0.77 ± 0.00
NO_3^-	0.00	0.00	0.00
I^-	1.29 ± 0.01	1.27 ± 0.01	1.32 ± 0.00 [(c)]
SCN^-	1.76 ± 0.02	1.84 ± 0.01	1.85 ± 0.00
ClO_4^-	3.04 ± 0.03	3.10 ± 0.02	3.06 ± 0.00

[(a)] Average and standard deviations from three electrodes, [(b)] Slope: average value of the individual Nernstian slopes of the examined ions between logα -1.4 and -1, [(c)] The slopes for these ions were far from Nernstian and thus excluded from the calculation of the average slope (see section of "Selectivity coefficients and data processing" for more information)

Two more studies (both from the same research group) were found in the literature that reported on the ionophore NI-V. [48,49] As in our case, the ionophore was purchased and according to the cited reference [17] the modified separate solutions method was used for the determination of selectivity coefficients. Also, the same membrane compositions were used in both studies, including 24 mmol·kg^{-1} NI-V, 50 % mol TDMAC (with respect to ionophore) and PCV: o-NPOE at a ratio 1:2. This composition is very similar to the one of the abovementioned reference studies and the comparison of the all the reported results should be straightforward. In their more recent study [49] the selectivity coefficients for chloride and nitrite are somewhat better than the ones reported in **Table 2.2** with approximate average values of $\log K^{pot}_{NO_3^-,Cl^-} = -2.9$ and $\log K^{pot}_{NO_3^-,NO_2^-} = -1.6$, respectively. These are approximate values estimated from the bar graph provided by the authors. The selectivity coefficients reported in their older study [48] for chloride and nitrite are even more improved with their logarithmic values ranging between -3.3 to -3.5 and -3.0 to -3.4 respectively. The authors attribute the improved selectivity to the addition of an intermediate tetrathiafulvalene (TTF) layer which is oxidized in the presence of nitrate during the preparation of the electrodes. It is also stated that the selectivity is improved when increasing the number

of cycles performed during TTF oxidation. However, this protocol raises some concerns since the described procedure introduces nitrate in the layer which risks leaching to the sensing membrane and become potential determining, thereby introducing a bias in the measurements. According to the modified separate solutions method [17] the membrane should not come in contact with the primary ion before all of the interfering ions are examined. This condition is violated in case nitrate is present in the membrane beforehand, as it happens in the study above, where TTF is oxidized in a concentrated solution of nitrate that consequently introduces the primary ion in the transducing layer. In such circumstances, the knowledge of the slopes obtained for all ions during the selectivity study would be valuable.

Overall, the three membrane compositions examined in this study exhibit similar values of selectivity coefficients for all ions tested. This indicates that NI-V does not offer significant advantages. As mentioned earlier, most studies on nitrate sensors found in the literature use the tetralkylammonium-based ion-exchangers as the nitrate sensing component and rely on the selectivity governed by the Hofmeister sequence of ions. Narrowing the selection to the studies using the separate solution method, the following logarithmic values of selectivity against chloride ($\log K^{pot}_{NO_3^-,Cl^-}$) were reported: -2.0 [39], -2.5 [40], -2.2 [41], -2.5 [42], -1.7 (reported as minimum value) [43], -2.2 [44] and -1.9 [45]. Again, these values are similar to the ones obtained here for membranes (IV) and (VI) where TDMAC is used as ion-exchanger for nitrate recognition.

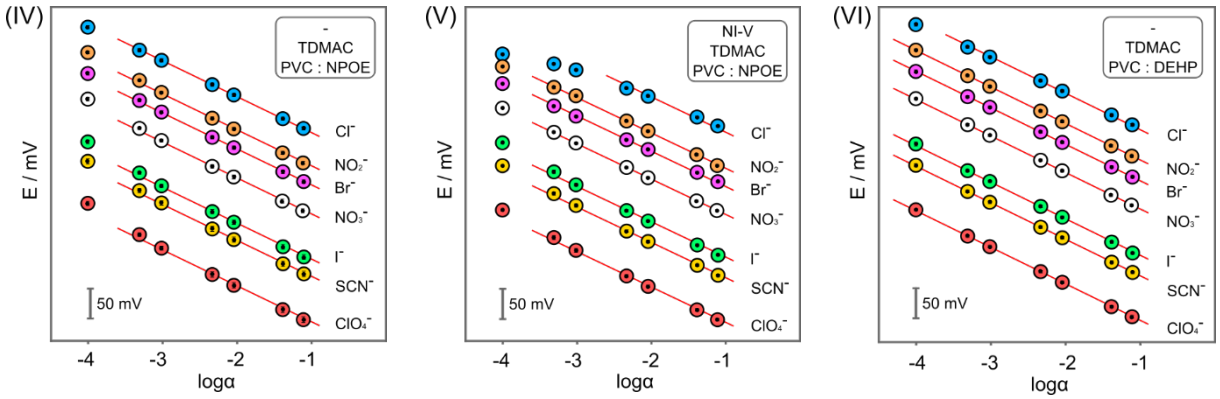

Figure 2.5: EMF responses of plasticized PVC membranes with compositions (IV), (V) and (VI) during the modified separate solutions method.

Apart from the studies using either tetralkylammonium-based ion-exchangers or the nitrate ionophores V and VI examined here, there are three other cases where nitrate ionophores synthetized in-house were examined for their selectivity using potentiometric techniques. [51–53] Interestingly, two of them reported excellent selectivity over any anion tested, including the lipophilic perchlorate and thiocyanate ions. These were not included in the comparisons made above since they used either the fixed interference method (FIM) or the matched potential method (MPM) for the calculation of the selectivity coefficients and a direct comparison with the results obtained from the SSM cannot be made.

Next, the sandwich membrane method was employed for the determination of the complex formation constant of nitrate ionophore V. The membranes used in the sandwich technique are schematically presented in **Figure 2.6** where (A) shows one of the two single homogenous membranes and (B) shows the two membranes fused together to obtain the two-layer confirmation that is subsequently used to measure the membrane potential. The data suggest that a mere 31% of the nitrate ions in the membrane are complexed by the ionophore (see Supporting Information for details), giving a very small complex formation constant of just $\log \beta_{NO_3^- L} = 1.36 \pm 0.14$.

The weak complexation is also evident in the graph of **Figure 2.6** (curve (ii)) where the sandwich membrane potential is shown to be almost equal to the single membrane, in contrast to what is expected when the interaction between an ionophore and ion is strong. In the latter case, the potential difference is expected to be large owing to the large ratio in concentrations of the uncomplexed primary ion between the two segments. In that case, the concentration of uncomplexed ions in the layer with the ionophore is expected to be significantly lower than the one in the layer without due to their complexation with the ionophore. An example of a strong interaction is given by the valinomycin-potassium complex. To make a direct comparison with the results obtained here, the membrane potential difference for this complex has been calculated to approximately 400 mV giving a value for the complex formation constant of $\log \beta_{K^+ L} = 10.0$. [20] Hence, as demonstrated, the complexation of nitrate ionophore V with nitrate is not superior to the one offered by the common ion-exchangers. Unfortunately, none of the studies mentioned above have investigated the formation constant of ionophores using the sandwich technique.

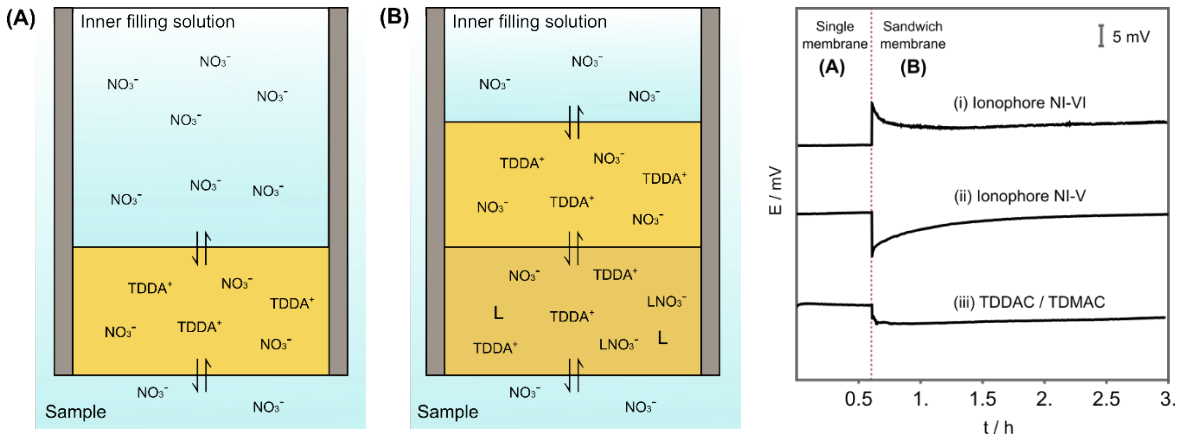

Figure 2.6: Schematic generic representation of single membrane segment without ionophore (A) and combined sandwich membrane with both segments (without and with ionophore L) (B), and graph of recorded potentials for the single and sandwich membranes from experiments performed with (i) ionophore NI-VI (with composition similar to membrane (II)), (ii) ionophore NI-V (with composition similar to membrane (V)) and (iii) TDDAC / TDMAC (see section of "Preparation of ISEs" for information on the membrane composition).

Membranes (I) to (VI) included either TDDAC or TDMAC as ion-exchangers. To examine whether there were any differences in the electrostatic interaction between these two ion-exchangers and nitrate which could result in potential differences, a similar sandwich membrane technique was employed. Here, the single membrane contained either TDDAC or TDMAC alone and the sandwich membrane contained both membrane segments, the one with TDDAC pressed together with the one with TDMAC. As shown in **Figure 2.6** (curve (iii)), the potential difference between the single and sandwich membrane segments was very small (6.3 ± 2.7 mV) which confirmed that both ion-exchangers can be used interchangeably without contributing to significant potential differences.

2.4 Conclusions

After a detailed examination of the studies reporting selectivity data on nitrate ionophores and ion-exchangers, there are some observations worth to be discussed. The majority of the studies limit the information provided to the type of the method used and the values of the calculated coefficients. For the studies using SSM, there is often missing information on the conditioning protocol (duration, type of solution, etc.) and the type of electrodes used for the study (solid- or liquid-contact ones). More importantly, it is essential to report the experimental electrode slopes based on which the selectivity coefficients are calculated and to mention the activity range to which they correspond. When the slopes are not Nernstian, it should be clearly stated. With the exception of one study [43] this practice has not been followed for most of the investigated ISEs. Also, it should be mentioned whether the theoretical slope is used for the calculations and even in these cases, the experimental slopes should be provided. In order to provide selectivity coefficients which are not biased, emphasis should be given on ensuring that the response for all investigated ions is Nernstian, or else, potential determining. [17] One recommendation is to avoid exposing the membrane to the primary ion before bringing it in contact with the most discriminated ions. This prerequisite was not met in the cases where TDMAN was used as ion-exchanger. Additionally, a more frequent use of the sandwich membrane method for the determination of complex formation constants is recommended. As a simple potentiometric technique, it does not require specialized equipment and can be used as a valuable tool for the determination of binding properties in solvent polymeric membranes.

Overall, the selectivity of commercially available nitrate ionophores is not superior to the one provided by the common tetralkylammonium-based ion-exchangers, a finding that can hardly justify their tenfold price. The selectivity coefficients over chloride determined in this study are $\log K^{pot}_{NO_3^-,Cl^-}$ = -2.4 and -2.2 for nitrate ionophore V and VI respectively, with the equivalent values found in the literature equal to $\log K^{pot}_{NO_3^-,Cl^-}$ = -3.5 and -2.5. It is unclear where the differences in the reported coefficients come from. Another study reports an equally low selectivity coefficient over chloride for nitrate ionophore VI with a value of $\log K^{pot}_{NO_3^-,Cl^-}$ = -3.6 which is more than an order of magnitude lower than the one obtained

in this study. For both nitrate ionophores examined here, the selectivity data for all investigated ions are similar to the ones obtained using just ion-exchangers. Finally, a complex formation constant of $\log \beta_{NO_3^- L}$ = 1.36 ± 0.14 is found for nitrate ionophore V underlying a weak complexation with nitrate that is also in agreement with the results from the selectivity study.

2.5 Supporting Information

2.5.1 Calculation of the complex formation constant

The membrane potential of a two-layer sandwich membrane in contact with two aqueous solutions of equal concentrations is described as follows (for a monovalent anion):

$$E_M = \frac{RT}{-F} ln \frac{a''_{I\,(org)}}{a'_{I\,(org)}} \quad (1)$$

where $a'_{I\,(org)}$ is the ion activity at the sample-membrane interface, $a''_{I\,(org)}$ is the ion activity at the membrane-inner electrolyte interface and R, T and F are the gas constant, the absolute temperature and the Faraday constant.

We assume that ion pairing in the membrane is negligible, which means that all ions are either in their dissociated form or complexed to the ionophore.

Layer without ionophore

The ion activity in the layer without the ionophore (which faces the inner electrolyte) is given by the charge balance in that layer:

$$c''_I = R_T \rightarrow a''_I = \gamma_I R_T \quad (2)$$

where R_T is the concentration of the ion-exchanger and γ_I the activity coefficient for ion I. We omit the notation (org) shown in (1) since we will only refer to the organic phase (membrane) from now on.

Layer with ionophore

The ion activity in the layer with the ionophore (which faces the sample) is given by the charge balance in that layer:

$$R_T = c'_I + c_{IL} \rightarrow c_{IL} = R_T - c'_I \quad (3)$$

where c'_I and c_{IL} are the concentrations of nitrate and complexed ionophore respectively. The concentration of the free ionophore is described as follows:

$$c_L = L_T - c_{IL} \quad (4)$$

where L_T is the total concentration of the ionophore in this layer. The ionophore may form complexes with the targeted ion with the stability constant β_{IL} which is described as follows, assuming a 1:1 stoichiometry and an activity coefficient for the neutral ionophore equal to one:

$$\beta_{IL} = \frac{a_{IL}}{a_I' c_L} \rightarrow a_I' = \frac{\gamma_{IL} c_{IL}}{\beta_{IL} c_L} \quad (5)$$

From (3) and (4) we get:

$$c_L = L_T - R_T + c_I' \quad (6)$$

From (3), (5) and (6) we get:

$$a_I' = \frac{\gamma_{IL}(R_T - c_I')}{\beta_{IL}(L_T - R_T + c_I')} \rightarrow a_I' = \frac{\gamma_{IL}\left(R_T - \frac{a_I'}{\gamma_I}\right)}{\beta_{IL}\left(L_T - R_T + \frac{a_I'}{\gamma_I}\right)} \rightarrow$$

$$(a_I')^2 \beta_{IL} + a_I'(\gamma_I \beta_{IL} L_T - \gamma_I \beta_{IL} R_T + \gamma_{IL}) - \gamma_I \gamma_{IL} R_T = 0 \rightarrow$$

$$a_I' = \frac{(-\beta_{IL}\gamma_I(L_T - R_T) - \gamma_{IL}) \pm \sqrt{(\beta_{IL}\gamma_I(L_T - R_T) + \gamma_{IL})^2 + 4\beta_{IL}\gamma_I\gamma_{IL}R_T}}{2\beta_{IL}} \quad (7)$$

Combining (1), (2) and (7) we get:

$$-\beta_{IL}\gamma_I(L_T - R_T) - \gamma_{IL} \pm \sqrt{(\beta_{IL}\gamma_I(L_T - R_T) + \gamma_{IL})^2 + 4\beta_{IL}\gamma_I\gamma_{IL}R_T} = 2\beta_{IL}\gamma_I R_T e^{\frac{E_M F}{RT}}$$

If both layers have the same ionic strength we can assume that the activity coefficients for the complexed ions are approximately equal to the ones for the uncomplexed ions ($\gamma_I = \gamma_{IL}$). Solving the above equation using the WolframAlpha engine (www.wolframalpha.com/) we get:

$$\beta_{IL} = \frac{-e^{-k}(e^k - 1)}{R_T e^k + L_T - R_T}$$

where $k = \frac{E_M F}{RT}$ ($F = 96500\ C\ mol^{-1}, R = 8.31\ J\ K^{-1}\ mol^{-1}, T = 298\ K$).

For membrane (V), where $L_T = 22\ mmol \cdot kg^{-1}, R_T = 11\ mmol \cdot kg^{-1}$ and E_M (as the difference of potentials of the single and sandwich membranes) equal to $-11.6\ mV, -9.0\ mV$ and $-7.2\ mV$ for the three repetitions performed, the logarithmic complex formation constant for nitrate ionophore V is equal to:

$$log\beta_{IL} = 1.36 \pm 0.14$$

2.5.2 Calculation of complexed and not complexed fraction of nitrate in the membrane

Knowing the binding constant of nitrate ionophore V enables us to calculate the complexed and not complexed fraction of nitrate in the membrane, using the equations presented in the section above. Considering concentrations instead of activities, the complex formation constant for nitrate ionophore V is given as:

$$\beta_{IL} = \frac{c_{IL}}{c_I' c_L} \rightarrow c_{IL} = \beta_{IL} c_I' c_L$$

Using (3), we can now eliminate the concentration of complexed ionophore as follows:

$$c_{IL} = \beta_{IL} c_I' \, c_L \rightarrow R_T - c_I' = \beta_{IL} c_I' \, c_L \quad (9)$$

From (6) and (9) we get:

$$R_T - c_I' = \beta_{IL} c_I' \, (L_T - R_T + c_I') \rightarrow$$

$$\beta_{IL} (c_I')^2 + (\beta_{IL} L_T - \beta_{IL} R_T + 1) c_I' - R_T = 0 \quad (10)$$

with the only unknown being the concentration of free nitrate (c_I') in the membrane.

Knowing the total concentration of ionophore and ion-exchanger added in the membrane and assuming that the density of the membrane is equal to the one of plasticizer used (d_{NPOE} = 1.04 g/mL) we first calculate the respective concentrations in mol/L as follows:

$L_T = 22 \; mmol \; kg^{-1} \rightarrow L_T = 0.0229 \; M$

$R_T = 11 \; mmol \; kg^{-1} \rightarrow R_T = 0.0114 \; M$

From the sandwich membrane experiment we calculate:

$log\beta_{IL} = 1.36 \rightarrow \beta_{IL} = 22.9 \; M^{-1}$

Using the above values to solve (10) we get the concentration of free nitrate in the membrane:

$c_I' = 7.9 \; mM$

Finally, from (3) we calculate the concentration of complexed ionophore in the membrane equal to:

c_{IL} = 3.5 mM

Hence, 31 % of the total nitrate is complexed to the ionophore and 69 % is in free form (not complexed).

2.5.3 Correction for the liquid junction potentials and calculation of activities

All the potentiometric measurements from the selectivity study were corrected for the liquid junction potentials originating from the double junction reference electrode (Ag/AgCl/ 3 M KCl/1 M LiOAc). Those were calculated with the Henderson equation using the ionic mobilities of the respective ions [59] and they were subtracted from the measured potential values for each ion ($u_{Na^+} = 5.19 \cdot 10^{-4} cm^2 \cdot s^{-1} \cdot V^{-1}, u_{NO_3^-} = 7.40 \cdot 10^{-4} cm^2 \cdot s^{-1} \cdot V^{-1}, u_{Cl^-} = 7.91 \cdot 10^{-4} cm^2 \cdot s^{-1} \cdot V^{-1}, u_{Br^-} = 8.13 \cdot 10^{-4} cm^2 \cdot s^{-1} \cdot V^{-1}, u_{I^-} = 7.96 \cdot 10^{-4} cm^2 \cdot s^{-1} \cdot V^{-1}, u_{ClO_4^-} = 7.05 \cdot 10^{-4} cm^2 \cdot s^{-1} \cdot V^{-1}, u_{OAc^-} = 4.24 \cdot 10^{-4} cm^2 \cdot s^{-1} \cdot V^{-1}, u_{Li^+} = 4.01 \cdot 10^{-4} cm^2 \cdot s^{-1} \cdot V^{-1}$).

For the nitrite and thiocyanate solutions, the ionic mobilities were replaced by the respective diffusion coefficients [60] due to the lack of available data ($d_{Na^+} = 1.33 \cdot 10^{-5} cm^2 \cdot s^{-1}, d_{NO_2^-} = 1.91 \cdot 10^{-5} cm^2 \cdot s^{-1}, d_{OAc^-} = 1.09 \cdot 10^{-5} cm^2 \cdot s^{-1}, d_{Li^+} = 1.03 \cdot 10^{-5} cm^2 \cdot s^{-1}, d_{SCN^-} = 1.76 \cdot 10^{-5} cm^2 \cdot s^{-1}$).

The resulting junction potentials are summarized in **Table S2.1** for the examined concentrations:

Table S2.1: Calculated junction potentials for the examined ions and concentrations.

C (M)	Ej (mV)						
	NaCl	$NaNO_2$	NaBr	$NaNO_3$	NaI	NaSCN	$NaClO_4$
$\mathbf{10^{-4}}$	-6.26	-6.39	-6.25	-6.29	-6.26	-6.42	-6.31
$\mathbf{5{\cdot}10^{-4}}$	-5.09	-5.20	-5.07	-5.12	-5.08	-5.24	-5.14
$\mathbf{10^{-3}}$	-4.57	-4.68	-4.55	-4.61	-4.57	-4.73	-4.63
$\mathbf{5{\cdot}10^{-3}}$	-3.28	-3.40	-3.26	-3.35	-3.28	-3.48	-3.40
$\mathbf{10^{-2}}$	-2.66	-2.79	-2.62	-2.75	-2.65	-2.90	-2.81
$\mathbf{5{\cdot}10^{-2}}$	-0.81	-1.05	-0.71	-1.04	-0.78	-1.33	-1.20
$\mathbf{10^{-1}}$	0.29	-0.06	0.43	-0.06	0.32	-0.48	-0.31

The following semi-empirical equation which is based on the extended Debye-Hückel theory was used for the calculation of the activity coefficients for each ion:

$$\log \gamma_{\pm} = -\frac{A|z_+ z_-|\sqrt{I}}{1 + B\sqrt{I}} + CI$$

where I is the ionic strength, $|z_+ z_-|$ is the absolute product of valencies, and A, B, C parameters given by Meier [61]. The logarithms of the resulting activities for each ion are summarized in **Table S2.2** for the examined concentrations.

Table S2.2: Calculated activities for the examined ions and concentrations.

C (M)	logα						
	Cl^-	NO_2^-	Br^-	NO_3^-	I^-	SCN^-	ClO_4^-
$\mathbf{10^{-4}}$	-4.005	-4.005	-4.005	-4.005	-4.005	-4.005	-4.005
$\mathbf{5{\cdot}10^{-4}}$	-3.312	-3.312	-3.312	-3.312	-3.312	-3.312	-3.312
$\mathbf{10^{-3}}$	-3.015	-3.016	-3.015	-3.016	-3.015	-3.015	-3.015
$\mathbf{5{\cdot}10^{-3}}$	-2.334	-2.334	-2.334	-2.334	-2.333	-2.333	-2.334
$\mathbf{10^{-2}}$	-2.044	-2.045	-2.044	-2.046	-2.044	-2.044	-2.044
$\mathbf{5{\cdot}10^{-2}}$	-1.386	-1.390	-1.385	-1.392	-1.383	-1.383	-1.387
$\mathbf{10^{-1}}$	-1.109	-1.114	-1.106	-1.119	-1.103	-1.103	-1.110

2.6 References

(1) Beer, P. D.; Gale, P. A. Anion Recognition and Sensing: The State of the Art and Future Perspectives. *Angewandte Chemie International Edition* **2001**, *40* (3), 486–516. https://doi.org/10.1002/1521-3773(20010202)40:3<486::AID-ANIE486>3.0.CO;2-P.

(2) Hay, B. P.; Gutowski, M.; Dixon, D. A.; Garza, J.; Vargas, R.; Moyer, B. A. Structural Criteria for the Rational Design of Selective Ligands: Convergent Hydrogen Bonding Sites for the Nitrate Anion. *J. Am. Chem. Soc.* **2004**, *126* (25), 7925–7934. https://doi.org/10.1021/ja0487980.

(3) Jia, C.; Zuo, W.; Zhang, D.; Yang, X.-J.; Wu, B. Anion Recognition by Oligo-(Thio)Urea-Based Receptors. *Chem. Commun.* **2016**, *52* (62), 9614–9627. https://doi.org/10.1039/C6CC03761E.
(4) Herges, R.; Dikmans, A.; Jana, U.; Köhler, F.; Jones, P. G.; Dix, I.; Fricke, T.; König, B. Design of a Neutral Macrocyclic Ionophore: Synthesis and Binding Properties for Nitrate and Bromide Anions. *Eur. J. Org. Chem.* **2002**, *2002* (17), 3004–3014. https://doi.org/10.1002/1099-0690(200209)2002:17<3004::AID-EJOC3004>3.0.CO;2-O.
(5) Nishizawa, S.; Bühlmann, P.; Iwao, M.; Umezawa, Y. Anion Recognition by Urea and Thiourea Groups: Remarkably Simple Neutral Receptors for Dihydrogenphosphate. *Tetrahedron Letters* **1995**, *36* (36), 6483–6486. https://doi.org/10.1016/0040-4039(95)01296-T.
(6) J. Mercer, D.; J. Loeb, S. Metal-Based Anion Receptors: An Application of Second-Sphere Coordination. *Chemical Society Reviews* **2010**, *39* (10), 3612–3620. https://doi.org/10.1039/B926226C.
(7) Bisson, A. P.; Lynch, V. M.; Monahan, M.-K. C.; Anslyn, E. V. Recognition of Anions through NH□π Hydrogen Bonds in a Bicyclic Cyclophane—Selectivity for Nitrate. *Angewandte Chemie International Edition in English* **1997**, *36* (21), 2340–2342. https://doi.org/10.1002/anie.199723401.
(8) Işiklan, M.; Saeed, M. A.; Pramanik, A.; Wong, B. M.; Fronczek, F. R.; Hossain, A. A C3 Symmetric Nitrate Complex with a Thiophene-Based Tripodal Receptor. *Cryst Growth Des* **2011**, *11* (4), 959–963. https://doi.org/10.1021/cg2001859.
(9) Blondeau, P.; Benet-Buchholz, J.; de Mendoza, J. Enthalpy Driven Nitrate Complexation by Guanidinium-Based Macrocycles. *New J. Chem.* **2007**, *31* (5), 736. https://doi.org/10.1039/b616409a.
(10) Singh, A. S.; Sun, S.-S. Recognition, Encapsulation, and Selective Fluorescence Sensing of Nitrate Anion by Neutral C3-Symmetric Tripodal Podands Bearing Amide Functionality. *J. Org. Chem.* **2012**, *77* (4), 1880–1890. https://doi.org/10.1021/jo202502f.
(11) Watt, M. M.; Zakharov, L. N.; Haley, M. M.; Johnson, D. W. Selective Nitrate Binding in Competitive Hydrogen Bonding Solvents: Do Anion–π Interactions Facilitate Nitrate Selectivity? *Angewandte Chemie International Edition* **2013**, *52* (39), 10275–10280. https://doi.org/10.1002/anie.201303881.
(12) Bakker, E.; Bühlmann, P.; Pretsch, E. Carrier-Based Ion-Selective Electrodes and Bulk Optodes. 1. General Characteristics. *Chem. Rev.* **1997**, *97* (8), 3083–3132. https://doi.org/10.1021/cr940394a.
(13) Pungor, E.; Tóth, K.; Hrabéczy-Páll, A. Selectivity Coefficients of Ion-Selective Electrodes. https://doi.org/10.1515/iupac.51.0504.
(14) Bakker, Eric.; Meruva, R. K.; Pretsch, Erno.; Meyerhoff, M. E. Selectivity of Polymer Membrane-Based Ion-Selective Electrodes: Self-Consistent Model Describing the Potentiometric Response in Mixed Ion Solutions of Different Charge. *Anal. Chem.* **1994**, *66* (19), 3021–3030. https://doi.org/10.1021/ac00091a600.
(15) Bakker, E. Determination of Improved Selectivity Coefficients of Polymer Membrane Ion-Selective Electrodes by Conditioning with a Discriminated Ion. *J. Electrochem. Soc.* **1996**, *143* (4), L83–L85. https://doi.org/10.1149/1.1836608.
(16) Bakker, E. Determination of Unbiased Selectivity Coefficients of Neutral Carrier-Based Cation-Selective Electrodes. *Anal. Chem.* **1997**, *69* (6), 1061–1069. https://doi.org/10.1021/ac960891m.
(17) Bakker, E.; Pretsch, E.; Bühlmann, P. Selectivity of Potentiometric Ion Sensors. *Anal. Chem.* **2000**, *72* (6), 1127–1133. https://doi.org/10.1021/ac991146n.
(18) Stefanova, O. K. On the effect of coupling of ionic and neutral ligand fluxes in membrane potentials. *Electrokhimiya* **1979**, *15*, 1707–1710.
(19) Mikhelson, K. N. Ion-Selective Electrodes in PVC Matrix. *Sensors and Actuators B: Chemical* **1994**, *18* (1–3), 31–37. https://doi.org/10.1016/0925-4005(94)87051-9.
(20) Mi, Y.; Bakker, E. Determination of Complex Formation Constants of Lipophilic Neutral Ionophores in Solvent Polymeric Membranes with Segmented Sandwich Membranes. *Anal. Chem.* **1999**, *71* (23), 5279–5287. https://doi.org/10.1021/ac9905930.
(21) Qin, Y.; Mi, Y.; Bakker, E. Determination of Complex Formation Constants of 18 Neutral Alkali and Alkaline Earth Metal Ionophores in Poly(Vinyl Chloride) Sensing Membranes Plasticized with

Bis(2-Ethylhexyl)Sebacate and o-Nitrophenyloctylether. *Analytica Chimica Acta* **2000**, *421* (2), 207–220. https://doi.org/10.1016/S0003-2670(00)01038-2.
(22) Mikhelson, K. M.; Bobacka, J.; Ivaska, A.; Lewenstam, A.; Bochenska, M. Selectivity of Lithium Electrodes: Correlation with Ion-Lonophore Complex Stability Constants and with Interfacial Exchange Current Densities. *Anal Chem* **2002**, *74* (3), 518–527. https://doi.org/10.1021/ac0155660.
(23) Lutov, V. M.; Mikhelson, K. N. A New pH Sensor with a PVC Membrane: Analytical Evaluation and Mechanistic Aspects. *Sensors and Actuators B: Chemical* **1994**, *19* (1), 400–403. https://doi.org/10.1016/0925-4005(93)01010-2.
(24) Mi, Y.; Bakker, E. Ion Binding Properties of the Lipophilic H + -Chromoionophore ETH 5294 in Solvent Polymeric Sensing Membranes as Determined with Segmented Sandwich Membranes. **2000**, 3.
(25) Szigeti, Z.; Malon, A.; Vigassy, T.; Csokai, V.; Grün, A.; Wygladacz, K.; Ye, N.; Xu, C.; Chebny, V. J.; Bitter, I.; Rathore, R.; Bakker, E.; Pretsch, E. Novel Potentiometric and Optical Silver Ion-Selective Sensors with Subnanomolar Detection Limits. *Analytica Chimica Acta* **2006**, *572* (1), 1–10. https://doi.org/10.1016/j.aca.2006.05.009.
(26) Jarolímová, Z.; Vishe, M.; Lacour, J.; Bakker, E. Potassium Ion-Selective Fluorescent and pH Independent Nanosensors Based on Functionalized Polyether Macrocycles. *Chemical Science* **2016**, *7* (1), 525–533. https://doi.org/10.1039/C5SC03301B.
(27) Ceresa, A.; Qin, Y.; Peper, S.; Bakker, E. Mechanistic Insights into the Development of Optical Chloride Sensors Based on the [9]Mercuracarborand-3 Ionophore. *Anal. Chem.* **2003**, *75* (1), 133–140. https://doi.org/10.1021/ac026055w.
(28) Gupta, V.; Goyal, R.; Sharma, R. Anion Recognition Using Newly Synthesized Hydrogen Bonding Disubstituted Phenylhydrazone-Based Receptors: Poly(Vinyl Chloride)-Based Sensor for Acetate. *Talanta* **2008**, *76* (4), 859–864. https://doi.org/10.1016/j.talanta.2008.04.046.
(29) Makarychev-Mikhailov, S.; Legin, A.; Mortensen, J.; Levitchev, S.; Vlasov, Y. Potentiometric and Theoretical Studies of the Carbonate Sensors Based on 3-Bromo-4-Hexyl-5-Nitrotrifluoroacetophenone. *Analyst* **2004**, *129* (3), 213–218. https://doi.org/10.1039/B310560A.
(30) Li, L.; Zhang, Y.; Li, Y.; Duan, Y.; Qian, Y.; Zhang, P.; Guo, Q.; Ding, J. Polymeric Membrane Fluoride-Selective Electrodes Using Lewis Acidic Organo-Antimony(V) Compounds as Ionophores. *ACS Sens.* **2020**, *5* (11), 3465–3473. https://doi.org/10.1021/acssensors.0c01481.
(31) Singh, A. K.; Singh, U. P.; Mehtab, S.; Aggarwal, V. Thiocyanate Selective Sensor Based on Tripodal Zinc Complex for Direct Determination of Thiocyanate in Biological Samples. *Sensors and Actuators B: Chemical* **2007**, *125* (2), 453–461. https://doi.org/10.1016/j.snb.2007.02.056.
(32) Peshkova, M. A.; Korobeynikov, A. I.; Mikhelson, K. N. Estimation of Ion-Site Association Constants in Ion-Selective Electrode Membranes by Modified Segmented Sandwich Membrane Method. *Electrochimica Acta* **2008**, *53* (19), 5819–5826. https://doi.org/10.1016/j.electacta.2008.03.030.
(33) Egorov, V. V.; Lyaskovski, P. L.; Il'inchik, I. V.; Soroka, V. V.; Nazarov, V. A. Estimation of Ion-Pairing Constants in Plasticized Poly(Vinyl Chloride) Membranes Using Segmented Sandwich Membranes Technique. *Electroanalysis* **2009**, *21* (17–18), 2061–2070. https://doi.org/10.1002/elan.200904639.
(34) Bühlmann, P.; Pretsch, E.; Bakker, E. Carrier-Based Ion-Selective Electrodes and Bulk Optodes. 2. Ionophores for Potentiometric and Optical Sensors. *Chem. Rev.* **1998**, *98* (4), 1593–1688. https://doi.org/10.1021/cr970113+.
(35) Jiang, C.; He, Y.; Liu, Y. Recent Advances in Sensors for Electrochemical Analysis of Nitrate in Food and Environmental Matrices. *Analyst* **2020**, *145* (16), 5400–5413. https://doi.org/10.1039/D0AN00823K.
(36) Singh, S.; Anil, A. G.; Kumar, V.; Kapoor, D.; Subramanian, S.; Singh, J.; Ramamurthy, P. C. Nitrates in the Environment: A Critical Review of Their Distribution, Sensing Techniques, Ecological Effects and Remediation. *Chemosphere* **2022**, *287*, 131996. https://doi.org/10.1016/j.chemosphere.2021.131996.
(37) Hofmeister, F. Zur Lehre von der Wirkung der Salze. *Archiv f. experiment. Pathol. u. Pharmakol* **1888**, *24* (4), 247–260. https://doi.org/10.1007/BF01918191.

(38) Kim, M.-Y.; Lee, J.-W.; Park, D. J.; Lee, J.-Y.; Myung, N. V.; Kwon, S. H.; Lee, K. H. Highly Stable Potentiometric Sensor with Reduced Graphene Oxide Aerogel as a Solid Contact for Detection of Nitrate and Calcium Ions. *Journal of Electroanalytical Chemistry* **2021**, *897*, 115553. https://doi.org/10.1016/j.jelechem.2021.115553.
(39) Wang, H.; Yuan, B.; Yin, T.; Qin, W. Alternative Coulometric Signal Readout Based on a Solid-Contact Ion-Selective Electrode for Detection of Nitrate. *Analytica Chimica Acta* **2020**, *1129*, 136–142. https://doi.org/10.1016/j.aca.2020.07.019.
(40) Fayose, T.; Mendecki, L.; Ullah, S.; Radu, A. Single Strip Solid Contact Ion Selective Electrodes on a Pencil-Drawn Electrode Substrate. *Anal. Methods* **2017**, *9* (7), 1213–1220. https://doi.org/10.1039/C6AY02860H.
(41) Wardak, C.; Grabarczyk, M. Analytical Application of Solid Contact Ion-Selective Electrodes for Determination of Copper and Nitrate in Various Food Products and Drinking Water. *Journal of Environmental Science and Health, Part B* **2016**, *51* (8), 519–524. https://doi.org/10.1080/03601234.2016.1170545.
(42) Cuartero, M.; Crespo, G. A.; Bakker, E. Tandem Electrochemical Desalination–Potentiometric Nitrate Sensing for Seawater Analysis. *Anal. Chem.* **2015**, *87* (16), 8084–8089. https://doi.org/10.1021/acs.analchem.5b01973.
(43) Yuan, D.; Anthis, A. H. C.; Ghahraman Afshar, M.; Pankratova, N.; Cuartero, M.; Crespo, G. A.; Bakker, E. All-Solid-State Potentiometric Sensors with a Multiwalled Carbon Nanotube Inner Transducing Layer for Anion Detection in Environmental Samples. *Anal. Chem.* **2015**, *87* (17), 8640–8645. https://doi.org/10.1021/acs.analchem.5b01941.
(44) Paczosa-Bator, B.; Cabaj, L.; Piech, R.; Skupień, K. Potentiometric Sensors with Carbon Black Supporting Platinum Nanoparticles. *Anal. Chem.* **2013**, *85* (21), 10255–10261. https://doi.org/10.1021/ac402885y.
(45) Tang, W.; Ping, J.; Fan, K.; Wang, Y.; Luo, X.; Ying, Y.; Wu, J.; Zhou, Q. All-Solid-State Nitrate-Selective Electrode and Its Application in Drinking Water. *Electrochimica Acta* **2012**, *81*, 186–190. https://doi.org/10.1016/j.electacta.2012.07.073.
(46) Khripoun, G. A.; Volkova, E. A.; Liseenkov, A. V.; Mikhelson, K. N. Nitrate-Selective Solid Contact Electrodes with Poly(3-Octylthiophene) and Poly(Aniline) as Ion-to-Electron Transducers Buffered with Electron-Ion-Exchanging Resin. *Electroanalysis* **2006**, *18* (13–14), 1322–1328. https://doi.org/10.1002/elan.200603532.
(47) Liu, Y.; Liu, Y.; Meng, Z.; Qin, Y.; Jiang, D.; Xi, K.; Wang, P. Thiol-Functionalized Reduced Graphene Oxide as Self-Assembled Ion-to-Electron Transducer for Durable Solid-Contact Ion-Selective Electrodes. *Talanta* **2020**, *208*, 120374. https://doi.org/10.1016/j.talanta.2019.120374.
(48) Pięk, M.; Piech, R.; Paczosa-Bator, B. Improved Nitrate Sensing Using Solid Contact Ion Selective Electrodes Based on TTF and Its Radical Salt. *J. Electrochem. Soc.* **2015**, *162* (10), B257. https://doi.org/10.1149/2.0631510jes.
(49) Pięk, M.; Piech, R.; Paczosa-Bator, B. TTF-TCNQ Solid Contact Layer in All-Solid-State Ion-Selective Electrodes for Potassium or Nitrate Determination. *J. Electrochem. Soc.* **2018**, *165* (2), B60. https://doi.org/10.1149/2.0161803jes.
(50) Watts, A. S.; Gavalas, V. G.; Cammers, A.; Andrada, P. S.; Alajarín, M.; Bachas, L. G. Nitrate-Selective Electrode Based on a Cyclic Bis-Thiourea Ionophore. *Sensors and Actuators B: Chemical* **2007**, *121* (1), 200–207. https://doi.org/10.1016/j.snb.2006.09.048.
(51) Gupta, V. K.; Singh, L. P.; Chandra, S.; Kumar, S.; Singh, R.; Sethi, B. Anion Recognition through Amide-Based Dendritic Molecule: A Poly(Vinyl Chloride) Based Sensor for Nitrate Ion. *Talanta* **2011**, *85* (2), 970–974. https://doi.org/10.1016/j.talanta.2011.05.014.
(52) Lee, H. K.; Song, K.; Ran Seo, H.; Jeon, S. Nitrate-Selective Electrodes Based on Meso-Tetrakis[(2-Arylphenylurea)-Phenyl]Porphyrins as Neutral Lipophilic Ionophores. *Talanta* **2004**, *62* (2), 293–297. https://doi.org/10.1016/j.talanta.2003.07.016.
(53) Mazloum Ardakani, M.; Salavati-Niasari, M.; Jamshidpoor, M. Selective Nitrate Poly(Vinylchloride) Membrane Electrode Based on Bis(2-Hydroxyacetophenone)Ethylenediimine Vanadyl (IV). *Sensors and Actuators B: Chemical* **2004**, *101* (3), 302–307. https://doi.org/10.1016/j.snb.2004.03.011.
(54) *Nitrate Ionophore VI Selectophore, function tested 1196157-85-3*. http://www.sigmaaldrich.com/ (accessed 2022-05-18).

(55) Zdrachek, E.; Forrest, T.; Bakker, E. Solid-Contact Potentiometric Cell with Symmetry. *Anal. Chem.* **2022**, *94* (2), 612–617. https://doi.org/10.1021/acs.analchem.1c04722.
(56) Zdrachek, E.; Bakker, E. Potentiometric Sensor Array with Multi-Nernstian Slope. *Anal. Chem.* **2020**, *92* (4), 2926–2930. https://doi.org/10.1021/acs.analchem.9b05187.
(57) Cuartero, M.; Crespo, G.; Cherubini, T.; Pankratova, N.; Confalonieri, F.; Massa, F.; Tercier-Waeber, M.-L.; Abdou, M.; Schäfer, J.; Bakker, E. In Situ Detection of Macronutrients and Chloride in Seawater by Submersible Electrochemical Sensors. *Anal. Chem.* **2018**, *90* (7), 4702–4710. https://doi.org/10.1021/acs.analchem.7b05299.
(58) Pankratova, N.; A. Crespo, G.; Ghahraman Afshar, M.; Coll Crespi, M.; Jeanneret, S.; Cherubini, T.; Tercier-Waeber, M.-L.; Pomati, F.; Bakker, E. Potentiometric Sensing Array for Monitoring Aquatic Systems. *Environmental Science: Processes & Impacts* **2015**, *17* (5), 906–914. https://doi.org/10.1039/C5EM00038F.
(59) Allen J. Bard; Larry R. Faulkner. *Electrochemical Methods: Fundamentals and Applications*, 2nd ed.; 2000.
(60) M Haynes, W. *CRC Handbook of Chemistry and Physics*, 95th ed.; 2014.
(61) Meier, P. C. Two-Parameter Debye-Hückel Approximation for the Evaluation of Mean Activity Coefficients of 109 Electrolytes. *Analytica Chimica Acta* **1982**, *136*, 363–368. https://doi.org/10.1016/S0003-2670(01)95397-8.

Chapter 3: Unconditioned Symmetric Solid-Contact Electrodes for Potentiometric Sensing

(This chapter is based on the following paper: Damala, P.; Zdrachek, E.; Forrest, T.; Bakker, E. Unconditioned Symmetric Solid-Contact Electrodes for Potentiometric Sensing. *Anal. Chem.* 2022, *94* (33), 11549–11556. https://doi.org/10.1021/acs.analchem.2c01728)

3.1 Introduction

Ever since potentiometry was established as an analytical method, a certain number of standard procedures for the preparation of the ion-selective electrodes (ISEs) has been adopted by the electroanalytical community. Among them, the "conditioning" step has the vital role of equilibrating the electrodes' response by hydrating and saturating the sensing membrane with the desired analyte ions. During conditioning, a potential drift is typically observed owing to processes that fall into three main categories[1]: i) ion-exchange between the sensing membrane and aqueous solution, ii) water uptake into the membrane and underlying transducing layer and iii) other factors including temperature changes and leaching of membrane components. Ion-exchange and water uptake occur at different time-scales as water diffuses faster than ions in membranes, with the diffusion coefficients ranging between 10^{-6} – 10^{-7} cm^2 s^{-1} [2,3] for water and approximately 10^{-8} cm^2 s^{-1} [4,5] for ions. The importance of water uptake on the potential was studied by measuring the drift of unconditioned electrodes based on silicone rubber membranes and POT as transducer. A drift of just 4 mV over 24 h was observed for the electrodes containing both silicone rubber and POT (compared to a 29 mV drift of electrodes without POT). The authors attributed the excellent potential stability on the hydrophobic nature of these materials that prevented the formation of an internal water layer. A follow-up study[6] from the same research group examined the water uptake of the same sensors fabricated with plasticized PVC instead of silicone rubber without prior conditioning. An increased water uptake was reported, possibly originating from the intermixing of the underlying transducer and the overlaid membrane. The electrode potentials drifted by approximately 30-40 mV during the first 9 h while the drift slowed for the next 9-24 h. Interestingly, even though the diffusion coefficients of silicone rubber and plasticized PVC membranes are almost the same, the silicone rubber resulted in the lowest rate of water uptake. [7] The ion-exchange in the membrane takes place at a slower rate, but it can also contribute to the potential drift. A distinction should be made between membranes that contain or do not contain the primary ion in the form of ion-exchanger. The effect of the presence or absence of the primary ion on the potential drift was examined with sodium-selective electrodes that contained either potassium or sodium-based ion exchangers. [8] It was shown that electrodes (Au and GC) with membranes containing potassium-based ion-exchangers needed approximately 5 more minutes to equilibrate compared to their sodium-based counterparts,

demonstrating the effect of the ion-exchange process on the drift. Moreover, the effect of temperature was recently examined in our group where a drift of 25 mV was measured for a change of 20 degrees Celsius for solid-contact nitrate-selective electrodes based on PEDOT-C_{14}. [9] These experiments were performed with conditioned electrodes, but such drifts are also expected with unconditioned electrodes. The leaching of membrane components can also lead to potential drifts and researchers have examined the leaching of ionophores[10], ion-exchangers[11] and plasticizers[12] using various techniques. As an example, in the latter study the authors observed a slow drift of the measured streaming current during the 2 first hours of conditioning which they partly attributed to the leaching of plasticizer.

Despite the resulting potential drift, performing an adequate conditioning step can have a decisive role on the performance of the electrodes. Yet, it is also one of the most time-consuming procedures during the electrode preparation and use. Depending on the application, it can last from a few hours up to several days. An outcome of a long-term conditioning procedure often reported is the formation of an internal water layer between the membrane and the transducing material, which can introduce potential instabilities. This phenomenon has been known for decades and the gradual shift to the use of more lipophilic membrane materials and transducers is indicative of the problem. [8,13–16] This water layer, once formed, can contain an accumulated amount of primary ions that risk to leach out when dilute samples are analyzed, posing an additional limitation for measurements at low sample concentration. [17] A method to lower the detection limit is to use a conditioning solution that contains only interfering ions, but the non-stationary processes prevailing in the membrane limit the universal use of this approach. [18] Performing measurements in an optimized time window during which the sensors function in a non-equilibrated state is another strategy to achieve even lower detection limits, which also drastically reduces the conditioning time. [19] To ensure the Nernstian behavior of the membrane, however, and avoid the prevalence of non-steady state conditions and transient calibration curves, it is important to include the primary ion in the conditioning solution. In addition, using a solution that contains both primary and interfering ions can offer the combined advantage of achieving low detection limits and Nernstian responses. Despite the obvious advantages of this method, the potentiometric response may be strongly influenced by the composition of the conditioning solution owing to the various equilibria established in the transducer and membrane phases. [20] Other factors related to the physicochemical properties of the membranes can also influence the conditioning requirements. For example, increasing the thickness of the sensing membrane increases the conditioning time[21] while a 1000-fold decrease of the membrane (from 200 um to 200 nm) can significantly shorten the conditioning period due to the faster diffusion processes taking place. [22]

The need for fast and reliable potentiometric measurements has driven the researchers in the quest of new methods to decrease or eliminate the conditioning requirement without the cost of decreased performance. Pretreating the membrane cocktail with the necessary quantity of primary ions[21,23,24] or both primary and interfering ions[25], storing the electrodes with a drop of pure water on top of the sensing

membrane or inside the membrane cocktail[26], as well as storing them in humid containers[15,27] have been used as methods to reduce the need for conditioning immediately before measurement. However, in the last three cases, an initial preconditioning step of at least 24 h is required. In addition, the inclusion of the analyte ions in the membrane might not always eliminate the potential drifts arising from the water uptake in the membrane. An alternative strategy to avoid extensive conditioning is to optimize the thickness of the transducing layer as demonstrated with PEDOT(PSS). [28] In that study, an increase of the transducing layer thickness resulted in an increased hydrophobicity and decreased the influence of the electrode-transducer interface on the membrane equilibration rate. Research on unconditioned ion-selective sensors was also extended to paper-based devices for the detection of chloride, potassium and sodium in biological media without prior conditioning. [29,30] In both cases, Nernstian behavior was reported with a linear response range that covered the physiologically relevant concentrations of the analytes in biological samples. However, the detection limits were higher than the ones observed in the conventional ISEs and the authors attributed this phenomenon to the anionic groups of the paper cellulose used as a substrate for the sensors. Apart from the clinically relevant ions, paper-based ion-sensing platforms have been fabricated and used without pretreatment for the detection of enzyme activities and ogranophosphate pesticides. [31] Using a sensing platform resembling an origami structure, the authors reported detection limits for the methyl parathion pesticide that are comparable or lower to the ones already reported in literature.

As shown from the examples above, the planar sensing platforms that have been used succesfully without prior conditioning target either clinically relevant ions in physiological media (e.g. whole blood) or enzymes and small molecule analytes. There is still a lack of progress on a solid-state potentiometric sensing system that can detect environmentally relevant ions (such as nitrate) using sensors that can be used without prior conditioning while maintaining long-term stability and detection limits of conventional ISEs.

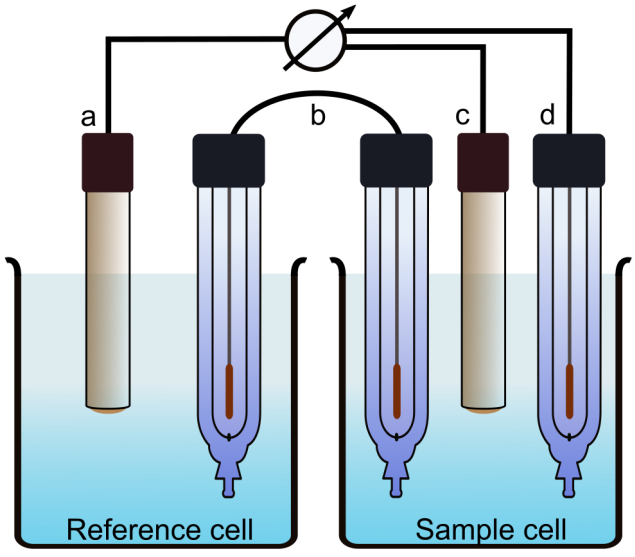

Figure 3.1: Symmetric setup consisting of a nitrate (or potassium)-selective electrode used as a (solid-contact) reference electrode (a), a bridge of two identical Ag/AgCl reference electrodes (b), a nitrate (or potassium)-selective electrode used as an indicator electrode (c) and an Ag/AgCl reference electrode used as the main reference electrode of the system to decouple potentials of solid-contact reference and indicator electrodes for characterization purpose (d). Any number of electrodes (a) and (c) can be added to the reference and sample cells respectively.

We examine here the performance of a setup using the principle of symmetry reported in a recent study by our group.[9] The novelty of the current work is to demonstrate stable potentiometric measurements using solid contact electrodes "out-of-the-box" without the need of conditioning. Moreover, with the suggested setup there is no need to fulfill any requirements for a bridge electrolyte mixture as with our earlier work, which facilitates the determination of a broader set of analytes. The principle is demonstrated with the measurement of nitrate of river water. Here, symmetry is established using two cells with identical solid-contact ISEs that serve as the reference and sample cells (**Figure 3.1**). By performing differential potential measurements between the two sides it is possible to cancel out all potential drifts unrelated to the analyte activity levels that may originate from (i) changes in the environment (temperature, light, pressure, air composition), (ii) changes in the quality of the electrode components, and (iii) changes related to the conditioning of the dry membranes upon initial contact with a solution. With this symmetric setup we demonstrate the successful use of unconditioned electrodes for the detection of nitrate and potassium ions.

3.2 Experimental

3.2.1 Reagents

Tridodecylmethylammonium nitrate (TDMAN), bis(2-ethylhexyl) phthalate (DEHP), tetradodecylammonium tetrakis(4-chlorophenyl)borate (ETH 500), bis(2-ethylhexyl)sebacate (DOS), potassium tetrakis[(3,5-bis(trifluoromethyl)phenyl]borate (KTFPB) and tetrahydrofuran (THF) were of Selectophore grade (Sigma-Aldrich, Switzerland). Octadecyl amine-functionalized single-walled carbon nanotubes (80-90 % carbon basis, D x L: 2-10 nm x 0.5-2 μm) were purchased from Sigma-Aldrich. Valinomycin (90+ %) was purchased from Alfa Aesar. Potassium nitrate (99+ %) and sodium nitrate (≥99 %) were purchased from Sigma-Aldrich. Aqueous solutions were prepared by dissolving the respective salts in Milli-Q water (18.2 MΩ cm).

3.2.2 Preparation of Ion-Selective Electrodes

Commercial glassy carbon macroelectrodes (Ø 3 mm) were used for the preparation of the nitrate and potassium-selective electrodes. The electrodes were polished with diamond spray (Kemet International, UK) of 6, 3, 1 and 0.25 μm size before use. The drop-casting protocol for the deposition of the transducer and the sensing membrane that followed was the same for both types of ISEs. Commercial octadecyl amine-functionalized single-walled carbon nanotubes (f-SWCNTs) were used as a transducer material. The respective solution was prepared by dispersing 1 mg f-SWCNTs in 1 mL THF. Eight layers (20 μL

each) of this solution were drop-cast on top of the electrodes, keeping 10 min of drying time before depositing the next layer. After the last coating, the electrodes were left to dry for at least 30 min before continuing with the deposition of the membrane layers. The sensing membrane of the nitrate-selective electrodes was prepared by dissolving 0.6 mg TDMAN (10 mmol·kg^{-1}), 1.7 mg ETH500 (14.8 mmol·kg^{-1}), 33.3 mg PVC and 64.4 mg DEHP in 1 mL THF. The membrane of the potassium-selective electrodes was prepared by dissolving 1.11 mg valinomycin (10 mmol·kg^{-1}), 0.45 mg KTFPB (5 mmol·kg^{-1}), 33.3 mg PVC and 65.5 mg DOS in 1 mL THF. Both membrane cocktails contained the primary ion in the form of ion-exchangers (TDMAN for nitrate-selective and KTFPB for potassium-selective membranes) to facilitate and shorten the equilibration process. Three layers (50 μL each) of the membrane solution were drop-cast on top of the transducer deposited earlier, keeping 20 minutes of drying time before the deposition of the next layer. The drop-cast electrodes were left to dry overnight in ambient air and temperature before use.

3.2.3 Electrochemical equipment

The potentiometric measurements were performed with a high impedance input 16-channel EMF monitor (Lawson Laboratories, Malvern, PA). Three identical double-junction reference electrodes (Ag/AgCl/ 3 M KCl/1 M LiOAc, Metrohm, Switzerland) were used in the symmetric setup; one was used as the main reference electrode connected to the Lawson and two were used as a bridge that connected the two cells (**Figure 3.1**). The liquid-junction reference electrodes used as a bridge were frequently cleaned and refilled with their respective electrolytes to minimize any additional potential drifts.

3.2.4 Symmetric setup and corrections in potential

The symmetric setup presented in **Figure 3.1** was used for all types of experiments performed in this study. The two liquid junction reference electrodes used as a bridge connecting the reference and sample cells contributed with their junction potentials to the final potential readings. During the calibration experiments, the reference cell was kept at a constant and relatively low concentration of the analyte ion, while the concentration in the sample cell varied between 10^{-6} M and 10^{-2} M. This discrepancy in concentration levels resulted in the rise of an additional potential that needed to be corrected. A detailed description of the potential corrections made is given in the Supporting Information.

3.2.5 Long-term and 5-day potential drift experiments

The 5-day drift was examined by calibrating the electrodes for five consecutive days. When not calibrated, the electrodes were kept in their conditioning solution (0.1 mM $NaNO_3$ for nitrate and 1 mM KNO_3 for potassium). For these experiments, the same set of electrodes was used for the five measurement days: six electrodes for nitrate (three in each cell) and four electrodes for potassium (two in each cell). Since the electrodes were used unconditioned, the first day of calibration (Day 1) can be considered as the conditioning day. During the measurements, stirring was performed for a short time

only after the addition of standard solutions; otherwise, the solutions were kept unstirred. The long-term drift of the ISEs was tested by keeping a constant concentration in the reference cell (0.1 mM $NaNO_3$ for nitrate and 1 mM KNO_3 for potassium-selective electrodes) while varying the analyte ion concentration in the sample cell (0.1/0.5/1 mM $NaNO_3$ for nitrate and 1/5/10 mM KNO_3 for potassium-selective electrodes). For each experiment, a new set of dry (unconditioned) electrodes was used. The potential was monitored for 20 h (except one case where the total duration was 15 h) in unstirred conditions and the drift was calculated on a minute-by-minute (or hour-by-hour) basis (as shown in **Figure 3.2**). All electrodes used in the long-term experiments were calibrated immediately after the 20-h monitoring period with standard nitrate solutions in Milli-Q water to ensure their proper functioning.

3.2.6 Data processing and statistics

The symmetric setup may include any number of reference and indicator electrodes in the reference and sample cells respectively (electrodes (a) and (c) in **Figure 3.1**). To apply the principle of symmetry, the potential readouts corresponding to the reference electrodes were subtracted from the ones of the indicator electrodes. For the 5-day drift experiments, the following data treatment took place. In the case of nitrate, six identical nitrate-selective electrodes were used; three electrodes placed in the reference cell (Ref_1, Ref_2, Ref_3) and three in the sample cell (Ind_1, Ind_2, Ind_3). The subtractions of the EMF readings between the reference and indicator electrodes (Ind_1-Ref_1, Ind_1-Ref_2, Ind_1-Ref_3, Ind_2-Ref_1, Ind_2-Re_2, Ind_2-Ref_3, Ind_3-Ref_1, Ind_3-Re_2, Ind_3-Ref_3) gave a dataset of nine deducted potential values, which were subsequently used for the statistics (the average and standard deviations came from these nine potential values). Hence, for all the results presented below that refer to the nitrate-selective electrodes, n=9 for the symmetric system and n=3 for the asymmetric system. In the case of potassium, four potassium-selective electrodes were used; two of them placed in the reference cell and two in the sample cell. The same statistical analysis presented above was also followed in the case of potassium. The average and standard deviations shown come from the four deducted potential values (Ind_1-Ref_1, Ind_1-Ref_2, Ind_2-Ref_1, Ind_2-Re_2). As before, for all the results presented below that refer to the potassium-selective electrodes, n=4 for the symmetric system and n=2 for the asymmetric system. For the long-term experiments, similar subtractions between the potential readouts of the indicator and reference electrodes were performed, resulting in four and nine potential traces, for potassium and nitrate respectively. For the calibrations performed during the 5-day drift experiments, the EMF readings were recorded every second and the average value of the last 60 readings was used every time as the final potential value corresponding to each nitrate activity.

For clarity purposes, the “symmetric system” mentioned below refers to the potentiometric response of the indicator electrode(s) (electrode (c) in **Figure 3.1**) measured against identical electrode(s) placed in the reference cell (electrode (a) in **Figure 3.1**), while the “asymmetric system” refers to the potentiometric response of the indicator electrode(s) (electrode (c) in **Figure 3.1**) measured against an

Ag/AgCl reference electrode (electrode (d) in **Figure 3.1**) without any data treatment between the EMF readings of the reference and sample cells.

3.2.7 Instrumentation and Protocols

Spectrophotometric Kit. The Spectroquant Nitrate Test from Merck was used as a reference method for the determination of the nitrate concentration in the river water sample. In this method, the nitrate ions reacted in sulfuric and phosphoric solution with 2,6-dimethylphenol to form 4-nitro-2,6-dimethylphenol, which is subsequently detected photometrically. The measuring range of the kit was 0.1 – 25 mg NO_3^- /L and the wavelength used for the photometric detection was 357 nm. The river water samples were filtered prior their measurement (0.45 μm).

Analysis of river water sample. To simulate the conditions in a real environment, the nitrate concentration of a river water sample (Arve river, Switzerland) was determined. The sample was tested without prior filtration or other treatment. Four nitrate-selective electrodes were used (two in the reference cell and two in the sample cell). The standard addition method was used for the determination of nitrate, using the following equation to linearize obtained data and calculate the concentration of the sample:

$$(V_{init} + V_{st}) \cdot 10^{\frac{E_2 - E_1}{s}} = V_{init} + \frac{1}{c_{sample,init}} \cdot c_{st} \cdot V_{st} \quad (1)$$

Where V_{init} is the initial volume of the river sample, V_{st} the volume of a standard nitrate solution added to the sample, E_2 is the potential value after the addition of the standard, E_1 is the initial potential value of the river sample, s is the response slope of the nitrate-selective electrodes determined during the calibration experiments, c_{st} is the concentration of the standard nitrate solution and $c_{sample,init}$ the unknown nitrate concentration of the river sample.

The initial potential reading corresponding to the untreated river sample was recorded. Then, a small aliquot of a known nitrate standard was added to the sample and the potential was recorded again. In total, nine sequential additions of standard nitrate solution were performed, and the nitrate concentration of the river sample was calculated using the slope of eq. 1. The EMF values were recorded every s and for each nitrate addition the last 60 potential readings (before the next addition) were averaged. This averaged potential value was used as the final EMF recording of each addition step (corresponding to E_2 from eq. 1). The detailed steps of the calculations related to the standard addition method are given in the Supporting Information.

The long-term drift of the nitrate-selective electrodes in the river water sample was examined by two additional experiments. In the first experiment, both reference and sample cells contained untreated sample while in the second experiment, the sample cell was spiked with a known quantity of nitrate

standard solution. In both cases, six nitrate-selective electrodes were used (three in the reference cell and three in the sample cell).

3.3 Results and Discussion

Typically, when a conditioning protocol is applied, the equilibration time is synonymous with the required conditioning time. The respective time period changes depending on the application; short conditioning times are preferred when rapid sensing with single-use sensors is desired while longer conditioning is acceptable when time is not of concern. [32] In addition, it is evident that any system may reach an equilibrated state after a certain time at constant environmental conditions. Taking this into account, the knowledge of the time required for the system to reach a certain potential drift becomes more important than merely the information on whether the system has reached equilibrium or not. This knowledge should be one of the characteristics used to evaluate the quality of a given ISE. [33] However, it is important to note that the threshold for defining what is considered as an acceptable drift is not universal. When the conditioning step is omitted, researchers choose their own threshold values to judge whether their system is equilibrated. For example, in an earlier study [8] the arbitrary value of 0.3 mV/min was used as threshold to enable the comparison between different potentiometric systems. Electrodes with a drift value lower than the threshold were considered sufficiently conditioned.

The advantage of using the principle of symmetry is here quite evident. In a conventional solid-contact potentiometric system, the potential reading corresponds to the indicator electrode measured against a reference electrode of different nature, as for example in the case of Ag/AgCl reference electrodes. Differences in the environment will affect differently the potential developed at the reference and indicator electrodes, as demonstrated in a recent study from our group. [9] In the symmetric system, the reference electrode is now an exact copy of the indicator electrode: both electrodes are influenced in the same way by the environment (e.g. from differences in temperature) and demonstrate very similar potential values. When one is measured against the other, any influence from the environment on the potential reading is cancelled, and what is remaining is the influence of the different analyte activities between the reference and sample cells. In this study the application of symmetry resulted in a potential drift that rapidly approached a zero value as opposed to the asymmetric system where the drift decreased at a slower rate. In the latter case, the contribution of ion-exchange to the potential drift observed during conditioning is expected to be minimal due to the presence of primary ions in the sensing membrane (use of TDMAN for nitrate-selective electrodes and KTFPB for potassium-selective electrodes). Instead, we expect that the water uptake -and maybe other factors like leaching of membrane components- are responsible for the potential drift (see **Figure 3.2**, orange trace). The influence of water penetration in the membrane has also been examined in other studies [26,28] that use membranes including the primary ion (as in our case) with the potential drifts observed ranging between 40 – 200 mV. The equilibration times in these studies were shorter compared to our case due to the highly concentrated conditioning solutions used.

The long-term potential drift of the unconditioned nitrate-selective electrodes upon first solution contact is shown in **Figure 3.2**. When both reference and sample cells were kept at the same concentration (0.1 mM $NaNO_3$), the potential in the symmetric system fluctuated around the value of 0 mV until the end of the 20-h period, reaching a drift of 0.3 mV/min in less than 10 minutes. The drift continued to decrease and approached a value close to zero (0.003 ± 0.002 mV/min) after 20 h. In the asymmetric system using a conventional Ag/AgCl outer reference element, the potential was continuously drifting until the end of the monitoring period. In total, it decreased by 20 mV with a drift of 0.98 ± 0.09 mV/h (at t = 20 h) compared to the drift for the symmetric system of 0.15 ± 0.09 mV/h. After the experiment, the electrodes were calibrated to give a slope close to 56 mV/dec, confirming their Nernstian behavior (**Figure S3.1**).

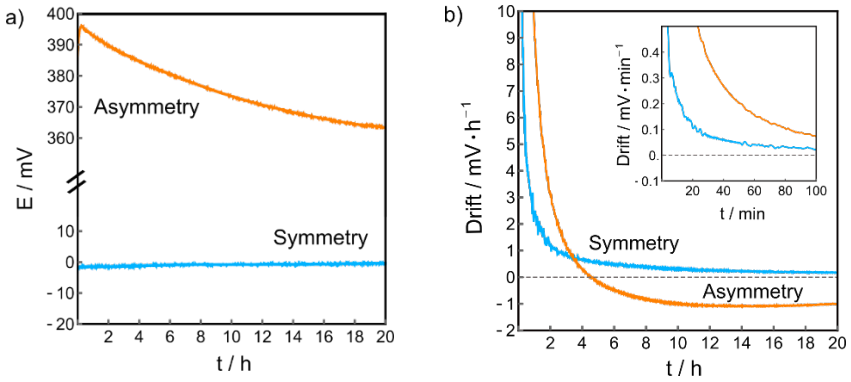

Figure 3.2: a) Observed potential change and b) corresponding potential drift in mV/h for 20-h following initial contact to a solution containing 0.1 mM NO_3^-. Inset: potential drift for the first 100 min shown for clarity.

The 5-day drift of nitrate-selective electrodes was examined using another set of unconditioned electrodes. The calibrations performed daily showing a clear difference between the symmetric and asymmetric system, mainly in relation to the first day of measurement, which corresponds to the actual conditioning of the electrodes (**Figure 3.3**a,b). The influence of the absence of conditioning disappears in the symmetric system where the electrodes used as reference are experiencing the same potential drift with the indicator electrodes. The average E^0 value of the five days was -231.4 ± 2.9 mV in the symmetric system and the zero potential value was measured at a nitrate activity of 0.073 ± 0.007 mM which is close to the nitrate activity in the reference cell (0.1 mM NO_3^-). In the asymmetric system, the average E^0 value of the five days was 121.7 ± 19.0 mV, showing a larger standard deviation, as expected. The slope remained stable in both cases, with an average value of 55.9 ± 0.3 mV/dec. To visualize the evolution of the electrodes response over time, **Figure 3.3**c shows the results from a single pair of electrodes, where the logarithmic activity that corresponds to the zero point (E = 0 mV) is plotted against the 5 days. The error bars presented here are standard deviations for the same electrode (n = 3). In the other two experiments of long-term potential monitoring (when the sample cell was kept at 0.5 mM and 1 mM $NaNO_3$) the drift for the symmetric system dropped below 0.1 mV/min in less than 10 minutes,

while the asymmetric system reached the same level of drift after more than an hour of monitoring. Detailed graphs are presented in the supporting information (**Figure S3.2**).

All results obtained from the long-term drift experiments correlated well with the actual response of the nitrate-selective electrodes when calibrated on a day-by-day basis. For example, in the long-term drift experiment where the sample and reference cells differed by one order of magnitude (in concentration terms), the potential in the symmetric system was -55.2 ± 3.4 mV at t = 0, remaining stable during the whole monitoring period ($E_{t=20h}$ = -54.6 ± 1.6 mV). These values were close to the electrodes slope measured during the 5-day experiments (55.9 ± 0.3 mV/dec, average value), confirming the excellent performance for both types of experiments.

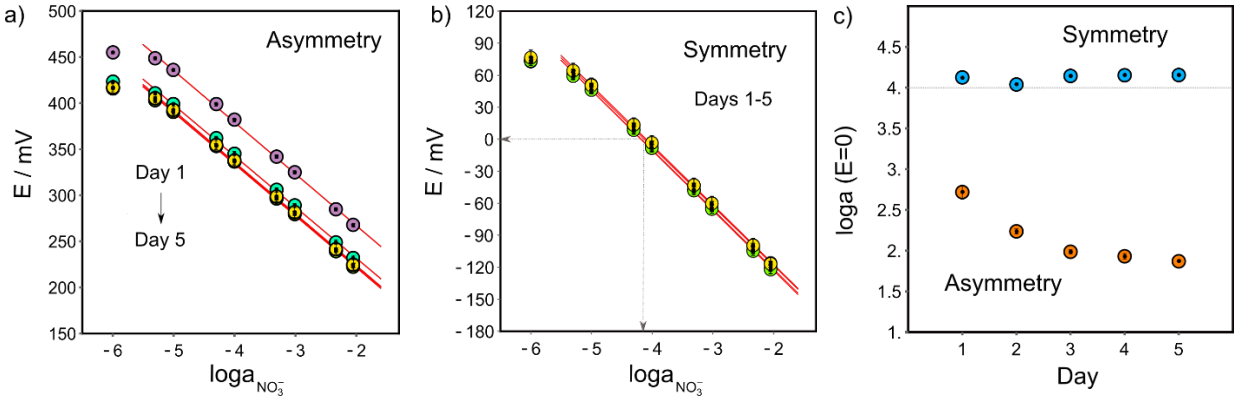

Figure 3.3: a) Calibration for days 1-5 in the asymmetric and b) symmetric system for nitrate and c) reproducibility of the zero point (the logarithmic nitrate sample activity giving a cell potential of zero) over 5 days for both systems.

By using the symmetric system presented in this study unconditioned ISEs may be used directly for potentiometric measurements while exhibiting the expected Nernstian response of conventional systems. The principle was initially tested with nitrate-selective electrodes, since nitrate is one of the target analytes for environmental studies and similar research on the use of unconditioned electrodes is missing.

Based on literature reports, potassium-selective electrodes are expected to give a low potential drift when used without prior conditioning.[8] To examine whether we would obtain a similar potential stability with our symmetric/asymmetric principle, we performed the same set of experiments as above, but by using potassium-selective electrodes. Indeed, during the 5-day drift experiments the electrodes remained relatively stable between the first and fifth day of measurements, even in the asymmetric system (**Figure 3.4**). The 5-day average E^0 value in the latter system was 281.7 ± 3.8 mV, compared to 164.2 ± 1.8 mV measured in the symmetric system. The slope in both cases remained stable, with an average value of 56.7 ± 0.5 mV. This result may explain the success of literature reports for the detection of potassium with unconditioned membranes, [29,30] although the reasons for this are as yet unclear.

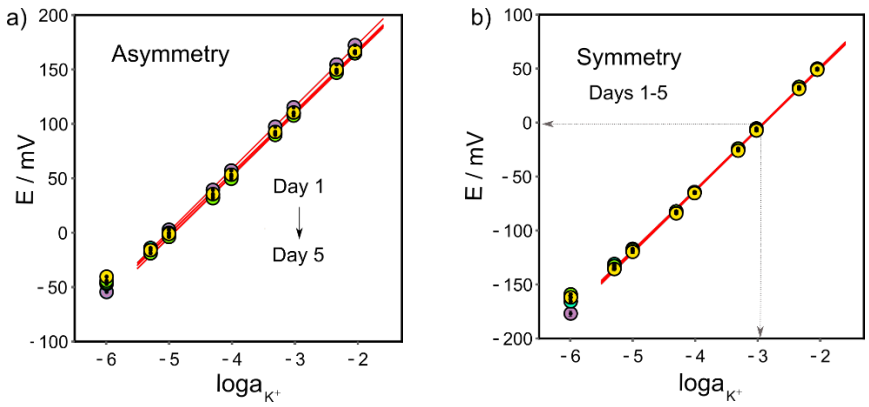

Figure 3.4: Calibration for days 1-5 in the asymmetric (a) and symmetric system (b) for measuring potassium.

Similarly, the long-term drift ranged between 0.10 – 0.13 mV/h (at t = 20 h) for both the symmetric and asymmetric systems when the activity in the reference/sample cells was 1 mM / 10 mM KNO_3 (1st experiment) and 1 mM / 5 mM (2nd experiment). In the third experiment (when both the reference and sample cells were kept in 1 mM KNO_3) the respective potential drift varied between 0.32 – 0.87 mV/h, however, it should be noted that the total duration here was 15 h instead of 20 h as in the previous two cases. Detailed graphs on the performance of the potassium-selective electrodes are given in the Supporting Information (**Figure S3.3**). Interestingly, the evolution of the drift over time showed the same trend as in the case of nitrate electrodes. In all three experiments, the drift minimized at a faster rate in the symmetric system. In the aforementioned literature study[8] where the threshold drift of 0.3 mV/min was used to determine the minimum equilibration time, the unconditioned K^+-ISEs stabilised after approximately 10 minutes. These results are surprising considering that the transducer used was the highly hydrophilic PEDOT(PSS), a conducting material that is prone to the formation of an internal aqueous layer between the membrane and the solid contact. [34] This water layer can induce an important potential instability, which is not expected to be present to that extent with the hydrophobic carbon nanotubes used in this study. Despite the differences in hydrophobicity between those two transducers, the average time to reach the same threshold of potential drift in the asymmetric system presented here was somewhat higher, but still comparable (30.6 ± 3.8 min instead of 10 min). Conversely, the 0.3 mV/min threshold was met in less than 10 minutes (5.3 ± 4.2 min) when symmetry was applied.

The applicability of the symmetric setup was examined by measuring the nitrate concentration of a river water sample using the standard addition method (**Figure S3.4**a,b). The slope used in the equation of the standard addition method was the average slope of the symmetric system from the 5-day drift experiment discussed above (-55.9 mV/dec) which did not change significantly in those five days (SD = 0.3 for the five days). The concentration of nitrate in the river sample was measured as 102.5 ± 0.5 µM NO_3^- (n = 4) which correlated well with the results from photometry (102.2 ± 1.4 µM NO_3^-, n = 3) used as a reference technique, with an error of just 0.3 %. After the determination of nitrate in the river

sample, the electrodes were calibrated with standard nitrate solutions in Milli-Q environment, showing a Nernstian response (**Figure S3.4**c).

The long-term potential drift was examined by keeping both reference and sample cells in the same untreated river sample. In the asymmetric system, the difference between the maximum and minimum potential value recorded for the 20-h monitoring period was 22 mV and the drift at t = 20 h was 0.60 ± 0.11 mV/h. The respective values for the symmetric system were 5 mV and 0.20 ± 0.10 mV/h. After just 10 min after initial solution contact the drift dropped to below 0.07 mV/min and remained at this level for the entire duration of the experiment (see blue trace in inset of **Figure 3.5**).

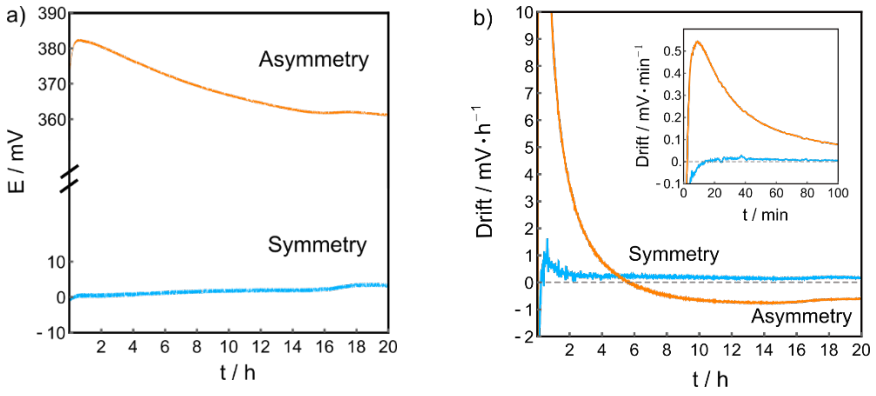

Figure 3.5: a) Observed potential change and b) corresponding potential drift in mV/h over a period of 20-h upon initial contact with an untreated river sample. Inset: potential drift for the first 100 min shown for clarity.

In a separate experiment, unconditioned nitrate-selective electrodes were immersed in river water. The reference cell contained untreated river sample while the sample cell was in contact with the same river water with an added quantity of nitrate standard solution, increasing its concentration from 102.2 µM NO_3^- to 372 µM NO_3^-. In the symmetric system, the average value of the potential reading for the entire 20 h duration of the monitoring period was -31.1 ± 2.1 mV (n = 18) (**Figure S3.5**a). Using the Nernstian equation, the slope corresponding to this potential value was calculated as -55.4 mV/dec, confirming the Nerstian behavior of the electrodes in the river water sample and the absence of a matrix effect. The drift at the end of the monitoring period was 0.76 ± 0.04 mV/h and 0.09 ± 0.07 mV/h for the asymmetric and symmetric system, respectively, with the latter maintaining a drift lower than 0.1 mV/min already from the third minute of exposure to the river sample (**Figure S3.5**b).

The above findings demonstrate that with the symmetric setup suggested here one may measure the nitrate concentration of a freshwater sample with unconditioned electrodes by using the slope from the calibration of unconditioned electrodes. We showed that the slope calculated in the laboratory setting (electrolyte in pure water) is almost identical to the one obtained in the real water sample (with a 0.9 % error), confirming that the knowldege of the latter is not required for the calculations of the nitrate concentration in the unknown freshwater sample. The application of the proposed system for the

detection of analytes in more complex media (e.g. biological samples) is also feasible. In this case, one may consider the potentials that can arise from the adsorption of sample components onto the membrane, which have been shown that are insignificant. The asymmetry potential that arises when sodium-selective membranes are brought in contact with diluted solution of bovine serum albumin (BSA) has been studied[35], demonstrating that the potential change after the protein contact with the membrane is in the order of few milivolts (< 3 mV). Another study [36] examining the influence of the adsorption of BSA and polyethylenimine on calcium-selective membranes showed that there is practically no effect in the response when the electrodes are used in the potentiometric mode, with the highest potential diffrence observed being approximately 3 mV. As stated, the potentiometric response is governed by local extraction equilibria and if the adsorbed components are not influencing these equilibria there will be no effect on the electrodes response. Overall, the small intereference observed by the adsorption of sample components in the membrane cannot be eliminated, but it is not expected to influence the function of the sensors. Nevertheless, the study of similar and other adsorption phenomena onto the surface of polymeric membranes is not the scope of the current study.

3.4 Conclusions

A symmetric setup with unconditioned solid-contact ISEs shows comparable long-term potential stability as well as detection ranges and Nernstian responses to conditioned membranes, and is clearly superior compared to asymmetric approaches with unconditioned electrodes. Identical electrodes in both compartments of the symmetric setup make it possible to achieve an effective differential potential measurement between reference and indicator electrodes. This allows for the near-complete elimination of potential drifts originating from environmental changes as well as those related to the water uptake of the membrane during the conditioning procedure. The nitrate- and potassium-selective electrodes tested here were based on plasticized PVC sensing membranes deposited on top of functionalized carbon nanotubes, but the principle can be applied to ion-selective electrodes of different membrane materials and transducers. The nitrate concentration of a river water sample was measured using the proposed system with an error of just 0.3 % compared to the reference technique. In addition, the potential drift reported during the long-term monitoring in the untreated river water sample dropped below 0.1 mV/min after a few minutes of initial contact with the sample. These promising results open the way for more applications based on the presented symmetric approach, enabling the use of solid contact electrodes "out-of-the-box" without the need of a lengthy conditioning step that limits the practical application of potentiometric measurements.

3.5 Supporting Information

3.5.1 Corrections in the potential values for the symmetric setup

All electrodes in the reference and sample cells were subject to the same junction potential, E_j, that arose from the main liquid double junction reference electrode. This is the principal reference electrode

connected to the Lawson potentiostat, together with the electrodes of both the reference and sample cells. Moreover, an additional junction potential emerged from the two liquid junction reference electrodes used as a bridge between the cells. Although these electrodes were identical, they each manifested a different junction potential, since they were subject to different concentrations of the principal ion: the reference cell was kept at a constant concentration, while the sample cell was subject to varying concentrations (during the calibration experiments). This additional contribution is denoted as dE and corresponded to the difference of the junction potential between the reference cell (E_j^{ref}) and the sample cell (E_j^{sample}). For the correction of this contribution, dE was added to the potential readout of the reference cell:

$$E^{sample} = E_{meas}^{sample} - E_j \qquad (1)$$

$$E^{ref} = E_{meas}^{ref} - E_j + dE \qquad (2)$$

$$dE = E_j^{sample} - E_j^{ref} \qquad (3)$$

where E_{meas}^{sample} and E_{meas}^{ref} refer to the raw EMF readouts from Lawson.

For applying the principle of symmetry between the two cells, the corrected potential of the reference cell was subtracted from the one of the indicator cell, resulting in the final potential value for the symmetric system, E_{sym}:

$$E^{sym} = E^{sample} - E^{ref} \xrightarrow{(1),(2)}$$

$$E^{sym} = E_{meas}^{sample} - E_{meas}^{ref} - dE$$

And the potential value for the asymmetric system, E^{asym}:

$$E^{asym} = E_{meas}^{sample} - E_j$$

The liquid junction potentials were calculated using the Henderson equation ($u_{NO_3^-} = 7.58 \cdot 10^{-4} cm^2 \cdot s^{-1} \cdot V^{-1}, u_{Na^+} = 5.47 \cdot 10^{-4} cm^2 \cdot s^{-1} \cdot V^{-1}, u_{OAc^-} = 4.38 \cdot 10^{-4} cm^2 \cdot s^{-1} \cdot V^{-1}, u_{Li^+} = 4.24 \cdot 10^{-4} cm^2 \cdot s^{-1} \cdot V^{-1}$, $u_{K^+} = 8.00 \cdot 10^{-4} cm^2 \cdot s^{-1} \cdot V^{-1}$).

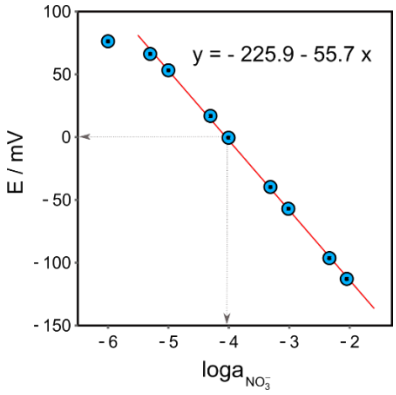

Figure S3.1: Calibration (symmetric system) after the long-term exposure of nitrate-selective electrodes in 0.1 mM $NaNO_3$ (both reference and sample cell).

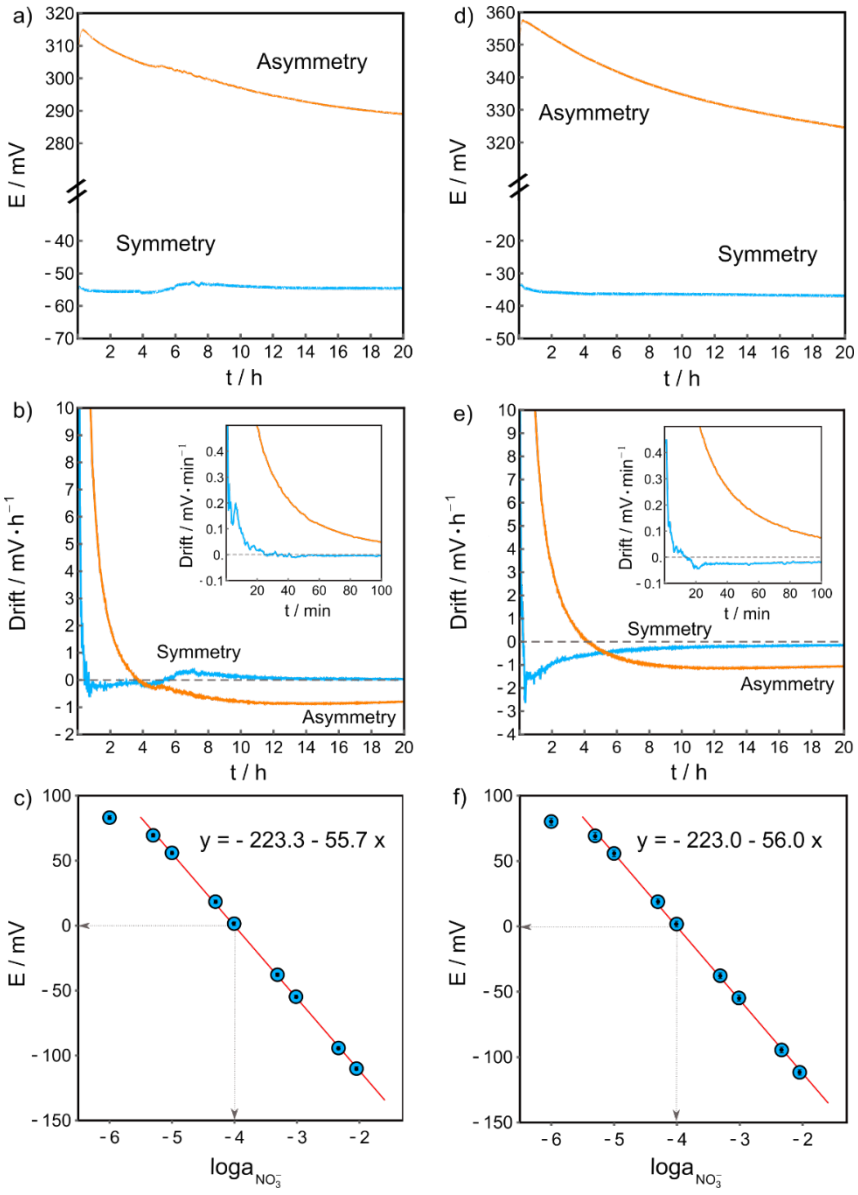

Figure S3.2: a) Observed potential change, b) corresponding potential drift in mV/h for 20-h following initial contact to a solution containing 1 mM NO_3^-, and c) calibration after the long-term exposure; d)

Observed potential change, e) corresponding potential drift in mV/h for 20-h following initial contact to a solution containing 0.5 mM NO_3^-, and f) calibration after the long-term exposure. The calibrations presented above refer to the symmetric system. Insets: potential drift for the first 100 min shown for clarity.

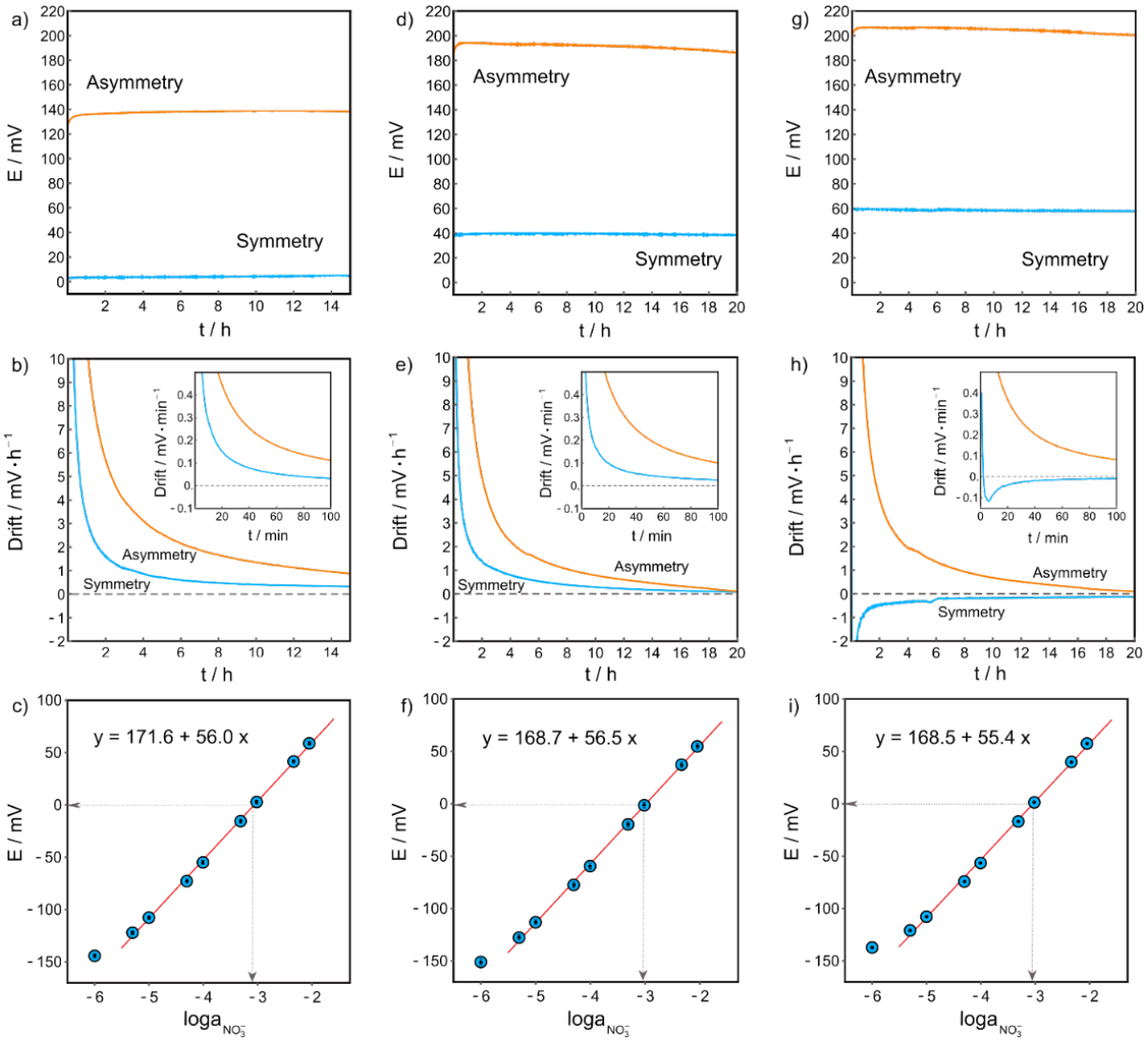

Figure S3.3: a) Observed potential change, b) corresponding potential drift in mV/h for 15-h following initial contact to a solution containing 1 mM K^+, and c) calibration after the long-term exposure; d) Observed potential change, e) corresponding potential drift in mV/h for 20-h following initial contact to a solution containing 5 mM K^+, and f) calibration after the long-term exposure; g) Observed potential change, h) corresponding potential drift in mV/h for 20-h following initial contact to a solution containing 10 mM K^+, and i) calibration after the long-term exposure; The calibrations presented above refer to the symmetric system. Insets: potential drift for the first 100 min shown for clarity.

3.5.2 Calculations for the application of the Standard Addition Method

The potentiometric response of the nitrate-selective electrode in the river water sample -before any standard addition- can be described by the following equation:

$$E_1 = E^0 + s \cdot loga_{sample,init} \rightarrow a_{NO_3^-} = \gamma_{sample} \cdot c_{sample,init} = 10^{\frac{E_1 - E^0}{s}} \rightarrow c_{sample,init} = \gamma_{sample}^{-1} \cdot 10^{\frac{E_1 - E^0}{s}} \quad (1)$$

where $c_{sample,init}$ is the nitrate concentration in the river water sample, E_1 the corresponding EMF readout, E^0 all the stable potential contributions present in the cell, γ_{sample} the activity of nitrate and s the potentiometric response slope of the nitrate-selective electrodes.

Similarly, after the addition of standard, the concentration of the sample can be described as following:

$$c_{sample} = \gamma_{sample}^{-1} \cdot 10^{\frac{E_2 - E^0}{s}} \quad (2)$$

where E_2 is the corresponding EMF readout after the standard addition.

When an aliquot of standard nitrate solution, V_{st} , is added to the sample, the following equilibrium is established:

$$n_{sample} = n_{sample,init} + n_{st} \rightarrow$$

$$c_{sample} \cdot V_{sample} = c_{sample,init} \cdot V_{init} + c_{st} \cdot V_{st} \rightarrow$$

$$c_{sample} \cdot (V_{init} + V_{st}) = c_{sample,init} \cdot V_{init} + c_{st} \cdot V_{st} \xrightarrow{(2)}$$

$$\gamma_{sample}^{-1} \cdot 10^{\frac{E_2 - E^0}{s}} \cdot (V_{init} + V_{st}) = c_{sample,init} \cdot V_{init} + c_{st} \cdot V_{st} \xrightarrow{\div c_{sample,init}}$$

$$\frac{10^{\frac{E_2 - E^0}{s}} \cdot (V_{init} + V_{st})}{\gamma_{sample} \cdot c_{sample,init}} = \frac{c_{sample,init} \cdot V_{init} + c_{st} \cdot V_{st}}{c_{sample,init}} \xrightarrow{(1)}$$

$$\frac{10^{\frac{E_2 - E^0}{s}} \cdot (V_{init} + V_{st})}{\gamma_{sample} \cdot \gamma_{sample}^{-1} \cdot 10^{\frac{E_1 - E^0}{s}}} = \frac{c_{sample,init} \cdot V_{init} + c_{st} \cdot V_{st}}{c_{sample,init}} \rightarrow$$

$$(V_{init} + V_{st}) \cdot 10^{\frac{E_2 - E_1}{s}} = V_{init} + \frac{1}{c_{sample,init}} \cdot c_{st} \cdot V_{st} \quad (3)$$

By plotting the potential readouts and concentrations from the nine standard additions performed to the above equation (which has the form $y = b + a \cdot x$), we found the initial nitrate concentration of the river water sample, which was equal to the reverse of the slope.

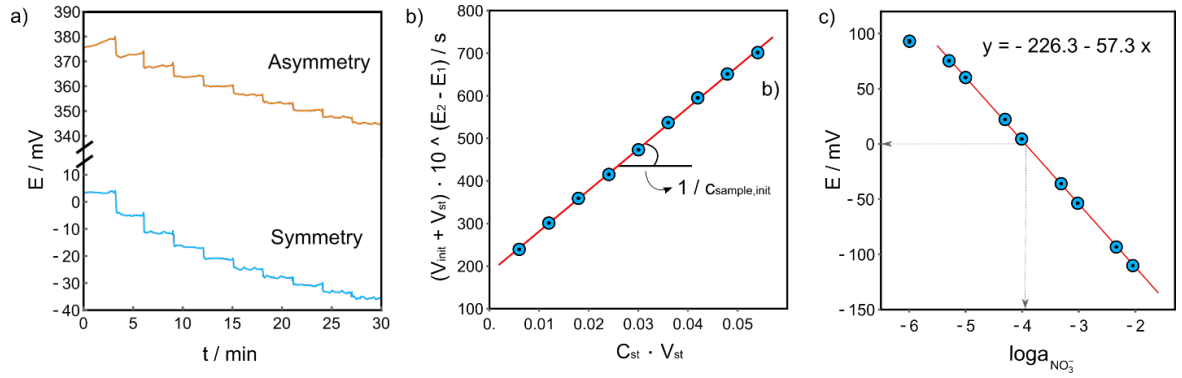

Figure S3.4: a) EMF readouts during the nine additions of standard nitrate aliquots for the symmetric and asymmetric system, b) plot of the equation of Standard Addition method (eq. 3) for the calculation of the initial nitrate concentration in the river water sample, and c) calibration (n = 4) of the nitrate-selective electrodes in Milli-Q after the 9-point determination of unknown river water sample.

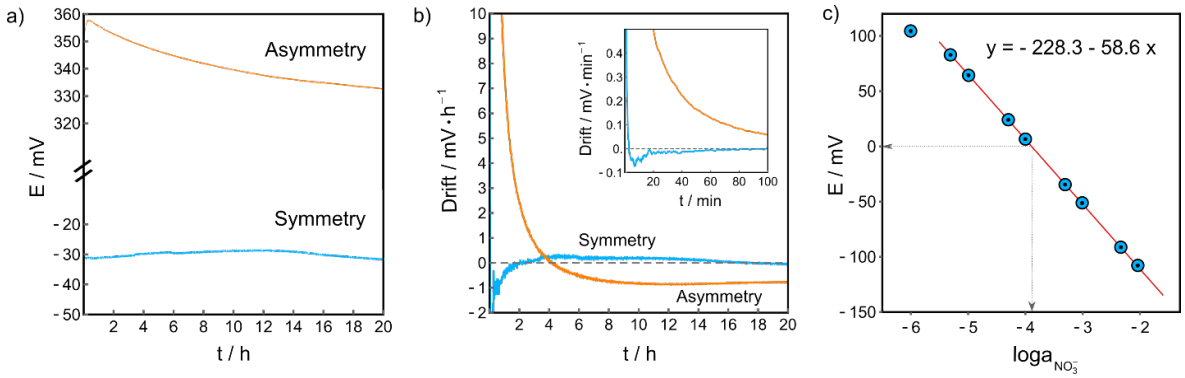

Figure S3.5: a) Observed potential change and b) corresponding potential drift in mV/h for 20-h following initial contact to a solution containing untreated river sample spiked with nitrate standard to a final concentration of 372 µM NO_3^- (with the reference cell containing untreated river water sample), and c) calibration (n=9) after the long-term exposure using nitrate standard solutions in Milli-Q. Inset: potential drift for the first 100 min shown for clarity.

3.6 References

(1) Hu, J.; Stein, A.; Bühlmann, P. Rational Design of All-Solid-State Ion-Selective Electrodes and Reference Electrodes. *TrAC Trends in Analytical Chemistry* **2016**, *76*, 102–114. https://doi.org/10.1016/j.trac.2015.11.004.

(2) Bakker, E.; Bühlmann, P.; Pretsch, E. Carrier-Based Ion-Selective Electrodes and Bulk Optodes. 1. General Characteristics. *Chem. Rev.* **1997**, *97* (8), 3083–3132. https://doi.org/10.1021/cr940394a.

(3) Lindfors, T.; Sundfors, F.; Höfler, L.; Gyurcsányi, R. E. FTIR-ATR Study of Water Uptake and Diffusion Through Ion-Selective Membranes Based on Plasticized Poly(Vinyl Chloride). *Electroanalysis* **2009**, *21* (17–18), 1914–1922. https://doi.org/10.1002/elan.200904609.

(4) Pocsai, D.; Höfler, L. Application of Potentiometric Ion-Breakthrough to Assess Individual Diffusion Coefficients of Ions in Ion-Selective Membranes. *J. Electrochem. Soc.* **2020**, *167* (14), 147506. https://doi.org/10.1149/1945-7111/abc35c.

(5) Hambly, B. P.; Sheppard, J. B.; Pendley, B. D.; Lindner, E. Voltammetric Determination of Diffusion Coefficients in Polymer Membranes: Guidelines to Minimize Errors. *Electroanalysis* **2018**, *30* (4), 681–689. https://doi.org/10.1002/elan.201700695.

(6) Lindfors, T.; Sundfors, F.; Höfler, L.; Gyurcsányi, R. E. The Water Uptake of Plasticized Poly(Vinyl Chloride) Solid-Contact Calcium-Selective Electrodes. *Electroanalysis* **2011**, *23* (9), 2156–2163. https://doi.org/10.1002/elan.201100219.

(7) Sundfors, F.; Lindfors, T.; Höfler, L.; Bereczki, R.; Gyurcsányi, R. E. FTIR-ATR Study of Water Uptake and Diffusion through Ion-Selective Membranes Based on Poly(Acrylates) and Silicone Rubber. *Anal. Chem.* **2009**, *81* (14), 5925–5934. https://doi.org/10.1021/ac900727w.

(8) Guzinski, M.; Jarvis, J. M.; Pendley, B. D.; Lindner, E. Equilibration Time of Solid Contact Ion-Selective Electrodes. *Anal. Chem.* **2015**, *87* (13), 6654–6659. https://doi.org/10.1021/acs.analchem.5b00775.

(9) Zdrachek, E.; Forrest, T.; Bakker, E. Solid-Contact Potentiometric Cell with Symmetry. *Anal. Chem.* **2022**, *94* (2), 612–617. https://doi.org/10.1021/acs.analchem.1c04722.

(10) de los A. Arada Pérez, M.; Marín, L. P.; Quintana, J. C.; Yazdani-Pedram, M. Influence of Different Plasticizers on the Response of Chemical Sensors Based on Polymeric Membranes for Nitrate Ion Determination. *Sensors and Actuators B: Chemical* **2003**, *89* (3), 262–268. https://doi.org/10.1016/S0925-4005(02)00475-6.

(11) Paczosa-Bator, B.; Piech, R.; Lewenstam, A. Determination of the Leaching of Polymeric Ion-Selective Membrane Components by Stripping Voltammetry. *Talanta* **2010**, *81* (3), 1003–1009. https://doi.org/10.1016/j.talanta.2010.01.048.

(12) Wojciechowski, K.; Linek, K. Anion Selectivity at the Aqueous/Polymeric Membrane Interface: A Streaming Current Study of Potentiometric Hofmeister Effect. *Electrochimica Acta* **2012**, *71*, 159–165. https://doi.org/10.1016/j.electacta.2012.03.113.

(13) Fibbioli, M.; Bandyopadhyay, K.; Liu, S.-G.; Echegoyen, L.; Enger, O.; Diederich, F.; Gingery, D.; Bühlmann, P.; Persson, H.; Suter, U. W.; Pretsch, E. Redox-Active Self-Assembled Monolayers for Solid-Contact Polymeric Membrane Ion-Selective Electrodes. *Chem. Mater.* **2002**, *14* (4), 1721–1729. https://doi.org/10.1021/cm0109589.

(14) Veder, J.-P.; Marco, R. D.; Clarke, G.; Jiang, S. P.; Prince, K.; Pretsch, E.; Bakker, E. Water Uptake in the Hydrophilic Poly(3,4-Ethylenedioxythiophene):Poly(Styrene Sulfonate) Solid-Contact of All-Solid-State Polymeric Ion-Selective Electrodes. *Analyst* **2011**, *136* (16), 3252–3258. https://doi.org/10.1039/C1AN15267J.

(15) Gyurcsányi, R. E.; Rangisetty, N.; Clifton, S.; Pendley, B. D.; Lindner, E. Microfabricated ISEs: Critical Comparison of Inherently Conducting Polymer and Hydrogel Based Inner Contacts. *Talanta* **2004**, *63* (1), 89–99. https://doi.org/10.1016/j.talanta.2003.12.002.

(16) Lindfors, T.; Höfler, L.; Jágerszki, G.; Gyurcsányi, R. E. Hyphenated FT-IR-Attenuated Total Reflection and Electrochemical Impedance Spectroscopy Technique to Study the Water Uptake and Potential Stability of Polymeric Solid-Contact Ion-Selective Electrodes. *Anal. Chem.* **2011**, *83* (12), 4902–4908. https://doi.org/10.1021/ac200597b.

(17) Sutter, J.; Radu, A.; Peper, S.; Bakker, E.; Pretsch, E. Solid-Contact Polymeric Membrane Electrodes with Detection Limits in the Subnanomolar Range. *Analytica Chimica Acta* **2004**, *523* (1), 53–59. https://doi.org/10.1016/j.aca.2004.07.016.

(18) Bratov, A.; Abramova, N.; Domínguez, C. Lowering the Detection Limit of Calcium Selective ISFETs with Polymeric Membranes. *Talanta* **2004**, *62* (1), 91–96. https://doi.org/10.1016/S0039-9140(03)00402-8.

(19) Lisak, G.; Ivaska, A.; Lewenstam, A.; Bobacka, J. Multicalibrational Procedure for More Reliable Analyses of Ions at Low Analyte Concentrations. *Electrochimica Acta* **2014**, *140*, 27–32. https://doi.org/10.1016/j.electacta.2014.02.091.

(20) Konopka, A.; Sokalski, T.; Michalska, A.; Lewenstam, A.; Maj-Zurawska, M. Factors Affecting the Potentiometric Response of All-Solid-State Solvent Polymeric Membrane Calcium-Selective Electrode for Low-Level Measurements. *Anal. Chem.* **2004**, *76* (21), 6410–6418. https://doi.org/10.1021/ac0492158.

(21) Szigeti, Z.; Vigassy, T.; Bakker, E.; Pretsch, E. Approaches to Improving the Lower Detection Limit of Polymeric Membrane Ion-Selective Electrodes. *Electroanalysis* **2006**, *18* (13–14), 1254–1265. https://doi.org/10.1002/elan.200603539.

(22) Forrest, T.; Zdrachek, E.; Bakker, E. Thin Layer Membrane Systems as Rapid Development Tool for Potentiometric Solid Contact Ion-Selective Electrodes. *Electroanalysis* **2020**, *32* (4), 799–804. https://doi.org/10.1002/elan.201900674.

(23) Ceresa, A.; Bakker, E.; Hattendorf, B.; Günther, D.; Pretsch, E. Potentiometric Polymeric Membrane Electrodes for Measurement of Environmental Samples at Trace Levels: New Requirements for Selectivities and Measuring Protocols, and Comparison with ICPMS. *Anal. Chem.* **2001**, *73* (2), 343–351. https://doi.org/10.1021/ac001034s.

(24) Rich, M.; Mendecki, L.; Mensah, S. T.; Blanco-Martinez, E.; Armas, S.; Calvo-Marzal, P.; Radu, A.; Chumbimuni-Torres, K. Y. Circumventing Traditional Conditioning Protocols in Polymer Membrane-Based Ion-Selective Electrodes. *Anal. Chem.* **2016**, *88* (17), 8404–8408. https://doi.org/10.1021/acs.analchem.6b01542.

(25) Michalska, A.; Pyrzyńska, K.; Maksymiuk, K. Method of Achieving Desired Potentiometric Responses of Polyacrylate-Based Ion-Selective Membranes. *Anal. Chem.* **2008**, *80* (10), 3921–3924. https://doi.org/10.1021/ac8000622.

(26) Kozma, J.; Papp, S.; Gyurcsányi, R. E. TEMPO-Functionalized Carbon Nanotubes for Solid-Contact Ion-Selective Electrodes with Largely Improved Potential Reproducibility and Stability. *Anal. Chem.* **2022**, *94* (23), 8249–8257. https://doi.org/10.1021/acs.analchem.2c00395.

(27) Cosofret, V. V.; Erdösy, M.; Lindner, E.; Johnson, T. A.; Buck, R. P.; Kao, W. J.; Neuman, M. R.; Anderson, J. M. Ion-Selective Microchemical Sensors with Reduced Preconditioning Time. Membrane Biostability Studies and Applications in Blood Analysis. *Analytical Letters* **1994**, *27* (15), 3039–3063. https://doi.org/10.1080/00032719408000310.

(28) Guzinski, M.; Jarvis, J. M.; Perez, F.; Pendley, B. D.; Lindner, E.; De Marco, R.; Crespo, G. A.; Acres, R. G.; Walker, R.; Bishop, J. PEDOT(PSS) as Solid Contact for Ion-Selective Electrodes: The Influence of the PEDOT(PSS) Film Thickness on the Equilibration Times. *Anal. Chem.* **2017**, *89* (6), 3508–3516. https://doi.org/10.1021/acs.analchem.6b04625.

(29) Ruecha, N.; Chailapakul, O.; Suzuki, K.; Citterio, D. Fully Inkjet-Printed Paper-Based Potentiometric Ion-Sensing Devices. *Anal. Chem.* **2017**, *89* (19), 10608–10616. https://doi.org/10.1021/acs.analchem.7b03177.

(30) Hu, J.; Stein, A.; Bühlmann, P. A Disposable Planar Paper-Based Potentiometric Ion-Sensing Platform. *Angew. Chem. Int. Ed.* **2016**, *55* (26), 7544–7547. https://doi.org/10.1002/anie.201603017.

(31) Ding, J.; Li, B.; Chen, L.; Qin, W. A Three-Dimensional Origami Paper-Based Device for Potentiometric Biosensing. *Angewandte Chemie International Edition* **2016**, *55* (42), 13033–13037. https://doi.org/10.1002/anie.201606268.

(32) Rousseau, C. R.; Bühlmann, P. Calibration-Free Potentiometric Sensing with Solid-Contact Ion-Selective Electrodes. *TrAC Trends in Analytical Chemistry* **2021**, *140*, 116277. https://doi.org/10.1016/j.trac.2021.116277.

(33) Lindner, E.; Gyurcsányi, R. E. Quality Control Criteria for Solid-Contact, Solvent Polymeric Membrane Ion-Selective Electrodes. *J Solid State Electrochem* **2009**, *13* (1), 51–68. https://doi.org/10.1007/s10008-008-0608-1.

(34) Pławińska, Ż.; Michalska, A.; Maksymiuk, K. Optimization of Capacitance of Conducting Polymer Solid Contact in Ion-Selective Electrodes. *Electrochimica Acta* **2016**, *187*, 397–405. https://doi.org/10.1016/j.electacta.2015.11.050.

(35) Duerselen, L. F. J.; Wegmann, Dorothee.; May, Kurt.; Oesch, Urs.; Simon, Wilhelm. Elimination of the Asymmetry in Neutral-Carrier Based Solvent Polymeric Membranes Induced by Proteins. *Anal. Chem.* **1988**, *60* (14), 1455–1458. https://doi.org/10.1021/ac00165a021.

(36) Xu, Y.; Xu, C.; Shvarev, A.; Becker, T.; De Marco, R.; Bakker, E. Kinetic Modulation of Pulsed Chronopotentiometric Polymeric Membrane Ion Sensors by Polyelectrolyte Multilayers. *Anal. Chem.* **2007**, *79* (18), 7154–7160. https://doi.org/10.1021/ac071201p.

Chapter 4. Avoiding Potential Pitfalls in Designing Wired Glucose Biosensors

(This chapter is based on the following paper: Damala, P.; Tiuftiakov, Yu. N.; Bakker, E. Avoiding Potential Pitfalls in Designing Wired Glucose Biosensors, *ACS Sens.* **2024**, *9* (1), 2–8. https://doi.org/10.1021/acssensors.3c01960)

4.1 Introduction

Glucose biosensors are today ubiquitous in diabetes management, with many commercialized blood tests exhibiting adequate sensitivity and reliability for single home use. [1] Today, one strives to perform glucose detection in situ and continuously, with minimally invasive sensors that are reliable, sensitive, low cost and often wearable. Many recent studies target alternative biofluids including tears, saliva, sweat and urine in the hopes of correlating the resulting glucose levels with those in blood. [2,3] Many newly developed biosensors focus more on the engineering side than on the understanding of the underlying chemistry. The same sensor preparation procedure is often repeated study after study, focusing more on form factor than on the principles governing their response. Principal limiting factors of the sensors are therefore often not studied or discussed, which hampers important progress. In this perspectives article, we focus on so-called "wired" glucose electrodes and aim to remind the reader of key aspects that govern and limit their response.

Enzyme "wiring" refers to the establishment of electrical communication between the enzyme and the electrode, made possible with the introduction of bound electron mediators that reduce or oxidize the active site of the enzyme and shuttle the electrons to and from the electrode surface. An important example of sensors employing such mediated electron transfer is found in Cass et al. who developed a second-generation glucose electrode based on ferrocene deposited on a graphite electrode with a top layer of covalently immobilized glucose oxidase. [4] In the late 80s, mediated amperometric glucose biosensors were brought to the market as single use home tests. [5] Meanwhile, it became clear that enzymes often cannot exchange electrons with the electrode on which they are adsorbed because their active sites are electrically inaccessible. This is typically caused by the protective glycosylation shell surrounding the enzyme, which protects against spontaneous electron transfer in living systems. [6] For a wired enzyme to be realized, part of the shell should be either stripped or modified with redox active compounds (known as "electron relays") to make it electrically conductive. [7] Electron mediators covalently attached to the enzyme were realized by the seminal work of Heller et al. and others and were the first attempts at wired enzyme biosensors.[6–9] This was followed by studies on the stability, kinetics and enzyme activity of glucose oxidase modified with ferrocene [11–13] while other redox mediators were also examined.[14,15] To improve long-term stability and minimize toxicity from leaching, redox polymers

containing groups that can be reversibly reduced or oxidized were introduced. [16] These redox reactions may occur either within the main polymeric chain, as in the case of the conductive polymer polyaniline, or in electron mediators immobilized within the polymer.

In amperometry, the observed current reflects the slowest kinetic step in the overall process of bringing the substrate glucose into the sensing film, transforming it enzymatically and generating a measurable electron flux at the electrode. A robust, continuously operating glucose sensor should always give a current reading proportional to glucose concentration. Imposing the appropriate rate limiting step is of utmost importance to achieve this. We may typically distinguish four potentially rate-limiting steps controlling the overall conversion of glucose (see Scheme 1): (1) mass transport of substrate from the sample bulk solution to the outer sensor surface; (2) diffusion of substrate across a diffusion limiting membrane separating the sample from the enzyme layer; (3) rate of enzyme turnover and (4) rate of electron transfer from the enzyme to the electrode. **Figure 4.1** shows a typical example of a wired enzyme biosensor that includes a layer of the redox mediator, enzyme and cross-linking agent immobilized in a polymeric matrix [17] overcoated with a diffusion limiting membrane, indicating the key kinetic process mentioned above.

Driven by the desire to understand the mechanisms of electron transfer in biological systems and translate the rate of enzymatic reactions to current measurements, Albery et al. [18] and later Bartlett and Pratt [19] published theoretical treatments for enzyme electrodes based on mediated electron transfer processes. The latter work explored the different rate-limiting processes involved in mediated enzyme biosensors and provided analytical solutions and numerical simulations for each case. According to their classification, the abovementioned system shown in **Figure 4.1** is case III in which the kinetics become substrate-limited and the enzyme-substrate kinetics remain unsaturated, resulting in a response that is independent of Michaelis-Menten kinetics.

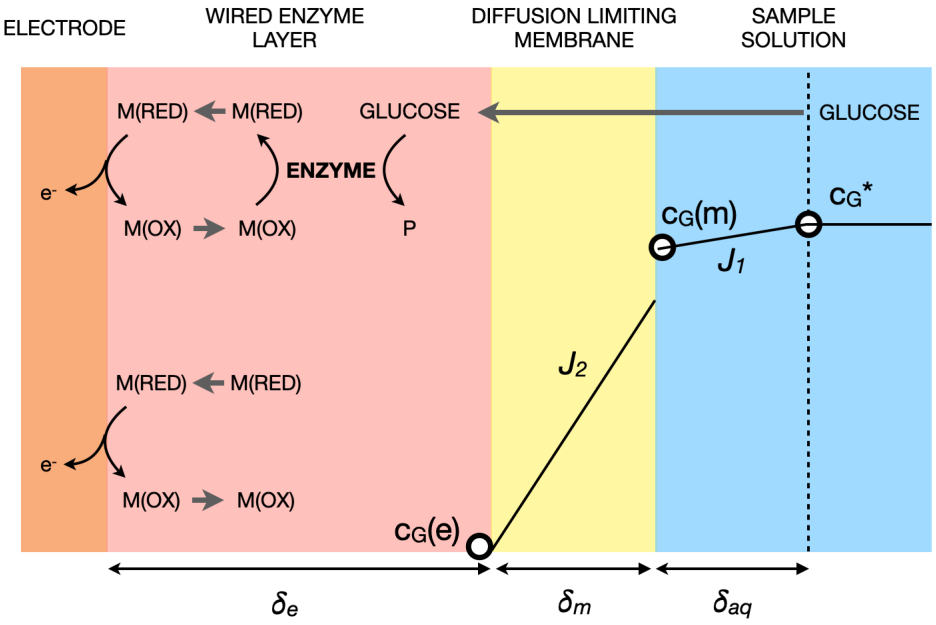

Figure 4.1: Potentially rate-limiting processes in a mediated wired enzyme biosensor: diffusion of substrate (glucose) from the sample bulk (c_G*) to the sensor surface (c_G(m)) shown as J_1; diffusion of substrate across the diffusion limiting membrane of thickness δ_m, shown as J_2; Enzyme turnover kinetics in the wired enzyme layer of thickness δ_e; Electron relay and transfer by the reduced mediator M(RED) to the electrode to produce an anodic current. If the rate limiting step is glucose diffusion across the membrane, glucose is assumed to be rapidly turned over in the enzyme layer, which explains why a glucose gradient is not drawn there. Note that current can also be produced in the absence of enzyme activity (bottom left), see also **Figure 4.4**.

The outer diffusion limiting membrane allows the diffusion of substrate to become the rate-limiting process instead of the enzyme turnover rate. In this way a partially denatured enzyme will not change the turnover rate because it does not define the rate limiting step. The membrane also shields the active electrode area against fouling and undesired interfering sample components and may help to achieve a reading independent of oxygen fluctuations.[20]

Mathematically, this is best understood by considering that there is only a single overall diffusional/reaction rate. Therefore, at steady-state the flux across each diffusional step must be the same. From Fick's law the flux J_1 across the sample diffusion layer δ_{aq} must be equal to that of J_2 across the diffusion limiting membrane of thickness δ_m (see **Figure 4.1**):

$$J_1 = D_{aq}\frac{c_G^* - c_G(m)}{\delta_{aq}} = J_2 = D_m p_G \frac{c_G(m) - c_G(e)}{\delta_m} \quad (1)$$

where p_G is the partition coefficient for glucose between the sample solution and the diffusion limiting membrane and D_{aq} and D_m are the diffusion coefficients of glucose in the indicated phase. The glucose concentration in the sample bulk is shown as c_G* while $c_G(m)$ and $c_G(e)$ are the glucose concentrations at the outer and inner side of the diffusion limiting membrane, respectively. For a continuous biosensor it seems important to suppress the influence of sample convection on the signal, which may be achieved

by imposing a sufficiently small flux J_2 across the membrane. One may further assume that $c_G(e)$ decreases substantially at the inner side of the membrane relative to $c_G(m)$ because of its turnover by the enzyme. So, if the concentration change across the sample diffusion layer should be just 1%, one obtains:

$$D_{aq}\frac{0.01c_G^*}{\delta_{aq}} = D_m p_G \frac{0.99c_G^*}{\delta_m} \qquad (2)$$

which gives the following condition:

$$\frac{\delta_{aq} D_m p_G}{\delta_m D_{aq}} < 10^{-2} \qquad (3)$$

Consequently, membranes of sufficient thickness exhibiting small partitioning coefficients and small diffusion coefficients for glucose may be suitable to achieve this goal.

A correctly formulated continuous glucose sensor should not exhibit concentration polarization at the sample side and one may substitute $c_G(m)$ with c_G* for this case. Moreover, enzyme turnover kinetics may be approximated by the established Michaelis-Menten equation and the rate should be multiplied by the enzyme layer thickness to obtain the flux J_3 in the correct units. As above, all fluxes are equal and we may write:

$$J_2 = D_m p_G \frac{c_G^*}{\delta_m} = J_3 = \delta_e \frac{v_{max} c_G(e)}{K_{max} + c_G(e)} \qquad (4)$$

where the maximum turnover is $v_{max} = k_{cat}\, c_e$ (catalytic constant multiplied by the enzyme concentration) and K_{max} is the Michaelis constant. Because the glucose concentration is greatly decreased thanks to the diffusion limiting membrane, $c_G(e) < Kmax$, and the enzyme turnover rate is proportional to substrate concentration. The relationship expressed as a function of current I for an electrode of area A is given as follows:

$$\frac{I}{2FA} = D_m p_G \frac{c_G^*}{\delta_m} = \delta_e \frac{k_{cat}\, c_e}{K_{max}} c_G(e) \qquad (5)$$

Ideally, the current is strictly limited by the second term. As the enzyme is lost by denaturization the glucose concentration in the enzyme layer, $c_G(e)$, will start to increase, and eventually the enzyme turnover process becomes the rate limiting step. This is demonstrated in **Figure S4.1** where gradual loss of enzyme activity results in a deterioration of the observed current, but only after most of the enzyme is lost. Experimental work supporting this has been beautifully demonstrated by Heller using well defined polyelectrolyte layers of variable thickness. [21]

Unfortunately, the challenges do not end here. One must make sure that the observed current quantitatively reflects enzyme turnover kinetics as shown in eq 5 to avoid background currents that may change in unpredictable ways. Two possible contributions are mentioned here. The first is the occurrence of non-faradaic charging currents which are always observed when a potential is imposed on an electrode surface because a transient current must flow to form the electrical double layer between the electrode and aqueous electrolyte solution. Depending on the solution resistance and the double layer

capacitance this charging process may be completed in a matter of milliseconds. Still, this effect has been shown to be problematic in recent work by Schuhmann with enzyme layers that are activated electrochemically after an equilibration step. [22] In continuous amperometric glucose sensors, however, charging currents are normally of no concern because the potential is not varied with time during measurement. More serious is faradaic current flow not connected to enzyme turnover.

4.2 Results & Discussion

Typical wired enzyme glucose biosensors often use relatively dense polymers containing covalently linked redox moieties that encapsulate the enzyme by cross-linking. A popular material is branched poly(ethyleneimine) (PEI) containing ferrocene (Fc), [23–26] reproduced in this work with an estimated ferrocene substitution degree of 10.7% or 1.49 M (see Supporting Information for details). PEI has characteristics that favor its use as a redox polymer. One of them is the low glass transition temperature (compared to e.g. poly(vinylpyrrolidone) or poly(vinylimidazole)) that gives it a high degree of flexibility and segmental mobility at room temperature, enhancing its electron transport capability. Its high amine density makes it chemically modifiable. By varying the degree of redox site substitution and controlling the density of cross-linking one obtains polymer structures with varying electrochemical characteristics and electrocatalytic performances. Increased cross-linking results in decreased segmental mobility, hence proper adjustment of cross-linking quantity is essential. The swelling properties of ferrocene-modified PEI films have also been studied with various electrolytes. Experiments at low and high pH have shown that modification with ferrocene moieties is not affecting the conformational changes undergone in the PEI backbone owing to protonation/deprotonation. Monobasic phosphate and perchlorate-based electrolytes have shown to cause deswelling of the films, but this does affect the confinement of ferrocene within the polymer since neither electrolyte has been shown to form hydrogen or nitrogen bonds with the PEI backbone. [25] In addition, studies with linear PEI modified with ferrocene moieties of different lengths have shown that apart from an increased electrochemical stability, ferrocene groups that are further distanced from the PEI backbone result in more stable enzymatic responses. [27] Interestingly, the same study showed that there is no correlation between mediator spacing and electron transport within the film, contrary to what has been demonstrated in previous studies. [28,29]

After cross-linking and enzyme encapsulation the thickness of the film was here estimated as 22.5 ± 3.0 µm by scanning electron microscopy. From the geometric electrode area one estimates a ferrocene quantity of 101 nmol with a corresponding charge of 9.7 mC required to convert all ferrocene in the polymer. In an ideal biosensor, the applied anodic potential should rapidly oxidize all addressable ferrocene moieties, after which time the steady-state current originating from the constant diffusional transport and transformation of glucose should dominate the signal. Unfortunately, this is often not the case. In the absence of glucose, a bell-shaped response curve should be observed in a linear potential sweep, returning the current to baseline after passing over the formal potential. As shown in **Figure 4.2**, however, one observes a diffusion limiting process, which is puzzling given the limited thickness of the

film and the immobilized nature of the redox probe. The anodic charge under the curve, calculated as 0.02 mC, represents just 0.2 % of the available ferrocene, clearly indicating that the charging process is not complete during the scan. In mediated glucose oxidase-based biosensors, oxygen acts as an additional electron acceptor competing with the mediator for the electrons from the reduced form of the enzyme, thus decreasing the current. This effect has been studied extensively with various mediators [30–33] as well as with the branched Fc-PEI [23] used in this study. Hence, since experiments were performed in normal (non O_2-deprived) conditions, the effect of oxygen should also be taken into consideration when interpreting the resulting voltammograms.

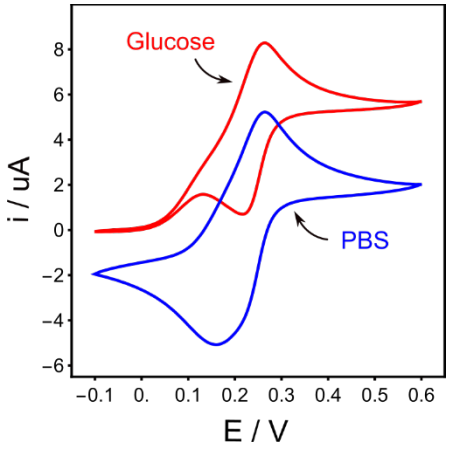

Figure 4.2: Cyclic voltammograms (vs. Ag/AgCl, 50 mV s^{-1}) for the Fc-C_6-bPEI/GOx/cross-linker biosensor in PBS (0.17 M, pH 7.49, blue trace) and 10 mM glucose (same PBS background, red trace). The last scan from a total of 10 cycles is shown.

Interdigitated array (IDA) electrodes may offer a convenient way of measuring diffusion coefficients. Both transient [34] and steady state [35,36] methods have been employed for such measurements using IDA. Here, a chronoamperometric experiment was performed to estimate the apparent diffusion coefficient (see SI for details) and found the value (9.7 ± 1.7) x 10^{-12} cm^2 s^{-1}. This suggests from $\delta = 2(Dt)^{1/2}$ that the diffusion layer thickness δ will approach the film thickness only after about 36 h. Unfortunately, this is a major problem for the realization of continuous enzyme biosensors because it means that one observes two major contributions to the current, one stemming from the desired enzyme turnover and the other from slowly turning over the remaining ferrocene not wired to an enzyme. The latter process approximately decays with the square root of time according to the Cottrell equation:

$$I = \frac{nFAD_e^{1/2}c_R}{\pi^{1/2}t^{1/2}} \qquad (6)$$

where D_e is the apparent electron diffusion coefficient of the redox polymer and c_R the effective electroactive site concentration.

Hence, one does not easily observe a current that adequately traces glucose concentration with time. This is experimentally demonstrated here by using the same electrode when alternating between 5 mM and 6 mM glucose concentration (**Figure 4.3**, black trace). The signal is indeed drifting monotonically

and signal reproducibility is too limited for practical work. The green trace shows the current response with time in the absence of glucose when applying the same potential. The non-specific charging process (green trace) is subtracted from the raw data (black trace) to give corrected glucose readings (orange trace). While the correction is not perfect, the data look much better and suggest that the principal reason for the signal drift is the charging of the ferrocene on the polymer.

But why is a ferrocene moiety so slow to charge when deposited directly onto an electrode surface? At such high density one would expect the electrons to easily hop between redox probes and result in rapid turnover. The reason is likely found in the need to maintain electroneutrality in this dense PEI film. As electrons are pulled from the polymeric film the resulting positive charge must be compensated, most likely by the incorporation of anionic solute from the outer side of the film. This process, which is often overlooked in the electrochemical community, may kinetically hinder redox turnover for dense films. [37] A second factor is the cationic nature of the polymer itself, which behaves differently depending on the electrolyte used. In the absence of covalent bonding between enzyme and redox polymer, electrolytes with increased ionic strength will result in screening of the charges by counterions and coiling of the polymer, hindering the complexation between the two and leading to a decreased glucose-dependent current. [38,39] The effect is reversed when ionic strength is low where the polymer is stretched due to internal interactions of the charges bound to the polymer backbone as demonstrated with poly(4-vinylpyridine) polymer not covalently bound to glucose oxidase. Note that a different result was observed in a later study with a ferrocene-poly(allylamine) polymer where the shrinking of the polymer with increased ionic strength led to shortening the distance between the redox centers, eventually resulting in an increased concentration of the redox sites available for mediation. [40]

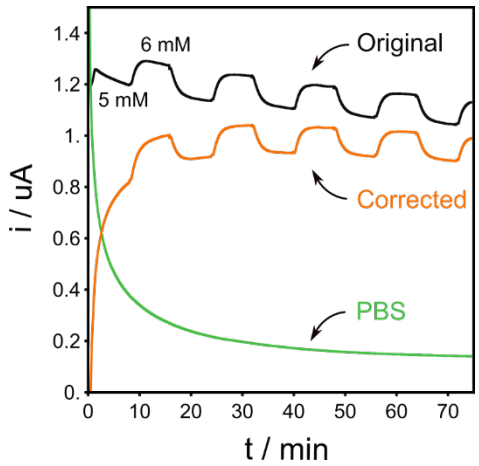

Figure 4.3: Chronoamperometric experiment (+0.6 V vs. Ag/AgCl) in PBS (0.17 M, pH 7.49, green trace) followed by amperometry (+0.6 V vs. Ag/AgCl) with alternating 5 mM and 6 mM glucose solutions (black trace), "corrected" (subtracted) trace (orange trace). A reduction potential (0 V vs. Ag/AgCl) preceded both experiments to reduce the ferrocene groups and avoid current contributions arising from their potentially mixed redox state.

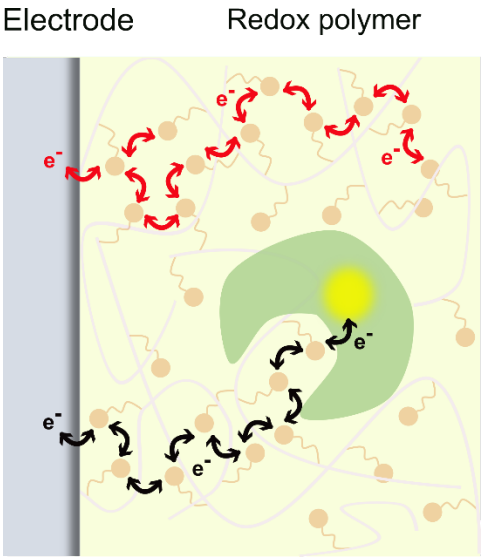

Figure 4.4: Redox moieties contributing to the enzyme turnover (black arrows) and those contributing to the charging of the film without being linked to the enzyme (red arrows)

Recent examples in the existing literature have reported glucose response currents for short chronoamperometric experiments on the order of 60 s after starting the enzyme reaction. [41–46] The amperometric curves in buffer solution (whenever available) show a similarly decaying current as the one presented above that, to the best of our knowledge, has not been accounted for during the reporting of the respective calibration curves. Available cyclic voltammograms in buffer solution show similar non-exhaustive behavior with large peak-to-peak separation and a current that does not decay to zero. In a recently published study, [47] Diaz-Gonzalez et al. reported the performance of wired enzyme glucose electrodes based on ferrocene moieties immobilized via cross-linking in PEI films. By performing short chronoamperometric experiments they demonstrated the current decay in the absence and presence of glucose. In the former case, the contribution of the "diffusion-like" electron transport within the film and the charging currents were underlined. In the latter, the initial current decay was attributed to the electron hopping in the film which was followed by the establishment of a glucose-dependent steady-state current. It was also argued that in the presence of glucose more complicated processes arise when the substrate and mediator availability vary across the film. The above examples are for when a large amount of mediator is deposited on the electrode, forming a three-dimensional network that extends beyond the surface of the electrode. If a much-reduced number of electroactive species are surface bound on the electrode, the application of a constant potential in the absence of substrate should more easily result in a complete depletion of the redox species in the time scale of the experiment. Examples of such behavior with osmium-based cross-linked enzyme electrodes may indeed be found in the literature and should be taken as guidance.[30,48,49]

As evidenced from the examples above, there is a direct link between the type and efficacy of "wiring" the enzyme to the electrode and the time-dependent signal observed in biosensors relying on mediated electron transfer processes. This article focused on this relationship and highlighted that the rate-limiting

steps that govern the response of a given sensor must be correctly understood. Detailed investigations on the rate-limiting processes should be part of the discussion when reporting the performance of new glucose biosensors. The "wired" enzymes play a key role in this respect, especially in the context of wearable sensors that are gaining in popularity. Choosing the right mediator is equally important. In this study we employed ferrocene, which in its oxidized form exhibits some instability that has been attributed to nucleophilic attack, causing its decomposition. [25,50] Earlier work has also confirmed the poor stability of ferrocenium ions through studies on the electrochemical stability of covalently bound ferrocene mediators to glucose oxidase [12] and on the half-lives of ferrocenium ion forms of carboxylic and acetic acid derivatives in aqueous buffered solutions. [51] The latter study attributed the instability of ferrocenium ions in hydrolysis reactions that gave rise to the formation of hydrous ferric oxides. To overcome the inherent drawbacks of the ferrocenium ion, alternate redox couples should be preferred. Surface bound redox moieties based on osmium derivatives are particularly promising, and combined with research on new materials and electroactive species, can provide a good base for the development of more reliable biosensors. Additionally, the importance of establishing a diffusion limited response cannot be overstated because a suitable membrane coating increases operational stability by overcoming limitations from loss of enzyme activity. Even if one may consider the field of glucose sensing mature, essential design characteristics should accompany contemporary work for the realization of reliable continuous glucose sensors.

4.3 Supporting Information

4.3.1 Calculations for the diffusion limiting case

We consider here the case of an enzyme-based glucose biosensor, where the sample is separated from the electrode by a diffusion limiting membrane and a layer containing the enzyme, redox mediator, and cross-linker. We assume that oxygen is not a rate limiting factor, and so the turnover rate of the enzyme is approximated by the Michaelis-Menten equation:

$$-\frac{dc_j^{aq}(0)}{dt} = \frac{v_{\max} c_j^{aq}(0)}{K_{\max} + c_j^{aq}(0)} \qquad (1)$$

where $c_j^{aq}(0)$ the concentration of glucose at the surface of the electrode, $v_{\max}$ is the maximum rate of conversion proportional to the enzyme concentration ($v_{\max} = c_e^{aq}(0) k_{cat}$ where k_{cat} is the turnover number) and $K_{\max}$ is the Michaelis constant.

The flux of glucose across the aqueous diffusion layer is given by:

$$J = -D_j^{aq} \frac{c_j^{aq,*} - c_j^{aq}(\delta^m)}{\delta^{aq}} \qquad (2)$$

where $c_j^{aq,*}$ the concentration of glucose in the sample, D_j^{aq} the diffusion coefficient of glucose in the sample, $c_j^{aq}(\delta^m)$ the concentration of glucose at the membrane (at the sample side) and δ^{aq} the thickness of the aqueous diffusion layer.

The flux of glucose across the membrane is given by:

$$J = -\frac{D_j^m}{\delta^m} p_j \left\{ c_j^{aq}(\delta^m) - c_j^{aq}(0) \right\} \tag{3}$$

where D_j^m the diffusion coefficient of glucose in the membrane, δ^m the thickness of the membrane layer and p_j the partition coefficient, equal to $p_j = c_j^m(\delta^m) / c_j^{aq}(\delta^m)$.

At steady state, the two fluxes are equal, so:

$$c_j^{aq}(\delta^m) = \left\{ \frac{D_j^{aq}\delta^m}{p_j D_j^m \delta^{aq}} c_j^{aq,*} + c_j^{aq}(0) \right\} \left\{ 1 + \frac{D_j^{aq}\delta^m}{p_j D_j^m \delta^{aq}} \right\}^{-1} \tag{4}$$

In addition, at steady state the rate of replenishment of the enzyme layer (of thickness δ^e) by diffusion across the membrane is equal to the turnover rate of the enzyme:

$$-\frac{dc_j^e}{dt} = \frac{v_{\max} c_j^{aq}(0)}{K_{\max} + c_j^{aq}(0)} \tag{5}$$

The diffusional concentration change in the enzyme layer is given by the flux divided by the enzyme layer thickness:

$$\frac{dc_j^e}{dt} = -\frac{D_j^m}{\delta^e \delta^m} p_j \left\{ c_j^{aq}(\delta^m) - c_j^{aq}(0) \right\} \tag{6}$$

By combining eq. 5 and 6 we obtain:

$$\frac{v_{\max} c_j^{aq}(0)}{K_{\max} + c_j^{aq}(0)} = \frac{D_j^m}{\delta^e \delta^m} p_j \left\{ c_j^{aq}(\delta^m) - c_j^{aq}(0) \right\} \tag{7}$$

Using eqs 3, 4 and 7 and the parameters presented below, we may now calculate the expected current density with respect to the glucose concentration in the sample. Parameters:

$p_j = 0.01$

$D_j^{aq} = 10^{-5} cm^2 / s$

$D_j^m = 10^{-7} cm^2 / s$

$\delta^e = \delta^m = 10 \mu m$

$\delta^{aq} = 50 \mu m$

$k_{cat} = 100 s^{-1}$

$K_{\max} = 0.1 M$

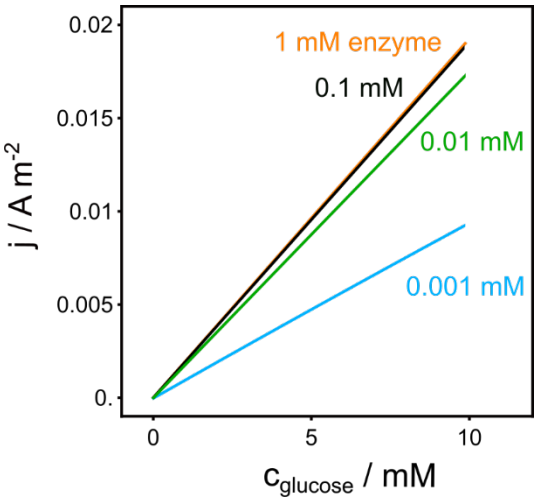

Figure S4.1: Steady state amperometric calibration curves for varying concentrations of enzyme

4.3.2 Reagents and solutions

Glucose oxidase from Aspergillus niger (type VII, lyophilized powder, ≥ 100000 units/g solid), (6-bromohexyl) ferrocene, poly(ethylene glycol) diglycidyl ether (PEGDE) (average Mn: 500), polyethylenimine (water-free, typical Mn: 10000, typical Mw: 25000), Nafion perfluorinated resin solution (5 wt. % in lower aliphatic alcohols and water, 15-20 % water), D-(+)-glucose (≥ 95 %), potassium chloride, sodium phosphate dibasic (ACS reagent, ≥ 99 %), sodium chloride (puriss, ≥ 99.5 %) were purchased from Sigma Aldrich, potassium phosphate monobasic (99+ %, extra pure) was purchased from Acros Organics and hydrochloric acid (1 M, NIST Standard Solution) was purchased by Fisher Chemical.

Phosphate buffered saline solution (PBS) of composition 137 mM sodium chloride, 2.7 mM potassium chloride, 10 mM sodium phosphate dibasic and 1.8 mM potassium phosphate monobasic with a pH 7.49 was prepared from stock solutions of the respective salts. Diluted Nafion solutions were prepared from the Nafion 5 wt. % stock solution with dilution in PBS. All other aqueous solutions were prepared in Milli-Q water (18.2 MΩ cm).

4.3.3 Electrochemical equipment & methods

The electrochemical measurements were performed with a PGSTAT204 (Metrohm Autolab) controlled by the Nova 2.1 software. A three-electrode configuration was used consisting of a glassy carbon rod (Ø 2 mm) used as working (WE), a Pt wire as counter (CE) and an Ag/AgCl wire as reference (RE) electrode. A flow cell built in-house accommodated the three-electrode setup with the electrodes placed in proximity to each other. The flow was controlled by an IPC pump (high precision multichannel dispenser, ISMATEC) and kept at a flowrate of ca. 255 uL/min during all the electrochemical experiments.

Cyclic voltammetry was performed from -0.1 V to +0.6 V at a 50 mV/s scan rate. The chronoamperometric and amperometric experiments were performed at +0.6 V. For both experiments

(in PBS and glucose solutions), the application of a reduction potential at 0 V preceded the measurements, to electrochemically reduce the ferrocene groups in the films and avoid potential current contributions that may arise from a mixed redox state. In the amperometric experiment with glucose, the solutions were switched in a continuous mode using the in-house flow cell system described above.

4.3.4 Preparation of glucose biosensor

First a 20 mg/mL redox polymer solution was prepared by dissolving 8 mg of the synthesized Fc-C_6-bPEI in 400 µL of MilliQ and 0.1 M HCl, with the pH adjusted to 5 (solution 1). The Fc-C_6-bPEI/GOx/cross-linker solution was then prepared by mixing 28 uL of solution 1, 12 uL of 50 mg/mL glucose oxidase solution (dissolved in MilliQ) and 1.5 uL of cross-linker solution (1:10 diluted solution of poly(ethylene glycol) diglycidyl ether in MilliQ). 2uL of this membrane cocktail were drop cast on a glassy carbon electrode (Ø 2 mm) which was previously polished with 0.3 um alumina and left to cure overnight in ambient atmosphere. Next, three layers (2 uL each) of 0.5 % diluted Nafion solution were drop cast on top, with a 30-minute waiting period before each deposition. The 0.5 % Nafion solution was prepared by dilution of the 5 % Nafion stock solution in the PBS buffer (pH 7.49).

4.3.5 Synthesis of hexylferrocene-modified branched poly(ethyleneimine) (Fc-C_6-bPEI)

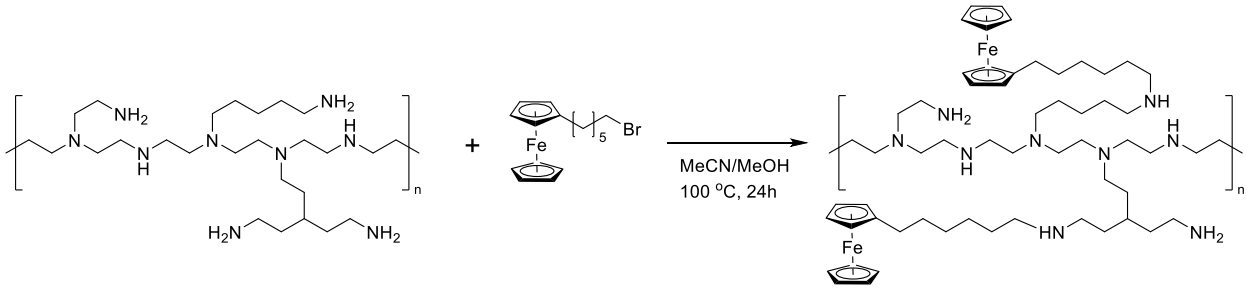

Figure S4.2: Synthetic reaction scheme of Fc-C_6-bPEI redox polymer

Fc-C_6-bPEI was obtained according to a modified procedure based on a previously reported protocol. [52] 0.2 g of branched poly(ethyleneimine) (bPEI) and 14 mL of MeCN were placed in a round bottom flask. The resulting suspension was heated to 80 °C and a small quantity of MeOH (approx. 1 mL) was added in order to achieve the full dissolution of the polymer. A solution of (6-bromohexyl)ferrocene (0.3 g) in MeCN (4mL) was added dropwise. The resulting mixture was stirred for 24 h at 100 °C. Subsequently, the reaction mixture was cooled down to room temperature and the solvent was removed *in vacuo*. The remaining solid was then washed with Et_2O (40 mL, soaked for 1h prior to decantation) and the product was dried *in vacuo* providing an orange oily residue.

^{1}H NMR (400 MHz, $CDCl_3$): 4.15-3.95 (m, Cp-Fe-Cp-**H**), 3.80-2.20 (m, broad, -C**H**$_2$-C**H**$_2$-NH-, Fc-C**H**$_2$-$(CH_2)_5$-, Fc-$(CH_2)_5$-C**H**$_2$-), 1.55-0.95 (m, Fc-$(CH_2)_n$-C**H**$_2$-$(CH_2)_m$), 0.92-0.75 (m, Fc-$(CH_2)_n$-C**H**$_2$-$(CH_2)_m$).

4.3.6 Characterization of Fc-C_6-bPEI

Nuclear Magnetic Resonance (NMR)

To calculate the PEI backbone substitution degree, the integral ratio of the peaks of the ferrocene moiety and the polymer backbone was investigated. Each monomer unit of the polymer chain contains the four non-exchanging methylene protons (-C**H**$_2$-C**H**$_2$-NH-) and the exchangeable hydrogen atoms of the amino groups (-N**H**-/-N**H**$_2$). While the peaks for the latter are absent from the spectrum due to their dynamic nature, the signal of the former is in the range 2.20 – 3.00 ppm in the spectrum of unsubstituted bPEI (**Figure S4.3**-A). This signal broadens significantly (2.20 – 3.80 ppm) with the introduction of hexylferrocene into the structure and overlaps with the signals of two methylene groups of the substituent (triplets at 2.45 and 3.43 ppm), while the ferrocene ring (Cp) hydrogens' signal is found outside (ca. 3.90 - 4.20 ppm) the region of interest and remains unperturbed (**Figure S4.3**-C). Setting the integral of the area under the peaks belonging to the ferrocene ring to nine and integrating other peaks relatively would allow one to obtain the number of backbone protons per one ferrocene moiety. This value, however, has to be lowered by 4 to account for the overlap of the signals of the polymer backbone and the ferrocene side-chain. Dividing the resulting value by 4 gives the number of monomer units per one ferrocene moiety, which is the reciprocal of the substitution degree (S), that can be calculated according to the following final equation:

$$S = \frac{4}{l_{\text{polymer backbone}} - 4} \cdot 100\% = 10.7\% \qquad (1)$$

Concentration of ferrocene functional groups per unit of mass of the substituted polymer (concentration "in the polymer") was calculated according to the following formula:

$$c_{Fc-C_6}^{polymer} = \frac{n_{Fc-C_6}}{m} = \frac{1}{\frac{M_m}{S} + M_{Fc-C_6} - 1} = 1.49 \frac{mmol}{g} \qquad (2)$$

where m the mass of the polymer, n_{Fc-C_6} the molar quantity of the hexylferrocene functional groups, M_m and M_{Fc-C_6} the molar mass of a monomer unit and hexylferrocene functional group respectively. To convert the concentration in mol/L, a density of 1 g/mL is used, giving a concentration of 1.49 M.

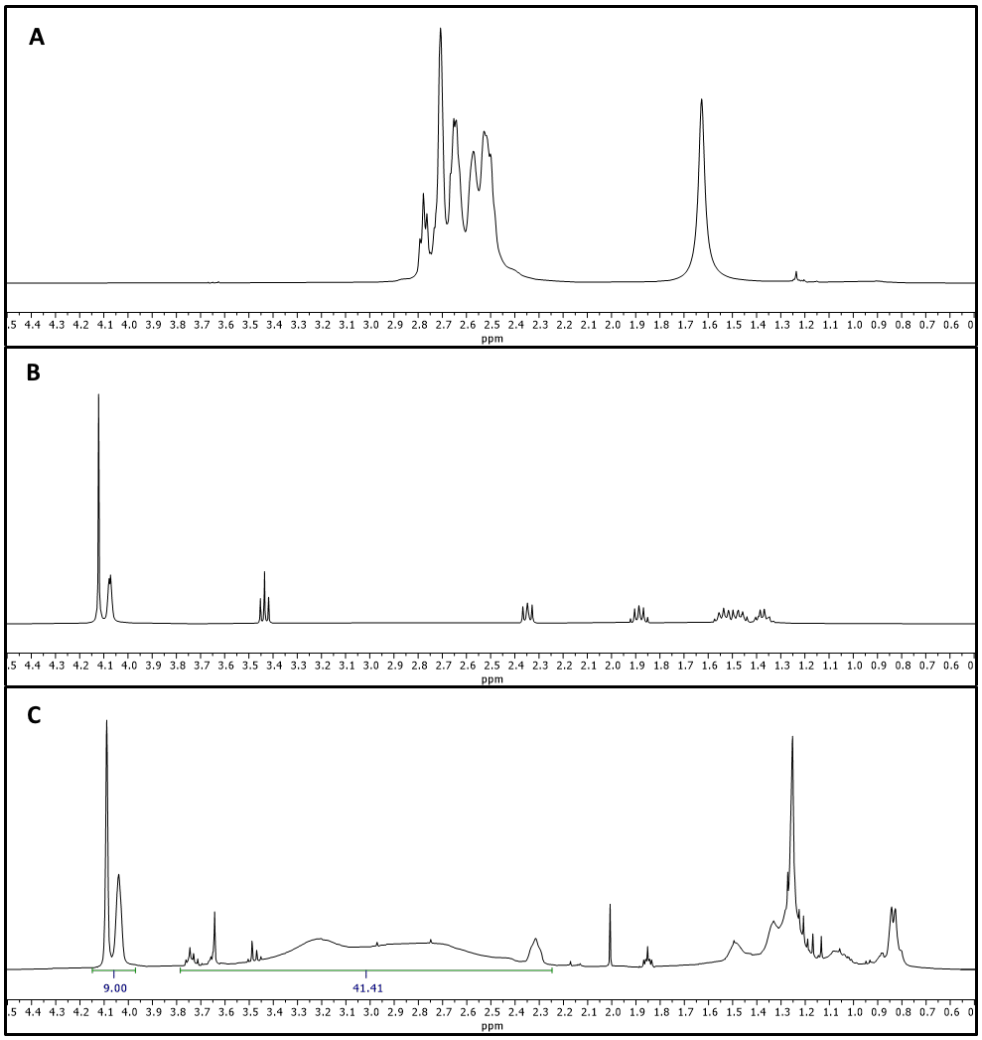

Figure S4.3: ^{1}H NMR spectra of bPEI (A), (6-bromohexyl)ferrocene (B) and Fc-C_6-bPEI product (C)

Scanning Electron Microscopy (SEM)

Cross-section

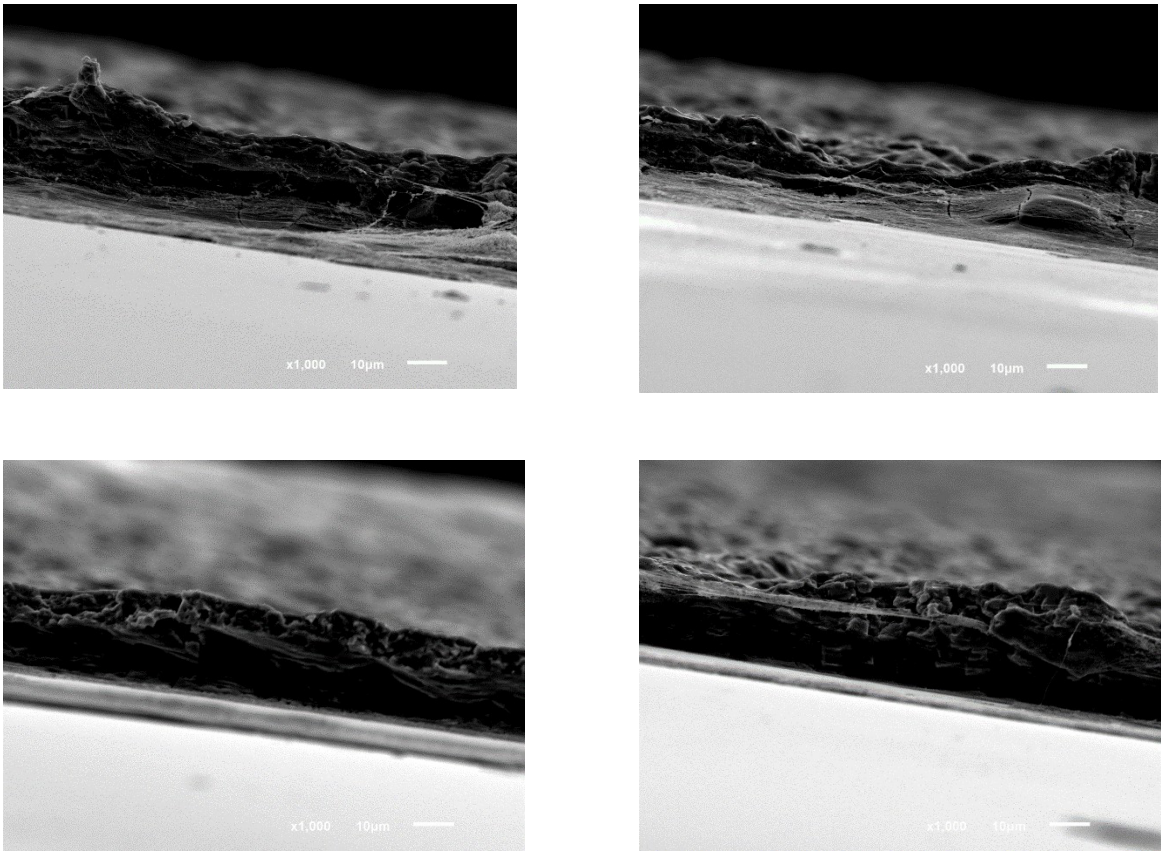

Overview

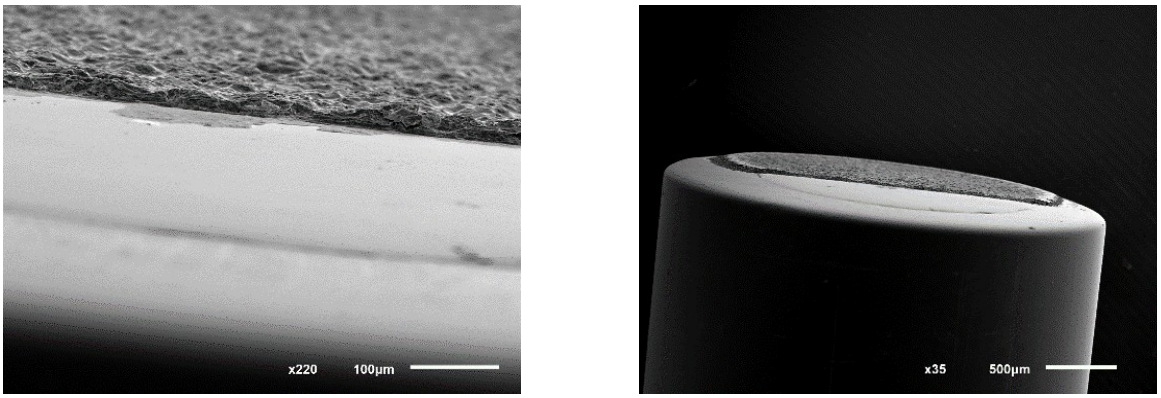

Figure S4.4: SEM images of the cross-section and overview of Fc-C_6-bPEI/GOx/cross-linker 2 uL drop cast films.

An average thickness of 22.5 ± 3.0 um was estimated by manually measuring the thicknesses at different parts of the films from the SEM images shown above.

4.3.7 Electrochemical properties of the biosensor

The electrochemical properties of the biosensor were evaluated through cyclic voltammetry in buffer solution (PBS, 0.17 M, pH 7.49) at a 50 mV s^{-1} scan rate. The redox potential of the Fc-C_6-bPEI film was estimated at 215 mV (vs. Ag/AgCl) with a peak-to-peak separation (ΔE_p) at 95 mV indicating a

quasi-reversible reaction (**Figure 4.2**). The oxidation and reduction peaks were located at +0.260 V and +0.165 V respectively, with similar values reported in the literature for other ferrocene-based redox polymers. [25,41,53,54]

The diffusion coefficient was calculated from the data of the chronoamperometric experiment (4500 s) carried out in PBS solution combined with the linearized version of the Cottrell equation:

$$i = \frac{nFAc_R D_e^{1/2}}{\pi^{1/2} t^{1/2}} \rightarrow i = Kt^{-1/2} \text{ (with } K = \frac{nFAc_R D_e^{1/2}}{\pi^{1/2}})$$

where F the Faraday constant (96485 C mol^{-1}), A the average area of electrode ($3 \cdot 10^{-6}$ m^2), c_R the concentration of electroactive sites (1.49 M) and D_e the apparent electron diffusion coefficient of the redox polymer.

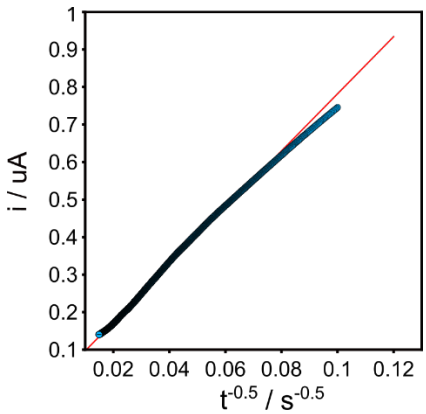

Figure S4.5: Current versus inverse of square root of time using data from the chronoamperometric experiment.

An average value of $9.70 \pm 1.71 \cdot 10^{-12}$ cm^2 s^{-1} was estimated considering the uncertainty of the electrode's surface area ($3.00 \pm 0.27 \cdot 10^{-6}$ m^2).

4.3.8 Calculation of ferrocene quantity and respective charge

Combining the average thickness (22.5 um) and electrode's surface area ($3 \cdot 10^{-6}$ m^2), the volume of the drop cast layer is estimated at $6.75 \cdot 10^{-11}$ m^3, which, combined with the ferrocene concentration (1.49 M) gives the following total quantity of ferrocene: $n = CV = 101$ nmol.

And the corresponding charge is (F= 96485 C mol^{-1}): $Q = nF \rightarrow Q = 9.74$ mC.

4.5 References

(1) Cha, K. H.; Qin, Y.; Meyerhoff, M. E. Origin of Low Detection Limit and High Selectivity of Roche Accu-Chek Test Strips That Enables Measurement of Tear Glucose Levels. *Electroanalysis* **2015**, *27* (3), 670–676. https://doi.org/10.1002/elan.201400576.

(2) Pullano, S. A.; Greco, M.; Bianco, M. G.; Foti, D.; Brunetti, A.; Fiorillo, A. S. Glucose Biosensors in Clinical Practice: Principles, Limits and Perspectives of Currently Used Devices. *Theranostics* **2022**, *12* (2), 493–511. https://doi.org/10.7150/thno.64035.

(3) Lee, H.; Hong, Y. J.; Baik, S.; Hyeon, T.; Kim, D.-H. Enzyme-Based Glucose Sensor: From Invasive to Wearable Device. *Adv Healthc Mater* **2018**, *7* (8), e1701150. https://doi.org/10.1002/adhm.201701150.

(4) Cass, A. E. G.; Davis, Graham.; Francis, G. D.; Hill, H. A. O.; Aston, W. J.; Higgins, I. John.; Plotkin, E. V.; Scott, L. D. L.; Turner, A. P. F. Ferrocene-Mediated Enzyme Electrode for Amperometric Determination of Glucose. *Anal. Chem.* **1984**, *56* (4), 667–671. https://doi.org/10.1021/ac00268a018.

(5) Turner, A. P. F. Biosensors: Sense and Sensibility. *Chem. Soc. Rev.* **2013**, *42* (8), 3184–3196. https://doi.org/10.1039/C3CS35528D.

(6) Demin, S.; Hall, E. A. H. Breaking the Barrier to Fast Electron Transfer. *Bioelectrochemistry* **2009**, *76* (1), 19–27. https://doi.org/10.1016/j.bioelechem.2009.03.006.

(7) Heller, A. Electrical Wiring of Redox Enzymes. *Acc. Chem. Res.* **1990**, *23* (5), 128–134. https://doi.org/10.1021/ar00173a002.

(8) Hill, H. A. O. *Eur. Pat. Appl. EPO* **1984**, *125*, 45−46.

(9) Degani, Y.; Heller, Adam. Direct Electrical Communication between Chemically Modified Enzymes and Metal Electrodes. I. Electron Transfer from Glucose Oxidase to Metal Electrodes via Electron Relays, Bound Covalently to the Enzyme. *J. Phys. Chem.* **1987**, *91* (6), 1285–1289. https://doi.org/10.1021/j100290a001.

(10) Degani, Yinon.; Heller, Adam. Direct Electrical Communication between Chemically Modified Enzymes and Metal Electrodes. 2. Methods for Bonding Electron-Transfer Relays to Glucose Oxidase and D-Amino-Acid Oxidase. *J. Am. Chem. Soc.* **1988**, *110* (8), 2615–2620. https://doi.org/10.1021/ja00216a040.

(11) N. Bartlett, P.; G. Whitaker, R.; J. Green, M.; Frew, J. Covalent Binding of Electron Relays to Glucose Oxidase. *Journal of the Chemical Society, Chemical Communications* **1987**, *0* (20), 1603–1604. https://doi.org/10.1039/C39870001603.

(12) Bartlett, P. N.; Bradford, V. Q.; Whitaker, R. G. Enzyme Electrode Studies of Glucose Oxidase Modified with a Redox Mediator. *Talanta* **1991**, *38* (1), 57–63. https://doi.org/10.1016/0039-9140(91)80009-O.

(13) Badia, A.; Carlini, R.; Fernandez, A.; Battaglini, F.; Mikkelsen, S. R.; English, A. M. Intramolecular Electron-Transfer Rates in Ferrocene-Derivatized Glucose Oxidase. *J. Am. Chem. Soc.* **1993**, *115* (16), 7053–7060. https://doi.org/10.1021/ja00069a001.

(14) Ikeda, T.; Katasho, I.; Kamei, M.; Senda, M. Electrocatalysis with a Glucose-Oxidase-Immobilized Graphite Electrode. *Agricultural and Biological Chemistry* **1984**, *48* (8), 1969–1976. https://doi.org/10.1080/00021369.1984.10866431.

(15) Albery, W. J.; Bartlett, P. N.; Craston, D. H. Amperometric Enzyme Electrodes: Part II. Conducting Salts as Electrode Materials for the Oxidation of Glucose Oxidase. *Journal of Electroanalytical Chemistry and Interfacial Electrochemistry* **1985**, *194* (2), 223–235. https://doi.org/10.1016/0022-0728(85)85006-3.

(16) Schuhmann, W.; Wohlschläger, H.; Lammert, R.; Schmidt, H.-L.; Löffler, U.; Wiemhöfer, H.-D.; Göpel, W. Leaching of Dimethylferrocene, a Redox Mediator in Amperometric Enzyme Electrodes. *Sensors and Actuators B: Chemical* **1990**, *1* (1), 571–575. https://doi.org/10.1016/0925-4005(90)80275-5.

(17) Schuhmann, W. Amperometric Enzyme Biosensors Based on Optimised Electron-Transfer Pathways and Non-Manual Immobilisation Procedures. *Reviews in Molecular Biotechnology* **2002**, *82* (4), 425–441. https://doi.org/10.1016/S1389-0352(01)00058-7.

(18) Albery, W. J.; Bartlett, P. N.; Driscoll, B. J.; Lennox, R. B. Amperometric Enzyme Electrodes: Part 5. The Homogeneous Mediated Mechanism. *Journal of Electroanalytical Chemistry* **1992**, *323* (1), 77–102. https://doi.org/10.1016/0022-0728(92)80004-N.
(19) Bartlett, P. N.; Pratt, K. F. E. Theoretical Treatment of Diffusion and Kinetics in Amperometric Immobilized Enzyme Electrodes Part I: Redox Mediator Entrapped within the Film. *Journal of Electroanalytical Chemistry* **1995**, *397* (1), 61–78. https://doi.org/10.1016/0022-0728(95)04236-7.
(20) Bollella, P. Enzyme-Based Amperometric Biosensors: 60 Years Later … Quo Vadis? *Analytica Chimica Acta* **2022**, *1234*, 340517. https://doi.org/10.1016/j.aca.2022.340517.
(21) Chen, T.; Friedman, K. A.; Lei, I.; Heller, A. In Situ Assembled Mass-Transport Controlling Micromembranes and Their Application in Implanted Amperometric Glucose Sensors. *Anal. Chem.* **2000**, *72* (16), 3757–3763. https://doi.org/10.1021/ac000348c.
(22) Alsaoub, S.; Ruff, A.; Conzuelo, F.; Ventosa, E.; Ludwig, R.; Shleev, S.; Schuhmann, W. An Intrinsic Self-Charging Biosupercapacitor Comprised of a High-Potential Bioanode and a Low-Potential Biocathode. *ChemPlusChem* **2017**, *82* (4), 576–583. https://doi.org/10.1002/cplu.201700114.
(23) Chuang, C. L.; Wang, Y. J.; Lan, H. L. Amperometric Glucose Sensors Based on Ferrocene-Containing B-Polyethylenimine and Immobilized Glucose Oxidase. *Analytica Chimica Acta* **1997**, *353* (1), 37–44. https://doi.org/10.1016/S0003-2670(97)00372-3.
(24) Wang, J.-Y.; Chen, L.-C.; Ho, K.-C. Synthesis of Redox Polymer Nanobeads and Nanocomposites for Glucose Biosensors. *ACS Appl. Mater. Interfaces* **2013**, *5* (16), 7852–7861. https://doi.org/10.1021/am4018219.
(25) Merchant, S. A.; Glatzhofer, D. T.; Schmidtke, D. W. Effects of Electrolyte and pH on the Behavior of Cross-Linked Films of Ferrocene-Modified Poly(Ethylenimine). *Langmuir* **2007**, *23* (22), 11295–11302. https://doi.org/10.1021/la701521s.
(26) Bracamonte, M. V.; Yañez, C.; Bollo, S.; Rivas, G. A.; Ferreyra, N. F. Physico-Chemical Characterization of Ferrocenyl-Modified Hyperbranched Poly(Ethylenimine) Self-Assembled Multilayers. *Journal of Electroanalytical Chemistry* **2014**, *712*, 124–131. https://doi.org/10.1016/j.jelechem.2013.11.018.
(27) Merchant, S. A.; Meredith, M. T.; Tran, T. O.; Brunski, D. B.; Johnson, M. B.; Glatzhofer, D. T.; Schmidtke, D. W. Effect of Mediator Spacing on Electrochemical and Enzymatic Response of Ferrocene Redox Polymers. *J. Phys. Chem. C* **2010**, *114* (26), 11627–11634. https://doi.org/10.1021/jp911188r.
(28) Hale, P. D.; Boguslavsky, L. I.; Inagaki, Toru.; Karan, H. I.; Lee, H. Sui.; Skotheim, T. A.; Okamoto, Yoshi. Amperometric Glucose Biosensors Based on Redox Polymer-Mediated Electron Transfer. *Anal. Chem.* **1991**, *63* (7), 677–682. https://doi.org/10.1021/ac00007a006.
(29) Mao, F.; Mano, N.; Heller, A. Long Tethers Binding Redox Centers to Polymer Backbones Enhance Electron Transport in Enzyme "Wiring" Hydrogels. *J. Am. Chem. Soc.* **2003**, *125* (16), 4951–4957. https://doi.org/10.1021/ja029510e.
(30) Gregg, B. A.; Heller, Adam. Cross-Linked Redox Gels Containing Glucose Oxidase for Amperometric Biosensor Applications. *Anal. Chem.* **1990**, *62* (3), 258–263. https://doi.org/10.1021/ac00202a007.
(31) Schuhmann, W.; Lammert, R.; Uhe, B.; Schmidt, H.-L. Polypyrrole, a New Possibility for Covalent Binding of Oxidoreductases to Electrode Surfaces as a Base for Stable Biosensors. *Sensors and Actuators B: Chemical* **1990**, *1* (1), 537–541. https://doi.org/10.1016/0925-4005(90)80268-5.
(32) Karan, H. I.; Hale, P. D.; Lan, H. L.; Lee, H. S.; Liu, L. F.; Skotheim, T. A.; Okamoto, Y. Quinone-Modified Polymers as Electron Transfer Relay Systems in Amperometric Glucose Sensors. *Polymers for Advanced Technologies* **1991**, *2* (5), 229–235. https://doi.org/10.1002/pat.1991.220020504.
(33) Wang, J. Electrochemical Glucose Biosensors. *Chem. Rev.* **2008**, *108* (2), 814–825. https://doi.org/10.1021/cr068123a.
(34) Feldman, B. J.; Feldberg, S. W.; Murray, R. W. An Electrochemical Time-of-Flight Experiment. *J. Phys. Chem.* **1987**, *91* (26), 6558–6560. https://doi.org/10.1021/j100310a027.

(35) Feldman, B. J.; Murray, R. W. Measurement of Electron Diffusion Coefficients through Prussian Blue Electroactive Films Electrodeposited on Interdigitated Array Platinum Electrodes. *Anal. Chem.* **1986**, *58* (13), 2844–2847. https://doi.org/10.1021/ac00126a056.
(36) Nishihara, Hiroshi.; Dalton, Frank.; Murray, R. W. Interdigitated Array Electrode Diffusion Measurements in Donor/Acceptor Solutions in Polyether Electrolyte Solvents. *Anal. Chem.* **1991**, *63* (24), 2955–2960. https://doi.org/10.1021/ac00024a028.
(37) Daum, P.; Lenhard, J. R.; Rolison, D.; Murray, R. W. Diffusional Charge Transport through Ultrathin Films of Radiofrequency Plasma Polymerized Vinylferrocene at Low Temperature. *J. Am. Chem. Soc.* **1980**, *102* (14), 4649–4653. https://doi.org/10.1021/ja00534a014.
(38) Degani, Y.; Heller, A. Electrical Communication between Redox Centers of Glucose Oxidase and Electrodes via Electrostatically and Covalently Bound Redox Polymers. *J. Am. Chem. Soc.* **1989**, *111* (6), 2357–2358. https://doi.org/10.1021/ja00188a091.
(39) Pishko, M. V.; Katakis, I.; Lindquist, S.-E.; Heller, A.; Degani, Y. Electrical Communication Between Graphite Electrodes and Glucose Oxidase/Redox Polymer Complexes. *Molecular Crystals and Liquid Crystals Incorporating Nonlinear Optics* **1990**, *190* (1), 221–249. https://doi.org/10.1080/00268949008047847.
(40) Battaglini, F.; Calvo, E. J.; Danilowicz, C.; Wolosiuk, A. Effect of Ionic Strength on the Behavior of Amperometric Enzyme Electrodes Mediated by Redox Hydrogels. *Anal. Chem.* **1999**, *71* (5), 1062–1067. https://doi.org/10.1021/ac971253m.
(41) Yang, J.; Gong, X.; Chen, S.; Zheng, Y.; Peng, L.; Liu, B.; Chen, Z.; Xie, X.; Yi, C.; Jiang, L. Development of Smartphone-Controlled and Microneedle-Based Wearable Continuous Glucose Monitoring System for Home-Care Diabetes Management. *ACS Sens.* **2023**, *8* (3), 1241–1251. https://doi.org/10.1021/acssensors.2c02635.
(42) Nikitina, V. N.; Daboss, E. V.; Vokhmyanina, D. V.; Solovyev, I. D.; Andreev, E. A.; Komkova, M. A.; Karyakin, A. A. The Widest Linear Range of Glucose Test Strips Based on Various Mediators and Membranes for Whole Blood Analysis. *Journal of Electroanalytical Chemistry* **2023**, *938*, 117445. https://doi.org/10.1016/j.jelechem.2023.117445.
(43) Dervisevic, M.; Alba, M.; Yan, L.; Senel, M.; Gengenbach, T. R.; Prieto-Simon, B.; Voelcker, N. H. Transdermal Electrochemical Monitoring of Glucose via High-Density Silicon Microneedle Array Patch (Adv. Funct. Mater. 3/2022). *Advanced Functional Materials* **2022**, *32* (3), 2270022. https://doi.org/10.1002/adfm.202270022.
(44) Jeon, W.-Y.; Kim, H.-H.; Choi, Y.-B. Development of a Glucose Sensor Based on Glucose Dehydrogenase Using Polydopamine-Functionalized Nanotubes. *Membranes* **2021**, *11* (6), 384. https://doi.org/10.3390/membranes11060384.
(45) Vargas, E.; Teymourian, H.; Tehrani, F.; Eksin, E.; Sánchez-Tirado, E.; Warren, P.; Erdem, A.; Dassau, E.; Wang, J. Enzymatic/Immunoassay Dual-Biomarker Sensing Chip: Towards Decentralized Insulin/Glucose Detection. *Angewandte Chemie International Edition* **2019**, *58* (19), 6376–6379. https://doi.org/10.1002/anie.201902664.
(46) Okurita, M.; Suzuki, N.; Loew, N.; Yoshida, H.; Tsugawa, W.; Mori, K.; Kojima, K.; Klonoff, D. C.; Sode, K. Engineered Fungus Derived FAD-Dependent Glucose Dehydrogenase with Acquired Ability to Utilize Hexaammineruthenium(III) as an Electron Acceptor. *Bioelectrochemistry* **2018**, *123*, 62–69. https://doi.org/10.1016/j.bioelechem.2018.04.007.
(47) Díaz-González, J. M.; Escalona-Villalpando, R. A.; Arriaga, L. G.; Minteer, S. D.; Casanova-Moreno, J. R. Effects of the Cross-Linker on the Performance and Stability of Enzymatic Electrocatalytic Films of Glucose Oxidase and Dimethylferrocene-Modified Linear Poly(Ethyleneimine). *Electrochimica Acta* **2020**, *337*, 135782. https://doi.org/10.1016/j.electacta.2020.135782.
(48) Aoki, A.; Heller, A. Electron Diffusion Coefficients in Hydrogels Formed of Cross-Linked Redox Polymers. *J. Phys. Chem.* **1993**, *97* (42), 11014–11019. https://doi.org/10.1021/j100144a019.
(49) Gao, Z.; Binyamin, G.; Kim, H.-H.; Barton, S. C.; Zhang, Y.; Heller, A. Electrodeposition of Redox Polymers and Co-Electrodeposition of Enzymes by Coordinative Crosslinking. *Angew Chem Int Ed Engl* **2002**, *41* (5), 810–813. https://doi.org/10.1002/1521-3773(20020301)41:5<810::aid-anie810>3.0.co;2-i.

(50) Calvo, E. J.; Etchenique, R.; Danilowicz, C.; Diaz, L. Electrical Communication between Electrodes and Enzymes Mediated by Redox Hydrogels. *Anal. Chem.* **1996**, *68* (23), 4186–4193. https://doi.org/10.1021/ac960170n.
(51) Szentrimay, R.; Yeh, P.; Kuwana, T. Evaluation of Mediator Titrants for the Indirect Coulometric Titration of Biocomponents. In *Electrochemical Studies of Biological Systems*; American Chemical Society: Washington, DC, 1977; pp 143–169.
(52) Hickey, D. P. Ferrocene-Modified Linear Poly(Ethylenimine) for Enzymatic Immobilization and Electron Mediation. In *Enzyme Stabilization and Immobilization: Methods and Protocols*; Minteer, S. D., Ed.; Methods in Molecular Biology; Springer: New York, NY, 2017; pp 181–191. https://doi.org/10.1007/978-1-4939-6499-4_14.
(53) Estrada-Osorio, D. V.; Escalona-Villalpando, R. A.; Gutiérrez, A.; Arriaga, L. G.; Ledesma-García, J. Poly-L-Lysine-Modified with Ferrocene to Obtain a Redox Polymer for Mediated Glucose Biosensor Application. *Bioelectrochemistry* **2022**, *146*, 108147. https://doi.org/10.1016/j.bioelechem.2022.108147.
(54) Meredith, M. T.; Hickey, D. P.; Redemann, J. P.; Schmidtke, D. W.; Glatzhofer, D. T. Effects of Ferrocene Methylation on Ferrocene-Modified Linear Poly(Ethylenimine) Bioanodes. *Electrochimica Acta* **2013**, *92*, 226–235. https://doi.org/10.1016/j.electacta.2013.01.006.

Chapter 5. A novel time-dependent potentiometric glucose biosensor

5.1 Introduction

The development of rapid, low-cost, and reliable sensors has been a long-standing goal. Glucose sensing is a common application of such sensors, with the majority of them being enzyme-based and working in amperometric mode. Here, the substrate is converted during an enzymatically catalyzed reaction, leading to changes in the redox state of either itself or another species participating in the reaction. With the application of a constant potential the initial redox state is regenerated, giving rise to a current that provides the signal of the sensor, which is ultimately correlated to the substrate concentration in the sample solution. [1] Amperometry is one of the most extensively used methods, but not the only one. Potentiometry has also found applications in the field of glucose sensing, where a potential difference is measured under zero-current conditions and serves as the signal of the sensor. Here there is no net consumption of material, which makes mass transport phenomena less important. In addition, specific control of the electrode dimensions and volumes of the electrochemical cell are not essential, as in the case of amperometric or coulometric sensors, while the system is free from undesired ohmic contributions. These advantages come with an important downside, which is the logarithmic dependence between the analyte concentration and the electrode signal. This makes it harder to track small variations in concentration. [2] In contrast, with amperometric sensors there is a linear dependance between the signal and the analyte concentration.

Over the decades, several efforts were made to overcome this limitation. Already in the late 50s, the development of precision null-point potentiometry [3] pointed out the benefits of potentiometry and inspired Malmstadt & Purdue [4] to develop a method demonstrating that glucose concentration was proportional to the reciprocal of the time required to produce a constant amount of iodine. The latter was produced at a rate proportional to the glucose concentration by a reaction that involved the hydrogen peroxide generated by the enzyme. These are the earliest attempts of applying potentiometry to demonstrate a linear dependence between sensor readout and glucose concentration. Several other potentiometric methods were developed a few decades later. Specifically, Nagy et al. developed a modified carbon electrode with a redox mediator adsorbed at the surface and employed a chronopotentiometric method consisting of an oxidation step followed by the measurement of open circuit potential (OCP) over time. The OCP followed a relaxation curve, the slope of which was then correlated with the concentration of nicotinamide adenine dinucleotide (NADH) coenzyme, which was used as an analyte. [5] Another potentiometry-based study incorporating the latest advances in redox mediators and wired enzymes was published by Yarnitzky et al. In this study, glucose oxidase enzyme was immobilized and wired to the electrode with the aid of an osmium-based redox polymer. [6] Their method included the application of a potential pulse to oxidize the redox centers in the film, followed

by the monitoring of the potential at the end of a fixed OCP period which was then correlated to the glucose concentration in the sample.

In the present study we report a novel method for monitoring glucose at zero current based on a time-dependent response. The principle of measurement is based on a two-step process that involves the oxidation of a mediator and the subsequent monitoring of the open-circuit potential over time. This process enables one to record a time-dependent response that is a function of the glucose in the sample. The readout is similar to that of chronopotentiometry where a transition time, rather than an electrochemical signal such as a current is monitored. The sensing membrane employed is based on ferrocene-modified poly(ethylenimine) used as mediator and the enzyme glucose oxidase. A diffusion limiting membrane enables the steady-state diffusion of glucose towards the electrode and can be used to fine tune the selectivity.

5.2 Experimental Section

5.2.1 Materials, Instruments & Electrochemical Methods

Glucose oxidase from Aspergillus niger (type VII, lyophilized powder, ≥ 100000 units/g solid), (6-bromohexyl) ferrocene, poly(ethylene glycol) diglycidyl ether (average Mn: 500), polyethylenimine (PEI) (water-free, typical Mn: 10000, typical Mw: 25000), Nafion perfluorinated resin solution (5 wt. % in lower aliphatic alcohols and water, 15-20 % water), D-(+)-glucose (≥ 95 %), potassium chloride, sodium phosphate dibasic (ACS reagent, ≥ 99 %), sodium chloride (puriss, ≥ 99.5 %), L-ascorbic acid (BioXtra, ≥ 99 %, crystalline) were purchased from Sigma Aldrich, potassium phosphate monobasic (99+ %, extra pure) from Acros Organics, hydrochloric acid (1 M, NIST Standard Solution) from Fisher Chemical and urea (≥ 99.5 %) from Fluka. Phosphate buffered saline solution (PBS) at a composition of 137 mM sodium chloride, 2.7 mM potassium chloride, 10 mM sodium phosphate dibasic and 1.8 mM potassium phosphate monobasic with a pH 7.49 was prepared from stock solutions of the respective salts. The glucose standard solutions used for all experiments were prepared (2–20 mM) in a PBS background. All other aqueous solutions were prepared in Milli-Q water (18.2 MΩ cm).

The electrochemical measurements were performed with a PGSTAT204 (Metrohm Autolab) controlled by the Nova 2.1 software. A three-electrode configuration was used, consisting of a glassy carbon electrode used as working (WE), a Pt wire as counter (CE) and an Ag/AgCl wire as reference (RE) electrode. The glassy carbon (GC) electrode used as WE was fabricated in-house by encasing a GC rod (Ø 2 mm) in a polyether ether ketone (PEEK) tube. The RE and CE electrodes were prepared similarly by encasing the Ag/AgCl and Pt wires respectively in PEEK tubes. An flow cell built in-house accommodated the three-electrode setup with the electrodes placed in proximity to each other (**Figure S5.1**). The flow was controlled by an IPC pump (high precision multichannel dispenser, ISMATEC) and kept at a flowrate of either 255 uL min^{-1} or 510 uL min^{-1} depending on the experiment.

Cyclic voltammetry was performed from -0.1 V to +0.6 V with a 50 mV s^{-1} scan rate in all cases except for the scan rate study. Amperometry was performed at +0.4 V keeping a 510 uL min^{-1} flowrate. Three repetitions were performed in total, washing with PBS in between. For the chronopotentiometric experiments, a two-step method was employed. First, an oxidation potential of +0.4 V was applied for 45 s, followed by monitoring of the OCP until the time needed for the potential to reach the cut-off value of +0.04 V. This period varied according to the concentration of glucose tested, with higher concentrations resulting in shorter time scales. For each glucose concentration, the above two-step protocol was repeated five times in total by sequentially applying the oxidation/OCP monitoring steps under constant flow of the glucose solutions (510 uL min^{-1} flow rate). The average and standard deviations were calculated from the results obtained during the last three repetitions. All electrochemical experiments (except for the ones of varying enzyme concentration and O_2 dependence) were performed in a flow cell built in-house (**Figure S5.1**) under constant flow in ambient temperature. All solutions were used without removing oxygen beforehand.

5.2.2 Synthesis of Fc-C_6-bPEI

The Fc-C_6-bPEI redox polymer used in this study was synthesized according to the procedure described in *Chapter 4. Avoiding Potential Pitfalls in Designing Wired Glucose Biosensors.*

5.2.3 Preparation of Glucose Biosensor

The glucose biosensor was prepared by drop casting two solutions on a glassy carbon electrode: a Fc-C_6-bPEI/GOx/cross-linker solution which formed the main sensing layer and an aqueous-based Nafion solution added on top as a diffusion limiting membrane. For the preparation of the Fc-C_6-bPEI/GOx/cross-linker solution, a 20 mg/mL redox polymer solution was first prepared by dissolving 8 mg of the synthesized Fc-C_6-bPEI in 400 µL of MilliQ and 0.1 M HCl (solution 1). The volume of HCl was adjusted to bring the pH of the final solution to 5. 28 uL of solution 1 were then mixed rapidly with 12 uL of 50 mg/mL glucose oxidase solution (dissolved in MilliQ) and 1.5 uL of cross-linker solution (1:10 diluted solution of poly(ethylene glycol) diglycidyl ether in MilliQ) using a vortex. 2 uL of this membrane cocktail were drop cast on the glassy carbon electrode (Ø 2 mm) which was previously polished with 0.3 um alumina and left to cure overnight in ambient atmosphere. Next, three layers (2 uL each) of 0.5 % diluted Nafion solution were drop cast on top, with a 30-minute waiting period before each deposition. The 0.5 % Nafion solution was prepared by diluting the 5 % Nafion stock solution in MilliQ. The sensors were ready for use after 3-4 h (kept in ambient T) following the last addition of Nafion layer to ensure that the film was completely dry.

5.2.4 Principle of the method

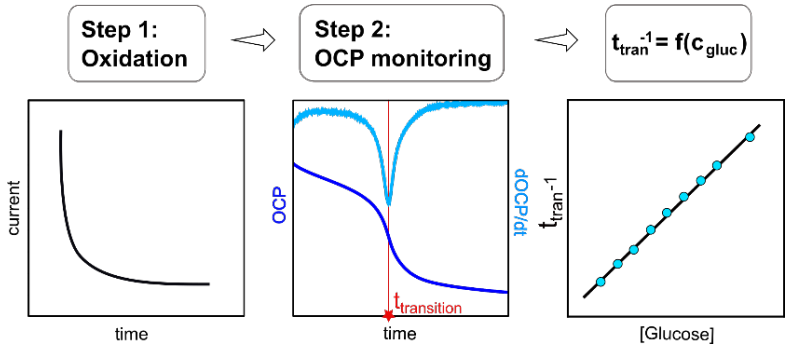

Figure 5.1: Schematic representation of the chronopotentiometric method. Oxidation of mediator (step 1), OCP monitoring (step 2), plotting of reciprocal transition time against glucose concentration (step 3).

The function of the sensor relies on the presence of glucose oxidase, the enzyme providing high specificity for glucose, and a ferrocene derivative that acts as an electron mediator establishing the electrical communication between enzyme and electrode. Both enzyme and mediator are immobilized on the surface of the glassy carbon electrode with a cross-linking agent. The electrode is placed in the flow cell where the glucose-containing sample is kept at constant solution flow. The chronopotentiometric method is initiated with an oxidation step in which the potential is kept at +0.4 V (step 1, **Figure 5.1**) for 45 s, resulting in the oxidation of the mediator and the production of ferrocenium ions. These ions act as an oxidant for glucose oxidase which is found in its reduced form due to the presence of glucose. Hence, the ferrocenium ions are reduced to ferrocene while the enzyme catalyses the oxidation of glucose to form gluconolactone. This turns the oxidized enzyme back to its reduced state (**Figure 5.2**). The application of the oxidation potential at +0.4 V is followed by the measurement of the OCP (step 2, **Figure 5.1**). When OCP monitoring initiates, a gradual decrease of the potential is observed owing to the reduction of the ferrocenium ions from the incoming electrons that are liberated during the oxidation of glucose. This process results in a distinct potential jump at a characteristic transition time that is a function of glucose concentration in the sample. When a certain potential cut-off value is reached (+0.04 V) the OCP monitoring step ends and a new cycle of step 1 and 2 begins, with the mediator being oxidized during step 1 and subsequently reduced during step 2 as described above. During the experiment, the incoming glucose flux is controlled by the diffusion limiting membrane (Nafion) placed on top of the sensing layer, ensuring that the conversion of glucose is not controlled by the enzyme kinetics but rather by the diffusion of substrate across the membrane and sensing layer (**Figure 5.2**). For the calibration curve, the reciprocal transition time is plotted against glucose concentration in some similarity to the Sand equation.

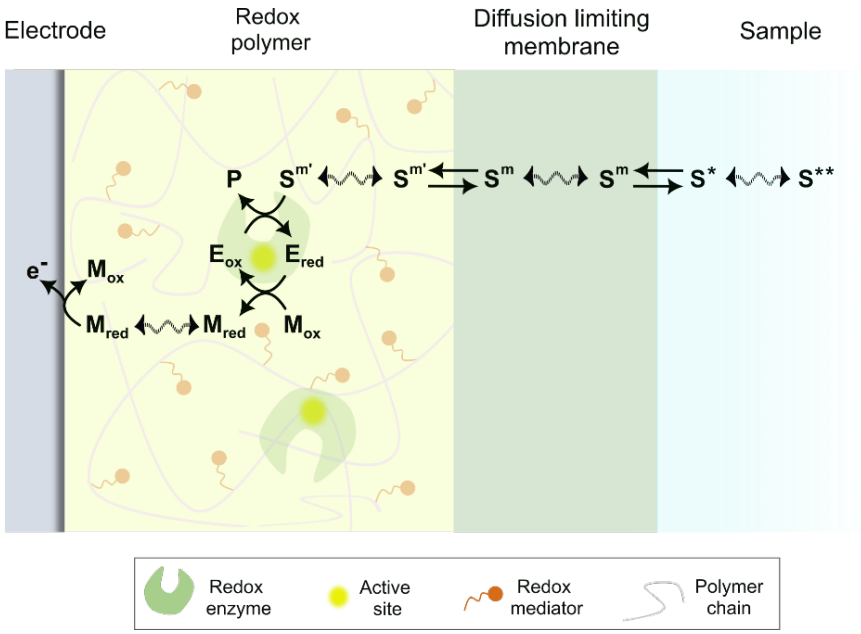

Figure 5.2: Sequence of events during the enzymatic oxidation of glucose in the examined mediated biosensor (S: substrate (glucose), P: product (gluconolactone), E_{red}: reduced form of enzyme (GOx-$FADH_2$), E_{ox}: oxidized form of enzyme (GOx-FAD), M_{red}: reduced form of mediator (Fc), M_{ox}: oxidized form of mediator (Fc^+)

5.3 Results and Discussion

5.3.1 Optimization of electrode components and characterization of the sensing film

Preliminary experiments to determine the optimal concentration of the enzyme in the Fc-C_6-bPEI/GOx/cross-linker film were performed by examining the chronopotentiometric response with varying GOx concentrations (40, 50 or 100 mg/mL). The solutions were deposited either by spin coating or drop casting on the GC electrodes. The effect of enzyme concentration on the response was similar for both depositions, with less enzyme amount resulting in longer transition times and the effect being more prominent in the drop cast films (**Figure S5.2**). Because the films containing 50 mg/mL GOx gave smaller standard deviations while maintaining reasonably fast transition times, this concentration was chosen as the final one. The Fc-C_6-bPEI concentration in the Fc-C_6-bPEI/GOx/cross-linker solution was kept at 20 mg/mL since earlier experiments with a lower amount of 10 mg/mL as suggested by the original protocol [7] did not always result in the expected OCP drop during the chronopotentiometric method. This is possibly because the amount of ferrocene was insufficient for completing the reaction cascade for the glucose conversion (**Figure 5.2**).

The two deposition methods used here (spin coating and drop casting) were characterized with microscopy techniques. Atomic force microscopy (AFM) on spin coated C_6-bPEI/GOx/cross-linker solutions (in the absence of Nafion layers) showed a dispersion of the solution components (**Figure S5.3**), which was confirmed by scanning electron microscopy (SEM) (**Figure S5.4**). The estimation of film thickness on spin coated films was difficult since ferrocene formed agglomerates dispersed on the

surface and not a homogeneous film. Conversely, SEM on the drop cast films revealed a uniform layer of 22.5 ± 3.0 um thickness, estimated by several cross-section points on the deposited films (**Figure 5.3**). Since the knowledge of thickness was necessary for the subsequent charge calculations, drop casting was selected as the preferred deposition method for the rest of the study. Next, nuclear magnetic resonance (NMR) was performed to determine the substitution degree of the ferrocene groups on the PEI backbone and the concentration of ferrocene in the redox polymer, which were estimated at 10.7 % and 1.49 M respectively (detailed calculations in *Chapter 4. Avoiding Potential Pitfalls in Designing Wired Glucose Biosensors*).

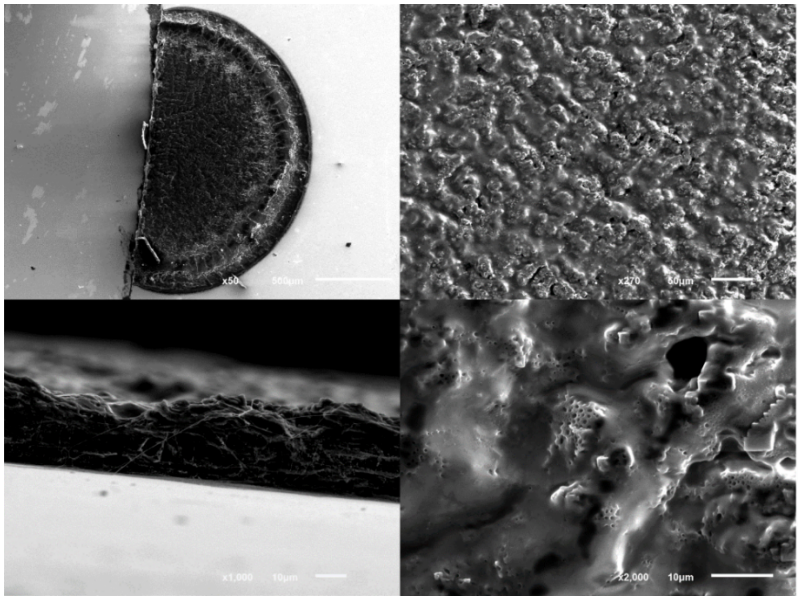

Figure 5.3: SEM on drop cast Fc-C_6-bPEI/GOx/cross-linker films (2 uL deposition).

The optimal amount of Nafion layers on top of the Fc-C_6-bPEI/GOx/cross-linker film, as well as various electrochemical properties of the biosensor, were determined by cyclic voltammetry. Comparison between no layer and 1, 3 and 5 Nafion layers (0.5 % w/v) with voltammograms taken both in PBS (absence of glucose) and 10 mM glucose (in PBS background) solutions showed that 5 layers were not optimal since glucose could not diffuse through the film (**Figure S5.5**). The results from one and three Nafion layers were comparable and given that more coverage with Nafion should theoretically result in better shielding against interfering compounds, the preferred amount of Nafion was chosen to be three layers. The electrocatalytic behavior of the films in the absence of a diffusion limiting membrane examined in the presence of 10 mM glucose showed an (almost) steady state catalytic current in the anodic region and a decreased cathodic peak. The addition of Nafion layers enhanced the effect of diffusion in the charge transfer process which was manifested by the appearance of the characteristic shoulders in both anodic and cathodic regions of the cyclic voltammogram. In all cases, the anodic peak of CVs in buffer solution was sharper compared to the cathodic one, with the latter often presenting signs of a second peak that tended to disappear over time. This could be the source of impurities of the film that leach out over time. Despite the existence of the diffusion limiting membrane which adds an

additional shield against leaching of the film components, a gradual loss of mediator was observed during a series of CV scans upon first contact with the PBS solution, before the peak current obtained a relatively stable value towards the end of 50 cycles (**Figure S5.6**). The same trend in decreasing peak current was also observed in the electrodes with varying Nafion coatings. Similar behavior has been reported in the literature for ferrocene-based redox polymers with the decrease attributed to either the loss of unbound polymer strands or to nucleophilic attacks that tend to destabilize the ferrocenium ion. [8,9]

The redox potential of the Fc-C_6-bPEI/GOx/cross-linker film was estimated at 204.5 mV (vs. Ag/AgCl) and the peak-to-peak separation at 102.5 mV by cyclic voltammetry (50 mV s^{-1}). A linear dependence between the anodic and cathodic peak currents and the square root of scan rate (**Figure 5.4**ii) is indicative of the diffusion-controlled electron transfer properties of the film, in agreement with previously reported mediated glucose biosensors based on redox polymers. [8–13]

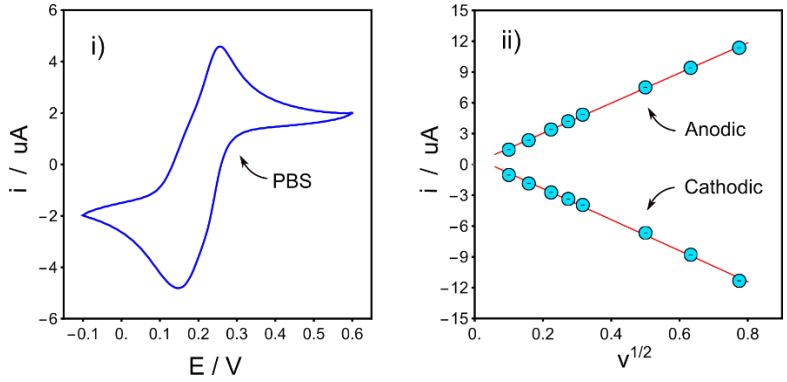

Figure 5.4: i) Cyclic voltammetry (50 mV s^{-1}) in PBS (0.17M, pH 7.49) upon first contact with solution. The last scan from a total of 15 cycles is presented. ii) Dependence of peak current on the square root of scan rate (10-600 mV s^{-1}). Experiments performed in PBS (0.17M, pH 7.49) with the same electrode used for the chronopotentiometric and amperometric experiments that followed (2 uL Fc-C_6-bPEI/GOx/cross-linker and 3 Nafion layers (2 uL each, 0.5% w/v) drop cast on the GC electrode).

As already discussed in *Chapter 1:* Introduction and *Chapter 4. Avoiding Potential Pitfalls in Designing Wired Glucose Biosensors*, CV is not an ideal method for quantitatively assessing the sensor film properties since a charging current is always overlaying the faradaic response, making the measurement of faradaic peak currents quite imprecise. However, we can still use the information under the oxidation and reduction peaks for a semi-quantitative assessment. By measuring the area under the oxidation and reduction peaks (**Figure 5.4**i), the number of electroactive species available for electrochemical oxidation or reduction was calculated at 0.18 nmol and 0.13 nmol respectively, which represents just 0.15 % of the total amount immobilized on the electrode as calculated from the thickness of the film and the ferrocene concentration. It is thus clearly demonstrated that the majority of deposited ferrocene is located far from the electrode surface and is difficult to convert electrochemically in the time scale of a voltammetric sweep. Because of this the current during cycling never reaches zero after attaining its maximum value. Biosensors relying on redox species that are exclusively surface-confined should

display such an exhaustive behavior. [14–16] These are typically characterized by well-defined and symmetrical cyclic voltammograms, where the peak currents are proportional to the scan rate, with the charge transfer and counter ion movement in the film not limited by diffusion, as in our case presented above.

The apparent electron diffusion coefficient was estimated at $1.53 \pm 0.05 \cdot 10^{-12}$ cm^2 s^{-1} using the Randles-Sevcik equation and the results from the scan rate study (**Figure S5.8**, detailed calculations in **5.5.4**). Factors that influence the diffusion coefficient include the mobility of the anchored redox group, the diffusion of counter-ions in and out of the film during the oxidation and reduction of the polymer and the cross-linking level (higher cross-linking results in lower mobility). [17] Other studies [18,19] on similar ferrocene-containing bPEI polymers with immobilized GOx have reported diffusion coefficients ranging from 10^{-7} cm^2 s^{-1} to 10^{-11} cm^2 s^{-1}. Given the wide range of methods employed for the calculation of these coefficients [15] and the different experimental conditions used (different chain length of ferrocene derivatives, cross-linking agents, etc.), a direct comparison between the reported diffusion coefficients is unfortunately meaningless.

5.3.2 Chronopotentiometric method

The influence of oxygen on the chronopotentiometric response was examined. Preliminary experiments on a spin coated electrode in the absence of Nafion coating were performed by comparing the transition time obtained in N_2-purged solutions with non-purged ones. A 3.5 kDa dialysis membrane was placed on top of the Fc-C_6-bPEI/GOx/cross-linker film to minimize leaching of membrane components. Although it is known that trace amounts of oxygen may still be present in a N_2-purged solution that could give rise to a pseudo-glucose response, [20] a qualitative interpretation of the results is still possible. As shown in **Figure S5.7**, in an oxygen depleted environment the transition time is found to decrease for the same glucose concentration. To understand the reason behind this we need to consider the role of oxygen during the enzymatic catalysis of the substrate. In a mediated glucose oxidase-based biosensor, GOx catalyses the two-electron glucose oxidation through its redox cofactor FAD/$FADH_2$ (eq. 1). [21] In an oxygen-containing solution, the oxidation of glucose to gluconolactone via the reductive half-reaction shown in eq. 1 is followed by two parallel oxidative half-reactions, with the oxidised mediator (eq. 2) and oxygen (eq. 3) acting both as electron acceptors, competing for the electrons arriving from the substrate-reduced enzyme.

$$\text{Glucose} + \text{GOx-FAD} \rightarrow \text{Gluconolactone} + \text{GOx-FADH}_2 \quad (1)$$

$$\text{GOx-FADH}_2 + 2\text{Fc}^+ \rightarrow \text{GOx-FAD} + 2\text{Fc} + 2\text{H}^+ \quad (2)$$

$$\text{GOx-FADH}_2 + \text{O}_2 \rightarrow \text{GOx-FAD} + \text{H}_2\text{O}_2 \quad (3)$$

In a classic amperometric glucose biosensor, an increased current density (compared to the case where oxygen is present) will be observed when the only electron acceptor is the redox mediator. [14] This is because in the N_2-purged solution, the mediator receives more electrons from the reduced enzyme (since

there is no oxygen to compete with) and more of it is reduced. This gives higher current densities when the biosensor is poised at a given oxidation potential to generate the oxidized mediator and trigger a new cycle of enzymatic catalytic reaction. Here, the transition time reflects how fast the mediator is reduced, with smaller transition times translating to faster reduction. Without competition by oxygen, the available (oxidized) mediator is the only electron acceptor, receiving all electrons from the reduced enzyme. Hence, a faster transition time is observed compared to the case where oxygen would also compete in this process. Even if GOx does not require oxygen for the glucose turnover in the presence of a suitable electron mediator, [20] the biosensor is expected to show minimal oxygen dependence with the application of the diffusion limiting membrane (Nafion) employed in the final system. Hence, all subsequent experiments were performed in oxygen-containing solutions.

Next, the optimal time for oxidation (step 1 in **Figure 5.1**) was determined. The amount of available oxidized redox mediator driving the potential inflection (characterized by a distinct transition time) varies with the duration of the oxidation step applied. The longer the oxidation time, the more ferrocene groups are oxidized. The more ferrocene groups are present, the more time needed for them to become reduced by the incoming electrons, eventually leading to longer transition times. To determine the optimal duration of the oxidation step, chronopotentiometric measurements in fixed glucose background were performed (4 mM glucose, PBS, pH 7.49) varying the oxidation time between 2 s and 60 s. At 45 s the maximum transition time was attained, followed by a slightly decreased value at 60 s (**Figure 5.5**i). Hence, an oxidation time of 45 s was kept for all subsequent experiments.

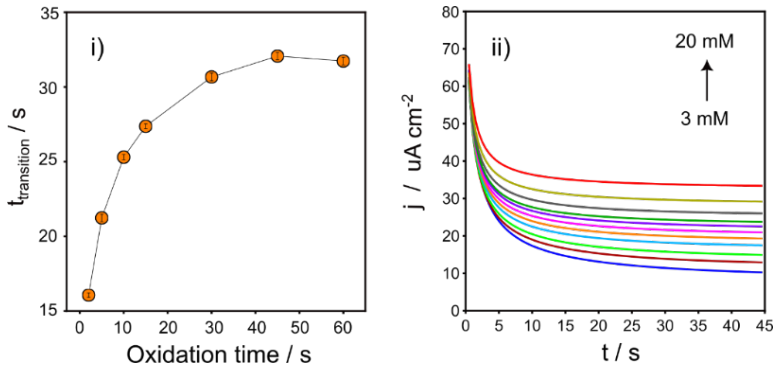

Figure 5.5: i) Varying oxidation time (+0.4 V) during chronopotentiometric measurements at 4 mM glucose (in PBS background) and ii) current density over time during the oxidation step (+0.4 V for 45 s) for varying glucose concentrations (3–20 mM). Five cycles of oxidation/OCP monitoring were performed for each concentration with the oxidation step during the 3rd cycle presented here. Same electrode as in **Figure 5.4**.

After determining the optimal duration of oxidation, the chronopotentiometric method was applied for glucose concentrations 3–20 mM, which is the range of interest for clinical applications. **Figure 5.5**ii shows the current response over time upon application of the oxidation potential at +0.4 V which transforms the mediator back to its oxidised form. This step is the equivalent of a chronoamperometric experiment with a Cottrell-like current decay. Comparing the charges from the oxidation step to the

charge calculated from the deposited ferrocene (**Table S5.1**) only a very small part of the deposited ferrocene (<1 %) is required for establishing the chronopotentiometric response. **Figure 5.6** shows the evolution of OCP over time after the application of the oxidation step and the resulting transition time for each glucose concentration (given by the time derivative of the OCP). As expected, higher glucose concentrations result in a faster depletion of the available oxidised ferrocene and give a shorter transition time. For each concentration tested, a series of five repetitions (cycles) of oxidation/OCP monitoring were performed (as described in **5.2.4**), with the average and standard deviations calculated from the last three repetitions.

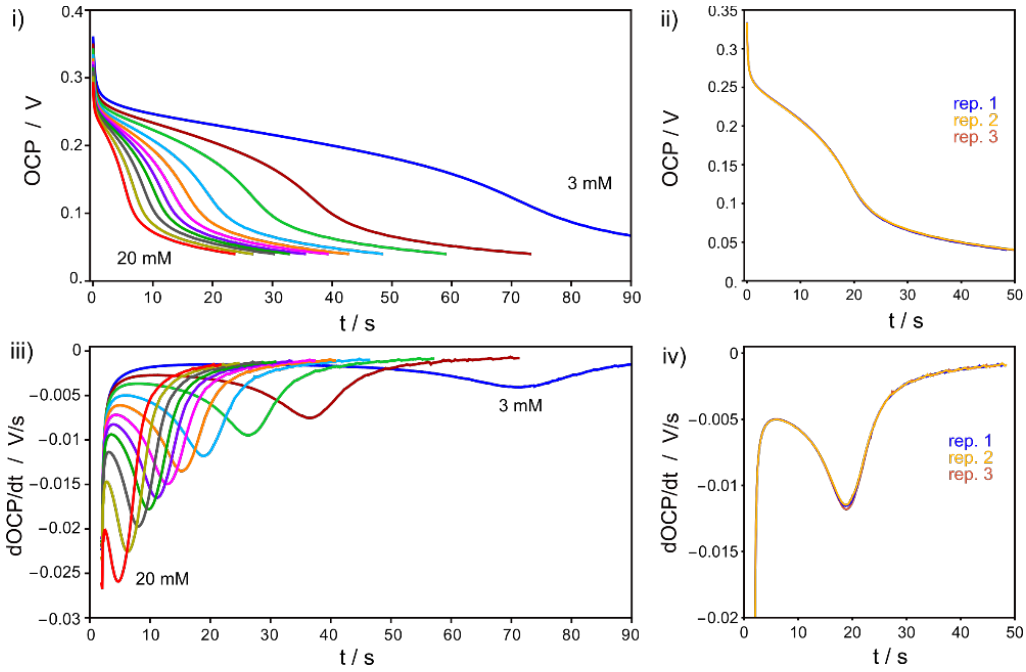

Figure 5.6: i) Evolution of OCP over time for all concentrations tested and ii) reversibility of response at 6mM (last 3 repetitions shown), iii) derivative of OCP over time for all concentrations tested and iv) reversibility of response at 6mM (last 3 repetitions shown). Same electrode as in **Figure 5.4**.

Plotting the reciprocal transition time as a function of glucose concentration, a linear response with a slope of 0.0117 ± 0.0002 is established for the concentration range of interest (3-12 mM) which serves as a calibration plot (**Figure 5.7**).

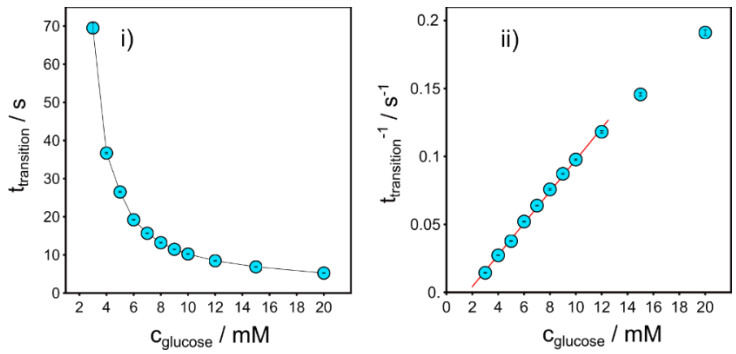

Figure 5.7: Calibration curve for glucose. Glucose concentration over i) the transition time and ii) the reciprocal transition time. Same electrode as in **Figure 5.4**.

5.3.3 Comparison with traditional amperometry and interference study

To evaluate the chronopotentiometric response, a comparison with traditional amperometry was performed by testing the same electrode in amperometry at + 0.4 V in the same concentration range for three sequential repetitions. **Figure 5.8** shows the resulting calibration curve and the evolution of current over time. The amperometric response was inferior to the chronopotentiometric one, with bigger standard deviations and a particularly decreased precision in the lower concentration range. From the evolution of current density over time, one can observe a degradation of response over time, possibly due to the prolonged exposure of the electrode (~3 h) to the flowing solution under the application of the constant anodic potential. With amperometry, an average response time of ~5 min is needed for the stabilization of the current for a single concentration tested, as opposed to the few seconds required for the establishment of the chronopotentiometric response. Five cycles of oxidation/OCP monitoring require approximately 5 min, resulting in a 3-fold shorter duration of measurement than the time needed to perform 3 amperometric repetitions at 5 min each. Another advantage of the former method is that the short duration of the oxidation step and subsequent OCP monitoring under zero current conditions prevent the long-term degradation of the sensor, which is a pronounced limitation with amperometric detection. In addition to this, the inherent drawbacks of amperometry, including the high charging currents and ohmic drop, are avoided with the zero current readout.

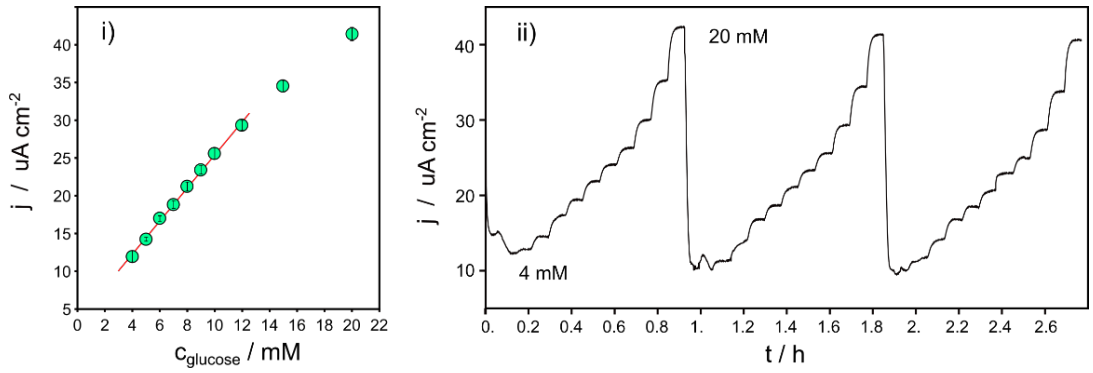

Figure 5.8: Amperometry in various glucose concentrations under constant flowrate (510 uL/min): i) calibration curve and ii) current density over time. Same electrode as in **Figure 5.4**.

Figure 5.9 shows the fluxes calculated from the charges involved during the oxidation step (chronopotentiometry) and the observed current values in amperometry. The fluxes are similar for both methods, with the slightly decreased curve of amperometry attributed to the prolonged use of the same electrode and the possible degradation of the sensing film that can occur under constant flow conditions.

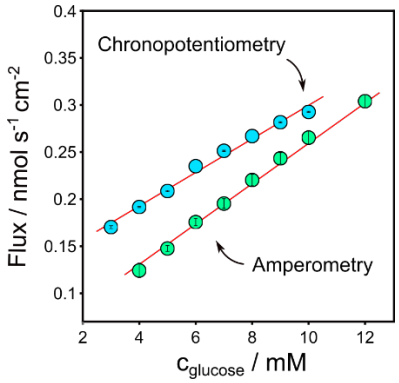

Figure 5.9: Comparison of fluxes with the chronopotentiometric and amperometric methods. Same electrode as in **Figure 5.4**.

Next, the interference of ascorbic acid and urea on the chronopotentiometric and amperometric responses was examined. Surprisingly, ascorbic acid interfered with both methods, despite the presence of the Nafion coating that should protect the sensing film. The study was performed in continuous flow by exchanging solutions of 5 mM glucose (in PBS) with solutions containing the interferents in the same glucose background. For the chronopotentiometric method, the transition time was recorded for four solutions tested sequentially containing glucose, glucose with ascorbic acid, glucose, glucose with urea (**Figure S5.10**). In the presence of ascorbic acid, the transition time decreased by 14% compared to the initial measurement. To evaluate whether the decreased response originated from the degradation of the film (in which case it would be unrelated to the presence of ascorbic acid), the same glucose solution without interferent was tested immediately afterwards, resulting again in an increased transition time, which however did not attain fully the initial level. The interference from ascorbic acid was therefore confirmed. Given that ascorbic acid is not interfering with the oxidase activity, [22] further investigations are needed to examine the reasons behind this behavior. In contrast, urea did not pose a problem as the transition time increased by only 3 % compared to glucose alone when the glucose/urea solution was examined. The same interfering patterns for both compounds were observed with amperometry (data not shown). A possible degradation of the Nafion coating, intensified from the constant flow applied during the measurements, may be responsible for this behavior. Similar experiments at less intense flow rates combined with the application of a protective membrane (e.g. dialysis membrane) should give a clearer view on the reasons behind the observed interferences.

5.4 Conclusions

A novel time-dependent potentiometric biosensor based on immobilized ferrocene on a PEI matrix containing glucose oxidase enzyme was developed. A two-step measurement with the application of a short-duration oxidation potential followed by the measurement of OCP is used to establish the chronopotentiometric response under zero-current conditions. This simple monitoring protocol requires low-power consumption, is less time-consuming and results in better reproducibility compared to the classic amperometric approach used for glucose sensing. The additional advantage of the specific

approach lies in its universality, which makes it possible to develop similar time-dependent sensors for other analytes. Further investigations on the effect of the diffusion limiting membrane on the interfering compounds typically present in biological fluids (e.g. serum, blood, etc) should be examined to allow the application of this principle to real sample measurements.

5.5 Supporting Information

5.5.1 Flow cell

An in-house built flow cell housing the working (glassy carbon, Ø 2mm), counter (Pt wire) and reference (Ag/AgCl wire) electrodes were used for the study. All three electrodes were kept in proximity to each other with the inlet placed opposite to the working electrode, see **Figure S5.*1***.

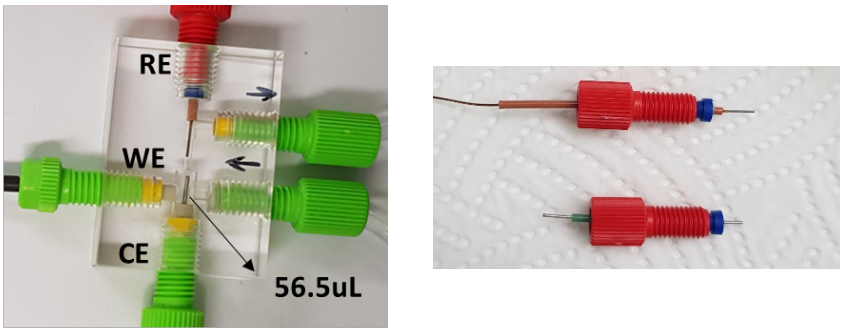

Figure S5.1: Flow cell used for all experiments (cyclic voltammetry, amperometry and chronopotentiometry) except for the ones of varying enzyme concentration (**Figure S5.2**) and O_2 dependence (**Figure S5.7**) (left), reference (Ag/AgCl wire) and counter (Pt wire) electrodes (right)

5.5.2 Optimization of electrode components and characterization of sensing film

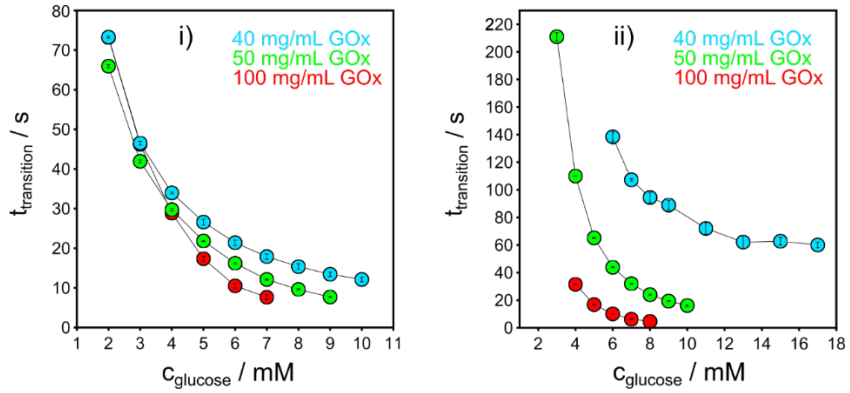

Figure S5.2: Influence of enzyme concentration on the transition time in i) spin coated and ii) drop cast C_6-bPEI/GOx/cross-linker films during the chronopotentiometric method. Electrodes (Ø 3 mm) were drop cast with 0.5% wt. Nafion solution, followed by the placement of a 3.5 kDa dialysis membrane. Experiments performed in beaker under stirring with sequential additions of standard glucose solution to reach the desired concentration. Oxidation step parameters: 30 s at +0.6 V.

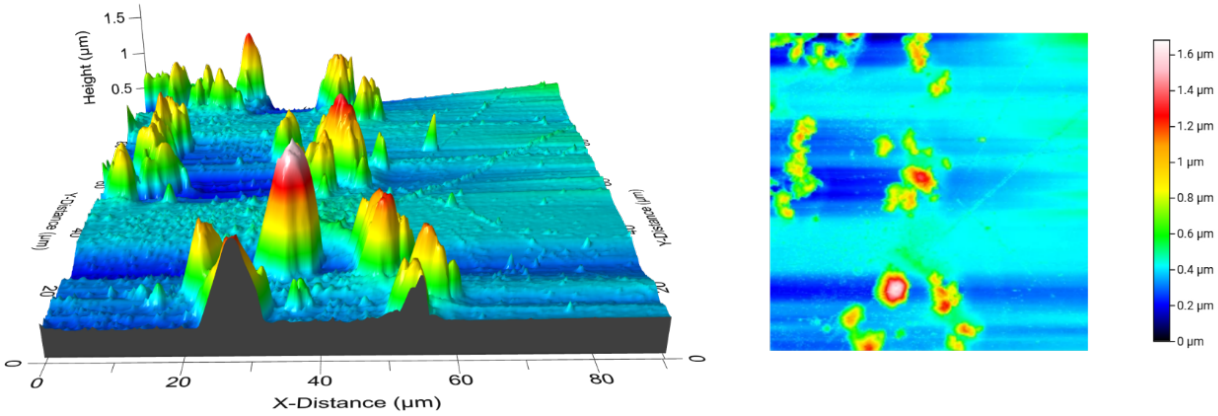

Figure S5.3: Atomic force microscopy (AFM) images in 3D (left) and 2D (right) of a spin coated film. For this, 3 uL of Fc-C_6-bPEI/GOx/cross-linker solution were drop cast on a silicon wafer followed by immediate spin coating. Spin coating parameters: 3000 rpm, 120 s duration.

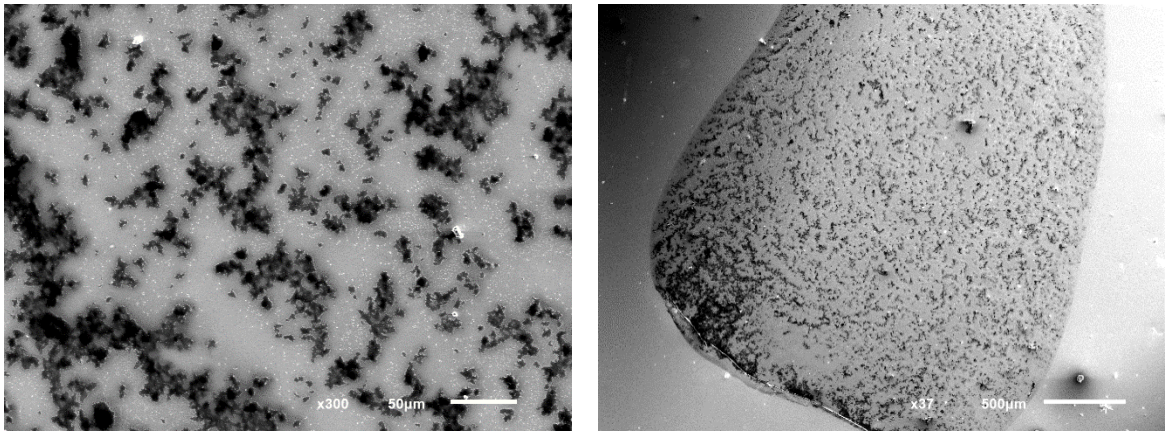

Figure S5.4: Scanning electron microscopy (SEM) of a spin coated film. Here, 3 uL of Fc-C_6-bPEI/GOx/cross-linker solution were drop cast on a Au-coated quartz crystal followed by immediate spin coating at 3000 rpm for 120 s.

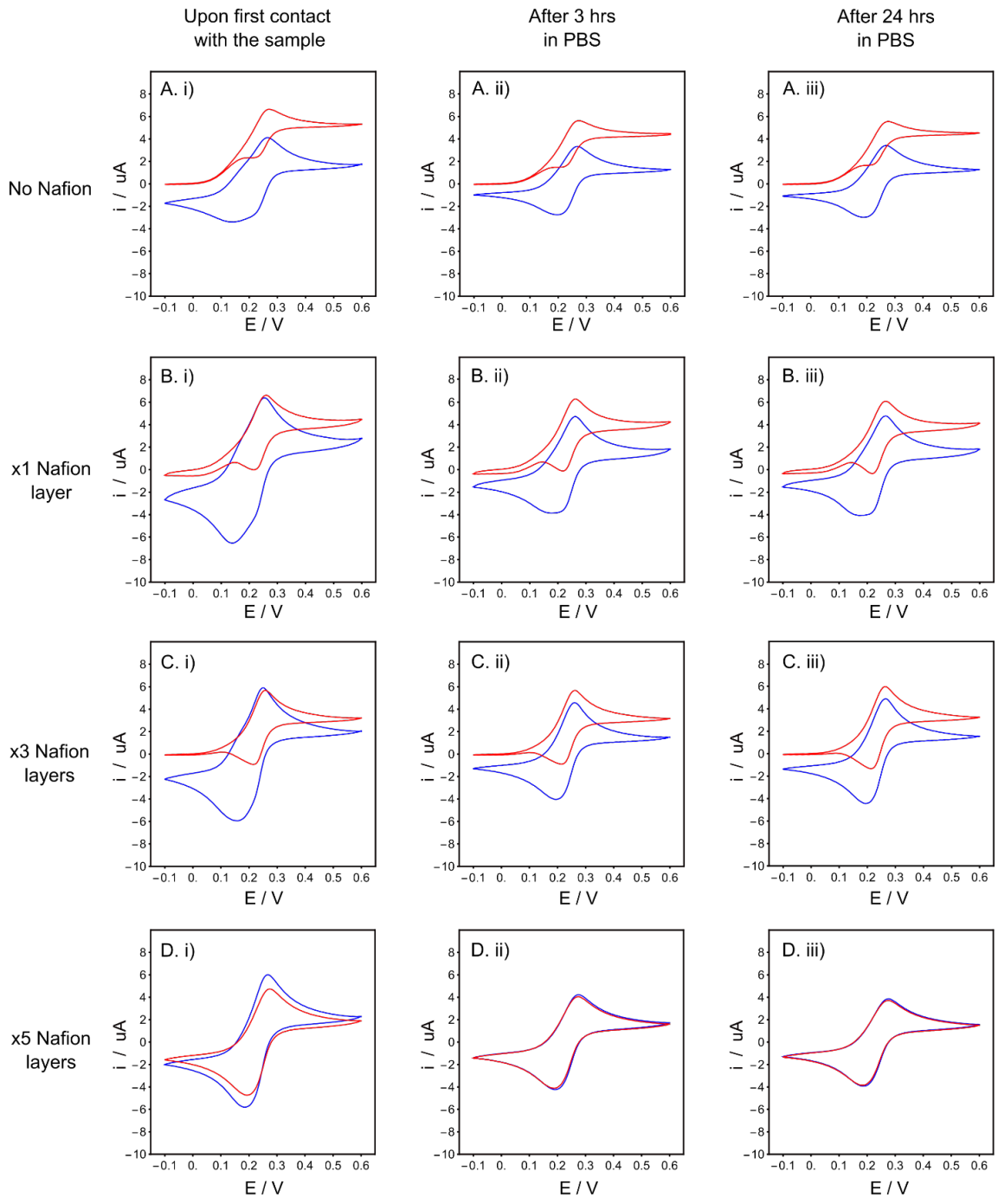

Figure S5.5: Cyclic voltammograms (50 mV s^{-1}) on electrodes with (A) absence of Nafion layer, (B) 1 Nafion layer (0.5% w/v), (C) 3 Nafion layers (0.5% w/v) and (D) 5 Nafion layers (0.5% w/v) upon first contact with the sample (i), after 3 hrs conditioning in PBS (ii) and after 24 hrs conditioning in PBS (iii). CVs taken in PBS (blue) and 10 mM glucose (red) under constant flowrate (510 uL/min). The last scan from a total of 10 cycles is presented. Electrodes were drop cast with 2 uL Fc-C_6-bPEI/GOx/cross-linker solution and left to dry overnight before testing the next day.

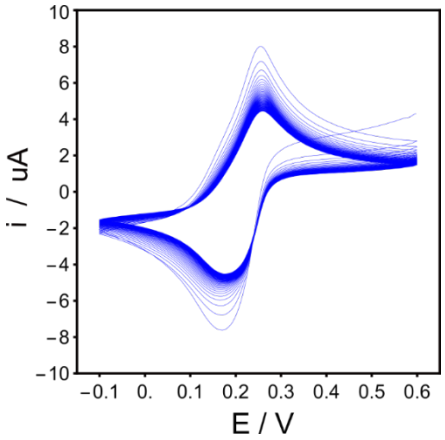

Figure S5.6: Cyclic voltammograms to examine stability over 50 scans (50 mV s^{-1}) in PBS at constant flowrate (510 uL/min). The electrode was drop cast with 2 uL Fc-C_6-bPEI/GOx/cross-linker and 3 Nafion layers (0.5% w/v).

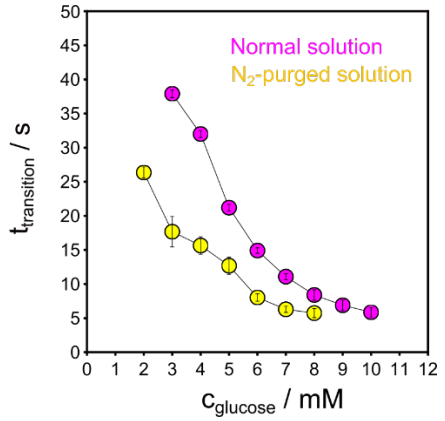

Figure S5.7: O_2 influence in the absence of Nafion membrane. The electrode was spin coated with Fc-C_6-bPEI/GOx/cross-linker covered by a 3.5kDa dialysis membrane for stability purposes. Oxidation step parameters: 30 s at +0.6V.

5.5.3 Calculation of charges during oxidation step and comparison with "recipe"

As calculated in *Chapter 4. Avoiding Potential Pitfalls in Designing Wired Glucose Biosensors (Calculation of ferrocene quantity and respective charge)*, the total quantity of ferrocene in the drop cast Fc-C_6-bPEI/GOx/cross-linker film (2 uL) is 101 nmol. Comparing this amount (defined as "mols from recipe") with the mols derived from the charge of the oxidation step (**Figure 5.5**ii), it is evident that only a very small part of the existing ferrocene is oxidised (<1 % for concentrations up to 20 mM) during the oxidation step (+0.4 V for 45 s) of the chronopotentiometric method.

Table S5.1: Charges during the oxidation step of the chronopotentiometric method (3-20 mM glucose)

mM	Average Q (uC)	n (=Q/F, in nmol)	Comparison with mols from "recipe" (%)
3	22.2	0.23	0.23
4	25.0	0.26	0.26
5	27.2	0.28	0.28
6	30.6	0.32	0.31

mM	Average Q (uC)	n (=Q/F, in nmol)	Comparison with mols from "recipe" (%)
7	32.8	0.34	0.34
8	34.8	0.36	0.36
9	36.8	0.38	0.38
10	38.2	0.40	0.39
12	41.1	0.43	0.42
15	45.2	0.47	0.46
20	50.7	0.53	0.52

5.5.4 Calculation of apparent electron diffusion coefficient (D_e) of the redox polymer

The apparent electron diffusion coefficient was estimated through cyclic voltammetry at varying scan rates and the application of Randles-Sevcik equation. The standard error was calculated from an analysis of variance (ANOVA) test using the data from the scan rate study (**Figure 5.4**ii and **Figure S5.8**).

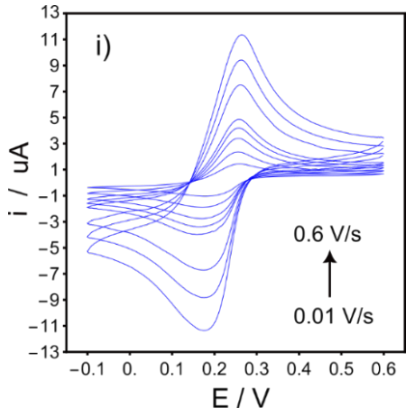

Figure S5.8: Scan rate study (50 mV s^{-1}) in PBS (0.17 M, pH 7.49) under constant flowrate (255 uL/min). The electrode was drop cast with 2 uL Fc-C_6-bPEI/GOx/cross-linker and 3 Nafion layers (0.5% w/v).

The slopes for the anodic and cathodic peak currents were $1.47 \cdot 10^{-5}$ and $1.51 \cdot 10^{-5}$ $A(V/s)^{-1/2}$, respectively, with standard errors of $1.50 \cdot 10^{-7}$ and $3.13 \cdot 10^{-7}$ $A(V/s)^{-1/2}$ respectively. The standard error for the diffusion coefficient was calculated with propagation of the error given for the slope ($i_p\, v^{-1/2}$) as follows (A= 0.030 cm^2, c_R=0.00149 mol cm^{-3}, n=1):

First, the Randles-Sevcik equation is solved to D_e:

$$i_p = (2.69*10^5) n^{3/2} A D_e^{1/2} c_R v^{1/2} \rightarrow D_e = \left(\frac{i_p / v^{1/2}}{2.69*10^5 n^{3/2} A c_R}\right)^2$$

where i_p the peak current (A), D_e the diffusion coefficient (cm^2 s^{-1}), v the scan rate (V s^{-1}), n the number of electrons linked to the redox reaction, A the electrode area (cm^2) and c_R the concentration of electroactive species.

The slope is then replaced with K and the error is propagated to find the ΔD_e:

$$D_e = (\frac{K}{2.69*10^5 n^{3/2} Ac_R})^2 \rightarrow D_e = K^2 * (\frac{1}{2.69*10^5 n^{3/2} Ac_R})^2 \rightarrow \Delta D_e = 2\mathrm{K} * (\frac{1}{2.69*10^5 n^{3/2} Ac_R})^2 \Delta \mathrm{K}$$

where ΔK the standard error of the slope.

Using the above equation, an average diffusion coefficient value of 1.53 ± 0.05 $\cdot 10^{-12}$ cm^2 s^{-1} was estimated from the respective values corresponding to the anodic and cathodic peak currents.

Note that a value of 4.66 ± 0.82$\cdot 10^{-13}$ cm^2 s^{-1} was obtained with chronoamperometry (at +0.4 V for 45 s) performed in PBS solution before the application of the chronopotentiometric experiment. The current was plotted against time (i=f(t$^{-1/2}$), **Figure S5.9**) for fitting the data to Cottrell equation and calculate the D_e. Standard deviation was calculated from the standard error of the regression slope (given by ANOVA test) and the uncertainty of the electrode area (3.00 ± 0.27$\cdot 10^{-6}$ m^2).

$$i = \frac{nFAc_R D_e^{1/2}}{\pi^{1/2} t^{1/2}} \rightarrow i = Kt^{-1/2} \quad (K = \frac{nFAc_R D_e^{1/2}}{\pi^{1/2}})$$

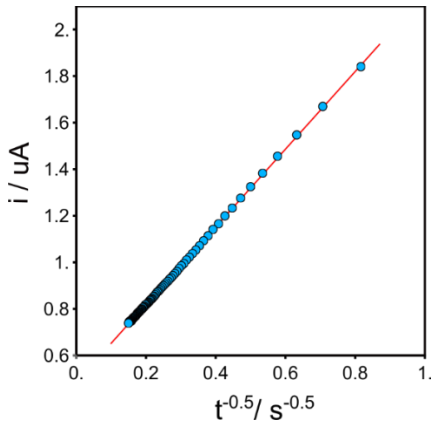

Figure S5.9: Cottrell experiment for the calculation of diffusion coefficient (+0.4 V for 45 s) in PBS (0.17 M, pH 7.49). The chronoamperometric experiment was performed before the application of chronopotentiometry in the absence of glucose.

5.5.5 Interference study

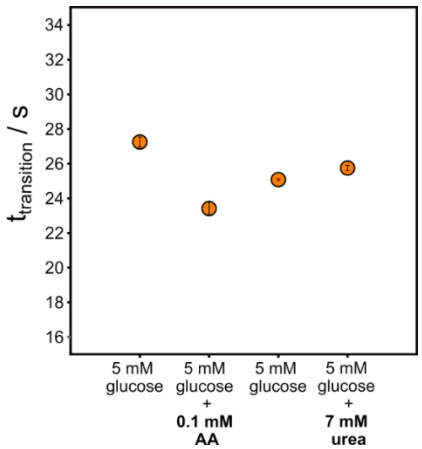

Figure S5.10: Interference study with the chronopotentiometric protocol. Solutions of glucose, ascorbic acid and urea were flowing sequentially through the cell under constant flowrate (510 uL/min). The electrode was drop cast with 2 uL Fc-C_6-bPEI/GOx/cross-linker and 3 Nafion layers (0.5% w/v).

5.6 References

(1) Schuhmann, W. Amperometric Enzyme Biosensors Based on Optimised Electron-Transfer Pathways and Non-Manual Immobilisation Procedures. *Reviews in Molecular Biotechnology* **2002**, *82* (4), 425–441. https://doi.org/10.1016/S1389-0352(01)00058-7.

(2) *Biosensors: Fundamentals and Applications*; Turner, A. P. F., Karube, I., Wilson, G. S., Eds.; Oxford University Press: Oxford [Oxfordshire] ; New York, 1987.

(3) Malmstadt, H. V.; Winefordner, J. D. Precision Null-Point Potentiometry: A Simple, Rapid and Accurate Method for Low Concentration Chloride Determinations. *Analytica Chimica Acta* **1959**, *20*, 283–291. https://doi.org/10.1016/0003-2670(59)80066-0.

(4) Malmstadt, H. V.; Pardue, H. L. Quantitative Analysis by an Automatic Potentiometric Reaction Rate Method. Specific Enzymatic Determination of Glucose. *Anal. Chem.* **1961**, *33* (8), 1040–1047. https://doi.org/10.1021/ac60176a054.

(5) Nagy, A.; Nagy, G.; Fehér, Z. Investigation of a Novel Chronopotentiometric Detection Method Using a Redox Mediator Modified Carbon Electrode. *Analytica Chimica Acta* **1995**, *310* (2), 241–249. https://doi.org/10.1016/0003-2670(95)00138-P.

(6) Yarnitzky, C.; Caruana, A. M.; Schmidtke, D. W.; Heller, A. Linear Dependence of the Potential of "Wired" Glucose Oxidase Electrodes on the Concentration of Glucose. *J. Phys. Chem. B* **1998**, *102* (49), 10057–10061. https://doi.org/10.1021/jp983176k.

(7) Hickey, D. P. Ferrocene-Modified Linear Poly(Ethylenimine) for Enzymatic Immobilization and Electron Mediation. In *Enzyme Stabilization and Immobilization: Methods and Protocols*; Minteer, S. D., Ed.; Methods in Molecular Biology; Springer: New York, NY, 2017; pp 181–191. https://doi.org/10.1007/978-1-4939-6499-4_14.

(8) Calvo, E. J.; Etchenique, R.; Danilowicz, C.; Diaz, L. Electrical Communication between Electrodes and Enzymes Mediated by Redox Hydrogels. *Anal. Chem.* **1996**, *68* (23), 4186–4193. https://doi.org/10.1021/ac960170n.

(9) Díaz-González, J. M.; Escalona-Villalpando, R. A.; Arriaga, L. G.; Minteer, S. D.; Casanova-Moreno, J. R. Effects of the Cross-Linker on the Performance and Stability of Enzymatic Electrocatalytic Films of Glucose Oxidase and Dimethylferrocene-Modified Linear Poly(Ethyleneimine). *Electrochimica Acta* **2020**, *337*, 135782. https://doi.org/10.1016/j.electacta.2020.135782.

(10) Al-Sagur, H.; Komathi, S.; Karakaş, H.; Atilla, D.; Gürek, A. G.; Basova, T.; Farmilo, N.; Hassan, A. K. A Glucose Biosensor Based on Novel Lutetium Bis-Phthalocyanine Incorporated Silica-Polyaniline Conducting Nanobeads. *Biosensors and Bioelectronics* **2018**, *102*, 637–645. https://doi.org/10.1016/j.bios.2017.12.004.

(11) Fritea, L.; J. Gross, A.; Gorgy, K.; K. O'Reilly, R.; Goff, A. L.; Cosnier, S. A Bifunctional Triblock Polynorbornene/Carbon Nanotube Buckypaper Bioelectrode for Low-Potential/High-Current Thionine-Mediated Glucose Oxidation by FAD-GDH. *Journal of Materials Chemistry A* **2019**, *7* (4), 1447–1450. https://doi.org/10.1039/C8TA10644D.

(12) Dervisevic, M.; Alba, M.; Yan, L.; Senel, M.; Gengenbach, T. R.; Prieto-Simon, B.; Voelcker, N. H. Transdermal Electrochemical Monitoring of Glucose via High-Density Silicon Microneedle Array Patch (Adv. Funct. Mater. 3/2022). *Advanced Functional Materials* **2022**, *32* (3), 2270022. https://doi.org/10.1002/adfm.202270022.

(13) Promsuwan, K.; Soleh, A.; Samoson, K.; Saisahas, K.; Wangchuk, S.; Saichanapan, J.; Kanatharana, P.; Thavarungkul, P.; Limbut, W. Novel Biosensor Platform for Glucose Monitoring via Smartphone Based on Battery-Less NFC Potentiostat. *Talanta* **2023**, *256*, 124266. https://doi.org/10.1016/j.talanta.2023.124266.

(14) Gregg, B. A.; Heller, Adam. Cross-Linked Redox Gels Containing Glucose Oxidase for Amperometric Biosensor Applications. *Anal. Chem.* **1990**, *62* (3), 258–263. https://doi.org/10.1021/ac00202a007.

(15) Aoki, A.; Heller, A. Electron Diffusion Coefficients in Hydrogels Formed of Cross-Linked Redox Polymers. *J. Phys. Chem.* **1993**, *97* (42), 11014–11019. https://doi.org/10.1021/j100144a019.
(16) Forster, R. J.; Walsh, D. A.; Mano, N.; Mao, F.; Heller, A. Modulating the Redox Properties of an Osmium-Containing Metallopolymer through the Supporting Electrolyte and Cross-Linking. *Langmuir* **2004**, *20* (3), 862–868. https://doi.org/10.1021/la035229h.
(17) Mao, F.; Mano, N.; Heller, A. Long Tethers Binding Redox Centers to Polymer Backbones Enhance Electron Transport in Enzyme "Wiring" Hydrogels. *J. Am. Chem. Soc.* **2003**, *125* (16), 4951–4957. https://doi.org/10.1021/ja029510e.
(18) Chuang, C. L.; Wang, Y. J.; Lan, H. L. Amperometric Glucose Sensors Based on Ferrocene-Containing B-Polyethylenimine and Immobilized Glucose Oxidase. *Analytica Chimica Acta* **1997**, *353* (1), 37–44. https://doi.org/10.1016/S0003-2670(97)00372-3.
(19) Wang, J.-Y.; Chen, L.-C.; Ho, K.-C. Synthesis of Redox Polymer Nanobeads and Nanocomposites for Glucose Biosensors. *ACS Appl. Mater. Interfaces* **2013**, *5* (16), 7852–7861. https://doi.org/10.1021/am4018219.
(20) Milton, R. D.; Minteer, S. D. Direct Enzymatic Bioelectrocatalysis: Differentiating between Myth and Reality. *Journal of The Royal Society Interface* **2017**, *14* (131), 20170253. https://doi.org/10.1098/rsif.2017.0253.
(21) Leskovac, V.; Trivić, S.; Wohlfahrt, G.; Kandrac, J.; Pericin, D. Glucose Oxidase from Aspergillus Niger: The Mechanism of Action with Molecular Oxygen, Quinones, and One-Electron Acceptors. *Int J Biochem Cell Biol* **2005**, *37* (4), 731–750. https://doi.org/10.1016/j.biocel.2004.10.014.
(22) Martinello, F.; Luiz da Silva, E. Mechanism of Ascorbic Acid Interference in Biochemical Tests That Use Peroxide and Peroxidase to Generate Chromophore. *Clinica Chimica Acta* **2006**, *373* (1), 108–116. https://doi.org/10.1016/j.cca.2006.05.012.

Conclusions and Outlook

Monitoring the level of essential analytes in the environmental and clinical context is crucial for sustaining society's well-being. Electrochemistry serves a key role in this respect, providing us with sensors that can yield real-time information on the examined analytes. Yet, achieving optimal sensor performance is a complex endeavour given the diverse parameters influencing their function. The goal of this thesis was to propose novel electrochemical methods that could form the basis of sensors with improved functionality.

First, an examination of the commercially available nitrate ionophores was made to evaluate their performance in comparison to the currently used ion-exchangers employed in nitrate-selective electrodes (**Chapter 2.** Commercially Available Nitrate Ionophores in Potentiometric Sensors Are Not Superior to Common Ion-Exchangers). Six different membrane compositions were tested, incorporating either the ionophores under investigation combined with ion-exchangers, or just ion-exchangers. Using the modified separate solution method, selectivity coefficients over chloride of -2.4 and -2.2 were calculated for nitrate ionophores V and VI respectively, which contradict the improved selectivity values reported in existing literature studies. The poor selectivity of both ionophores was later confirmed with the sandwich membrane method employed for determining the complex formation constants, highlighting a notably weak complexation with nitrate. The origin of the discrepancies in the reported coefficients with the ones from this work remains uncertain, but it could be linked to different approaches adopted in the execution of the studies. Considering these inconsistencies, several recommendations for improving the reporting of similar data were provided. The inclusion of experimental slopes used for the calculation of coefficients and the activity range to which they correspond is often lacking, but it is nonetheless essential. In addition, membranes should not be exposed to the primary ion before encountering the most discriminated ions, and the more frequent use of sandwich membrane method for calculating complex formation constants is strongly advocated.

Next, a novel yet simple method to eliminate the need for conditioning preceding the potentiometric measurements was proposed (**Chapter 3**: Unconditioned Symmetric Solid-Contact Electrodes for Potentiometric Sensing). The method is based on a symmetric setup incorporating identical indicator and reference electrodes. The application of differential potential measurements between the two permits the suppression of potential drifts originating from environmental fluctuations and those linked to the membrane's water uptake during conditioning. Using the proposed symmetric system, the nitrate concentration of a river water sample was determined with a marginal error of just 0.3% compared to the reference technique. In addition, the potential drift over long-term monitoring dropped below 0.1 mV min^{-1} after only few minutes of initial contact with the sample. The symmetric method was tested with nitrate- and potassium-selective electrodes using plasticized PVC for the sensing layer and carbon nanotubes for the transducer layer. However, the concept is adaptable to ISEs with different membrane

materials and transducers. Beyond its universal applicability, the suggested approach offers the benefit of substantially accelerating the preparation procedure preceding the potentiometric measurements, given that conditioning is typically the most time-consuming step.

The following topic shifted the discussion to the development of wired glucose biosensors (**Chapter 4.** Avoiding Potential Pitfalls in Designing Wired Glucose Biosensors). The motivation for this study originated from the realization that many of the newly developed sensors prioritize the engineering facets, neglecting the understanding of the fundamental working principles inherent in glucose sensing. A mediated glucose biosensor based on glucose oxidase and ferrocene immobilized in poly(ethylenimine) was used as a widespread example to investigate the intricate relationship between the observed amperometric signal and the type of mediated electron transfer process taking place. It was demonstrated that the observed signal is significantly influenced by the charging of the redox mediator that is not directly linked to the enzyme's active sites, resulting in a monotonically drifting signal. This factor is often overlooked when reporting the performance of similar sensors in literature and insights into the rate limiting steps governing the response are often insufficient. The negative implications of the undesired charging inducing a drifting response can be circumvented using surface bound redox moieties that facilitate rapid electron transfer between the enzyme and electrode. In addition, the use of diffusion limiting membranes is highly recommended to prevent complications arising from a potential loss of enzyme activity and enhance the sensors' operational stability. These aspects should be thoroughly addressed in the design phase of new glucose biosensors aiming to be reliable, affordable and minimally invasive.

To address some of the constraints imposed by amperometry, a time-dependent potentiometric glucose biosensor was proposed in the following chapter (**Chapter 5.** A novel time-dependent potentiometric glucose biosensor). The biosensor uses the same membrane composition as in chapter 4 and follows a two-step measurement protocol, including a short oxidation step succeeded by the monitoring of open circuit potential (OCP). During the OCP monitoring a shift in potential is observed due to the changing redox state of the mediator. This shift is marked by a characteristic transition time that is a direct function of the glucose concentration and serves as the sensor readout. The proposed chronopotentiometric method is shown to outperform traditional amperometry, offering better reproducibility and a 3-fold shorter measurement time. In addition, since the readout is based on zero current measurements, charging currents and ohmic drop contributions are eliminated. By adjusting the composition of the sensing membrane, the method may be customized for detecting different analytes. As with the symmetric system presented in Chapter 3 it should be broadly applicable.

In view of the impending technological advancements, the future of sensing applications looks bright. Within the environmental scope, advanced sensing technologies are anticipated to provide measurements of higher precision and temporal resolution in monitoring air, water, and soil quality. As an example, a notable outcome from this would be the improvement of agricultural practices, leading to

increased crop yields while mitigating the use of resources. In a clinical setting, wearable sensors and non-invasive devices are expected to attract considerable interest by facilitating continuous health monitoring, detecting abnormalities, and providing real-time data to healthcare providers while enhancing patient comfort and awareness. Biosensors, in particular, will play a key role in the area of non-invasive diagnostics and personalized medicine, enabling the realization of customized therapeutic interventions. Nevertheless, the promising future of sensing technologies brings with it certain challenges. Addressing the necessity for improved sensitivity and selectivity will remain one of the priorities, while enhancing the durability and lifespan of the newly developed sensors under various environmental conditions are essential. Scaling the production of sensing materials while ensuring the developed sensors remain both affordable and high-performing presents another challenge. Several environmental and sustainability concerns also come into play, including the necessity of fabricating and disposing sensors in an eco-friendly way and regulating the use of scarce materials, such as rare-earth elements, during sensor design. In addition, the mitigation of energy consumption in sensors, particularly in remote or wearable applications, along with the development and application of energy harvesting technologies for autonomous sensor operation will become essential.

Chemistry serves a critical role in tackling these challenges, functioning as the basis upon which advancements in sensing technology will be developed and refined. Nanomaterials and polymer science emerge as the sectors that will yield the most substantial progress. Fabricating electronic devices from materials that are both biodegradable and environmentally friendly is vital in addressing the persistent problem of electronic waste. Various polymers and carbon-based materials stand out as promising candidates thanks to their innate biodegradability or ability to be modified to biodegradable forms. Self-powered sensors which eliminate the need for external power sources relying on the energy harvested during their operation are gaining ground, particularly in the biosensing field. Wearable devices will particularly benefit from breakthroughs in this area, incorporating materials that combine flexibility, biocompatibility, and functionality. Moving forward, the field of printed electronics will progressively adopt the use of more sustainable, economically viable and widely accessible materials for inks and substrates and promote techniques with extensive production capabilities. Significant advancements in sensing applications will be driven by the development of advanced materials with enhanced sensitivity and selectivity, which exploit their distinctive properties to overcome the shortcomings of conventional materials. Among them, scaffold materials that combine the advantages of increased electroactivity, favorable spectroscopic characteristics and a porous 3D structure are expected to find extensive use in biomedical applications for the detection and quantification of various biomolecules. Other types of advanced materials that combine the facets of multifunctionality (e.g. light-responsive and shape-memory polymers, piezoelectric materials, metal-organic frameworks), enhanced durability (e.g. robust polymer composites, ceramic materials) and miniaturization (e.g. quantum dots, graphene) will also give

rise to innovative sensing solutions that are not only more efficient and precise, but are also adaptable to diverse and challenging application environments.

Acknowledgements

First, I would like to express my gratitude to Prof. Eric Bakker for granting me the opportunity to join his group back in 2019. Thank you for your guidance, patience, and confidence in me throughout the last five years.

I am very grateful to Prof. Aleksandar Radu from Lincoln University and Prof. Ross Milton from University of Geneva for accepting the request to review my thesis and join the jury for my defense.

I would like to thank my colleagues and friends in the group: Elena Zdrachek, for her scientific guidance and discussions, always willing to help with patience and understanding. Tara Forrest, who together with Elena formed my office companions, created a great ambiance in the lab, always eager to share her knowledge and help. Nikolai, Gabriel, Andrea, Robin, Yaotian, Ayian, Aori, Yupu and Marylou, for making this group vibrant with their presence, building a great and enthusiastic team of friends. I would also like to thank our old members, Yoshiki, Pitchnaree, Mao, Sutida, Sunil, Lu and Kye for the time spent together and the positive vibes brought into the group. A special thanks belongs to my former colleague and dear friend Melina Abdou, who made my stay in Geneva unique with her charismatic presence and kind personality, and to Liam Scarratt for his exceptional ability to bring people together and unlock their full potential.

Many thanks to Thomas Cherubini for his passion, enthusiasm, and readiness to support our team with the materials and equipment needed for our research needs, as well as to Stéphane Jeanneret for his kindness and continuous support in crafting all sorts of electronic material. I would also like to thank Magali, our kind secretary who is always willing to help and deal with all our administrative issues.

I am grateful to my dear friends that make my stay in Geneva truly special: Jerca, Gregor, Mil, Judith, Nikos, Chrysa, Richard, Guillaume, Maja, Elizabeta, Horace, Alex, Valentina, and to all those that are abroad, and particularly Katerina, Eirini, Céline, and Pamela for sharing their love from afar. Thank you all for being part of my extended family.

I would like to express my deepest gratitude to my family, and especially my parents Christos and Vasso, for giving their utmost so that I can stand here today. Finally, I would like to thank my husband Gregor for being my inspiration, and for his continuous support and love throughout these years.